



Michigan Technological University
Create the Future Digital Commons @ Michigan Tech

Dissertations, Master's Theses and Master's
Reports - Open

Dissertations, Master's Theses and Master's
Reports

2012

USING AUTO- AND CROSS-CORRELATIONS FROM SEISMIC NOISE TO MONITOR VELOCITY CHANGES AT VILLARRICA VOLCANO, CHILE

Kathleen F. McKee
Michigan Technological University

Follow this and additional works at: <https://digitalcommons.mtu.edu/etds>



Part of the [Geology Commons](#), and the [Geophysics and Seismology Commons](#)

Copyright 2012 Kathleen F. McKee

Recommended Citation

McKee, Kathleen F., "USING AUTO- AND CROSS-CORRELATIONS FROM SEISMIC NOISE TO MONITOR VELOCITY CHANGES AT VILLARRICA VOLCANO, CHILE", Master's Thesis, Michigan Technological University, 2012.

<https://doi.org/10.37099/mtu.dc.etds/479>

Follow this and additional works at: <https://digitalcommons.mtu.edu/etds>



Part of the [Geology Commons](#), and the [Geophysics and Seismology Commons](#)

USING AUTO- AND CROSS-CORRELATIONS FROM SEISMIC NOISE TO
MONITOR VELOCITY CHANGES AT VILLARRICA VOLCANO, CHILE

By

Kathleen Frances McKee

A THESIS

Submitted in partial fulfillment of the requirements for the degree of

MASTER OF SCIENCE

In Geology

MICHIGAN TECHNOLOGICAL UNIVERSITY

2012

© 2012 Kathleen Frances McKee

This thesis has been approved in partial fulfillment of the requirements for the Degree of MASTER OF SCIENCE in Geology.

Department of Geological/Mining Engineering and Sciences

Thesis Advisor: *Gregory P. Waite*

Committee Member: *Simon Carn*

Committee Member: *Petra Huentemeyer*

Department Chair: *Wayne Pennington*

Table of Contents

List of Figures	vii
List of Tables	xi
Acknowledgements.....	xiii
Abstract.....	xv
1 Introduction	1
2 Background	5
3 Methods & Analysis	6
3.1 Data Collection.....	6
3.2 Preparation of Data	7
3.3 Auto and Cross Correlation and Stacking	8
3.4 Stretching.....	13
4 Discussion	21
4.1 Seasonal Variations	21
4.2 Regional Tectonics	22
4.3 Volcanic	25
5 Conclusions	30
6 References	31
7 Appendices.....	34
7.1 2010 Auto-correlations with total stack and velocity change.....	34
7.2 2010 Cross-correlations with total stack and velocity change, positive and negative lag in separate plots	39
7.3 2011 Auto-correlations with total stack and velocity change.....	50
7.4 2010 Earthquakes and peak surface wave amplitudes	53

List of Figures

Figure 1.1 Cross-correlation of seismic noise, arrows indicate randomly scattered noise	2
Figure 1.2 Cross-correlation functions from two time periods showing an increase in arrival time of prominent signal.	3
Figure 2.1 Villarrica Volcano with plume from degassing (Taken: March 4, 2011).....	5
Figure 3.1 Villarrica hill-shade with stations V01 through V08.....	6
Figure 3.2 Station V01 to V03 2010 CCFs and total stack, A. Daily stacks of CCFs where red is positive correlation and blue is negative to the degree indicated in color bar to right, B. is the total stack of CCFs normalized by the number of CCFs. Positive time (+lag) is the CCF from V03 to V01 and negative time (-lag) is the CCF from V01 to V03.	8
Figure 3.3 Station V01 2010 vertical channel ACFs and total stack, A. Daily stacks of ACFs where red is positive correlation and blue is negative to the degree indicated in color bar to right, B. is the total stack of ACFs normalized by the number of ACFs. Here only positive time (+lag) from 2 to 10 seconds of the ACF is displayed because the time lag closer to zero is dominated by the positive correlation at zero and negative time (-lag) is the mirror image of +lag.	9
Figure 3.4 A. Station V01 east channel ACF and B. normalized total stack	10
Figure 3.5 A. Station V01 north channel ACF and B. normalized total stack.....	10
Figure 3.6 A. Station V06 2011 ACFs stacked daily and B. normalized total stack	11
Figure 3.7 CCFs from V01Z to V03R, daily stacks and normalized total stack	12
Figure 3.8 Vertical to vertical channel cross-correlation total stacks	12
Figure 3.9 Vertical to vertical channel cross-correlation total stacks continued	13
Figure 3.10 Examples of different stretching windows	14
Figure 3.11 Examples of different overlap window.....	15
Figure 3.12 Station V08 stretching function with best-fit line.....	15
Figure 3.13 2010 ACF vertical channel velocity changes.....	16
Figure 3.14 2010 ACF east channel velocity changes	17
Figure 3.15 2010 ACF north channel velocity changes	17
Figure 3.16 2010 CCF velocity changes from the negative lag for station pairs V01 to V03, V05, V07 and V08	18
Figure 3.17 2010 CCF velocity changes from the positive lag for station pairs V01 to V03, V05, V07 and V08.....	19
Figure 3.18 2010 CCF velocity changes from the negative lag for station pairs V05 to V03, V07 to V03, V05 and V08, and V08 to V03 and V05	19
Figure 3.19 2010 CCF velocity changes from the positive lag for station pairs V05 to V03, V07 to V03, V05 and V08, and V08 to V03 and V05	20
Figure 3.20 2011 ACF velocity changes from the vertical channel	20
Figure 4.1 A. 2010 velocity changes and B. total stack of 2010 velocity changes.....	21
Figure 4.2 2010 Velocity changes with regional earthquakes (gray lines), $6.5 > M > 5.4$..	23
Figure 4.3 V07 vertical channel surface wave amplitude versus stacked $\% \Delta v/v$	25

Figure 4.4 Distance from the edifice in kilometers versus magnitude of velocity change at each station during the perturbation that starts on day 123 of 2010.	27
Figure 4.5 2010 stacked velocity change compared to frequency of long-period events ..	27
Figure 4.6 2010 stacked velocity change compared to MODIS radiant heat output data from MODVOLC http://modis.higp.hawaii.edu/	28
Figure 4.7 2010 stacked velocity change compared to 60min RSAM from station V03 ..	29
Figure 4.8 OMI SO ₂ mass compared to 2010 stacked velocity change.....	29
Figure 7.1 Station V01 ACFs, A. daily stacks, B. normalized total stack and C. stretching function, y-axis is the same for A and C	34
Figure 7.2 Station V02 ACFs, A. daily stacks, B. normalized total stack and C. stretching function, y-axis is the same for A and C	35
Figure 7.3 Station V03 ACFs, A. daily stacks, B. normalized total stack and C. stretching function, y-axis is the same for A and C	35
Figure 7.4 Station V04 ACFs, A. daily stacks, B. normalized total stack and C. stretching function, y-axis is the same for A and C	36
Figure 7.5 Station V05 ACFs, A. daily stacks, B. normalized total stack and C. stretching function, y-axis is the same for A and C	36
Figure 7.6 Station V06 ACFs, A. daily stacks, B. normalized total stack and C. stretching function, y-axis is the same for A and C	37
Figure 7.7 Station V07 ACFs, A. daily stacks, B. normalized total stack and C. stretching function, y-axis is the same for A and C	37
Figure 7.8 Station V08 ACFs, A. daily stacks, B. normalized total stack and C. stretching function, y-axis is the same for A and C	38
Figure 7.9 CCFs from V01 to V03, -lag, A. daily stacks, B. normalized total stack and C. stretching function, y-axis is the same for A and C	39
Figure 7.10 CCFs from V01 to V03, +lag, A. daily stacks, B. normalized total stack and C. stretching function, y-axis is the same for A and C	40
Figure 7.11 CCFs from V01 to V05, -lag, A. daily stacks, B. normalized total stack and C. stretching function, y-axis is the same for A and C	41
Figure 7.12 CCFs from V01 to V05, +lag, A. daily stacks, B. normalized total stack and C. stretching function, y-axis is the same for A and C	41
Figure 7.13 CCFs from V01 to V07, -lag, A. daily stacks, B. normalized total stack and C. stretching function, y-axis is the same for A and C	42
Figure 7.14 CCFs from V01 to V07, +lag, A. daily stacks, B. normalized total stack and C. stretching function, y-axis is the same for A and C	42
Figure 7.15 CCFs from V01 to V08, -lag, A. daily stacks, B. normalized total stack and C. stretching function, y-axis is the same for A and C	43
Figure 7.16 CCFs from V01 to V08, +lag, A. daily stacks, B. normalized total stack and C. stretching function, y-axis is the same for A and C	43
Figure 7.17 CCFs from V05 to V03, -lag, A. daily stacks, B. normalized total stack and C. stretching function, y-axis is the same for A and C	44

Figure 7.18 CCFs from V05 to V03, +lag, A. daily stacks, B. normalized total stack and C. stretching function, y-axis is the same for A and C	44
Figure 7.19 CCFs from V07 to V03, -lag, A. daily stacks, B. normalized total stack and C. stretching function, y-axis is the same for A and C	45
Figure 7.20 CCFs from V07 to V03, +lag, A. daily stacks, B. normalized total stack and C. stretching function, y-axis is the same for A and C	45
Figure 7.21 CCFs from V07 to V05, -lag, A. daily stacks, B. normalized total stack and C. stretching function, y-axis is the same for A and C	46
Figure 7.22 CCFs from V07 to V05, +lag, A. daily stacks, B. normalized total stack and C. stretching function, y-axis is the same for A and C	46
Figure 7.23 CCFs from V07 to V08, -lag, A. daily stacks, B. normalized total stack and C. stretching function, y-axis is the same for A and C	47
Figure 7.24 CCFs from V07 to V08, +lag, A. daily stacks, B. normalized total stack and C. stretching function, y-axis is the same for A and C	47
Figure 7.25 CCFs from V08 to V03, -lag, A. daily stacks, B. normalized total stack and C. stretching function, y-axis is the same for A and C	48
Figure 7.26 CCFs from V08 to V03, +lag, A. daily stacks, B. normalized total stack and C. stretching function, y-axis is the same for A and C	48
Figure 7.27 CCFs from V08 to V05, -lag, A. daily stacks, B. normalized total stack and C. stretching function, y-axis is the same for A and C	49
Figure 7.28 CCFs from V08 to V05, +lag, A. daily stacks, B. normalized total stack and C. stretching function, y-axis is the same for A and C	49
Figure 7.29 Station V01 2011 ACFs, A. 6 hour stacks, B. normalized total stack and C. stretching function, y-axis is the same for A and C	50
Figure 7.30 Station V02 2011 ACFs, A. daily stacks, B. normalized total stack and C. stretching function, y-axis is the same for A and C	51
Figure 7.31 Station V03 2011 ACFs, A. daily stacks, B. normalized total stack and C. stretching function, y-axis is the same for A and C	51
Figure 7.32 Station V06 2011 ACFs, A. daily stacks, B. normalized total stack and C. stretching function, y-axis is the same for A and C	52
Figure 7.33 Station V08 2011 ACFs, A. daily stacks, B. normalized total stack and C. stretching function, y-axis is the same for A and C	52
Figure 7.34 V07 radial channel surface wave amplitude versus stacked $\% \Delta v/v$	57
Figure 7.35 V07 tangential channel surface wave amplitude versus stacked $\% \Delta v/v$	58

List of Tables

Table 3.1.1 2010 Station names, sensor type, dates used in Julian Days, and latitude/longitude	7
Table 3.1.2 2011 Station names, sensor type, dates used in Julian Days, and latitude/longitude	7
Table 4.2.1 Date, location, depth, magnitude and distance to Villarrica of the earthquakes displayed in Figure 4.2.1	23
Table 7.4.1 Magnitude, depth, date, location, and distance to Villarrica of the earthquakes M6 and greater displayed in Figure 4.2.2	53
Table 7.4.2 Magnitude, depth, date, location, and distance to Villarrica of the earthquakes M5.5-5.9 displayed in Figure 4.2.2.....	56

Acknowledgements

Teigan A. Gulliver, Jessica L. H. Smith, Bret M. Koehler, and Patrick Orr got me through the toughest and greatest moments of Peace Corps service. Thanks for always laughing with me.

Rüdiger Escobar Wolf, Joshua Richardson, and Kyle Brill helped me navigate the waters of MATLAB and of being a master's student again.

Simon Carn and Petra Huentemeyer served on my committee. Thank you for the constructive criticism and support.

Greg Waite. Thank you for the guidance and inspiration.

Mom, Dad, Sean and Ian encouraged and rejuvenated me with each visit home and phone call.

This material is based upon work supported by the National Science Foundation under Grant Numbers PIRE 0530109 and GEO 0948526.

Abstract

We used the Green's functions from auto-correlations and cross-correlations of seismic ambient noise to monitor temporal velocity changes in the subsurface at Villarrica volcano in the Southern Andes of Chile. Campaigns were conducted from March to October 2010 and February to April 2011 with 8 broadband and 6 short-period stations, respectively. We prepared the data by removing the instrument response, normalizing with a root-mean-square method, whitening the spectra, and filtering from 1 to 10 Hz. This frequency band was chosen based on the relatively high background noise level in that range. Hour-long auto- and cross-correlations were computed and the Green's functions stacked by day and total time. To track the temporal velocity changes we stretched a 24 hour moving window of correlation functions from 90% to 110% of the original and cross correlated them with the total stack. All of the stations' auto-correlations detected what is interpreted as an increase in velocity in 2010, with an average increase of 0.13%. Cross-correlations from station V01, near the summit, to the other stations show comparable changes that are also interpreted as increases in velocity. We attribute this change to the closing of cracks in the subsurface due either to seasonal snow loading or regional tectonics. In addition to the common increase in velocity across the stations, there are excursions in velocity on the same order lasting several days. Amplitude decreases as the station's distance from the vent increases suggesting these excursions may be attributed to changes within the volcanic edifice. In at least two occurrences the amplitudes at stations V06 and V07, the stations farthest from the vent, are smaller. Similar short temporal excursions were seen in the auto-correlations from 2011, however, there was little to no increase in the overall velocity.

1 Introduction

Scientists study the behaviors and hazards of volcanoes in an effort to prevent future disaster to those who live in their shadows. Seismologists use several techniques to monitor volcanic activity including mean seismic amplitudes (RSAM), numbers, and locations of volcano tectonic (VT), long-period (LP) or other seismic events, and occurrences of tremor that compliment geodetic, hydrologic, geophysical, and gas geochemical observations. Over the last decade, advances made in the using ambient seismic noise have enabled studies of structure without the use of ballistic waves. In addition, the use of interferometry with both natural and noise-derived waveforms has allowed volcano seismologists to image the volcanic subsurface with better spatial and temporal resolution. Studies at Erebus (Chaput et al., 2012) and Mt. Asama (Nagaoka et al., 2012) have used interferometric methods to model the structure. But interferometry has also resolved very small changes in seismic velocity over time that may be due to seasonal effects on volcanic systems (Sens-Schönfelder and Wegler, 2006), or changes in volcanic activity (Brenguier et al., 2011).

In recent studies, cross-correlations from ambient seismic noise have been used to observe velocity changes at volcanoes as a potential monitoring tool (Brenguier et al., 2011; Brenguier et al., 2008; Duputel et al., 2009). At Piton de la Fournaise Duputel et al. (2009) and Brenguier et al. (2011) found decreases in velocity that diminished in magnitude outside of the Dolomieu crater, which were followed by eruption. They attribute the changes to dilation of the subsurface due to magma migrating from the chamber to the surface. In Duputel et al. (2009) they do not have velocity information once the eruption starts, but their GPS, tiltmeter and extensometer data support a relaxation in the subsurface.

Given two receivers, A and B, and randomly scattered noise (Figure 1.1), the cross correlation of the seismograms from those receivers returns an approximation to the seismic record as if one station were a source and the other a receiver, the Green's function (Draganov et al., 2006; Shapiro and Campillo, 2004; Wapenaar and Fokkema, 2006; Weaver and Lobkis, 2001).

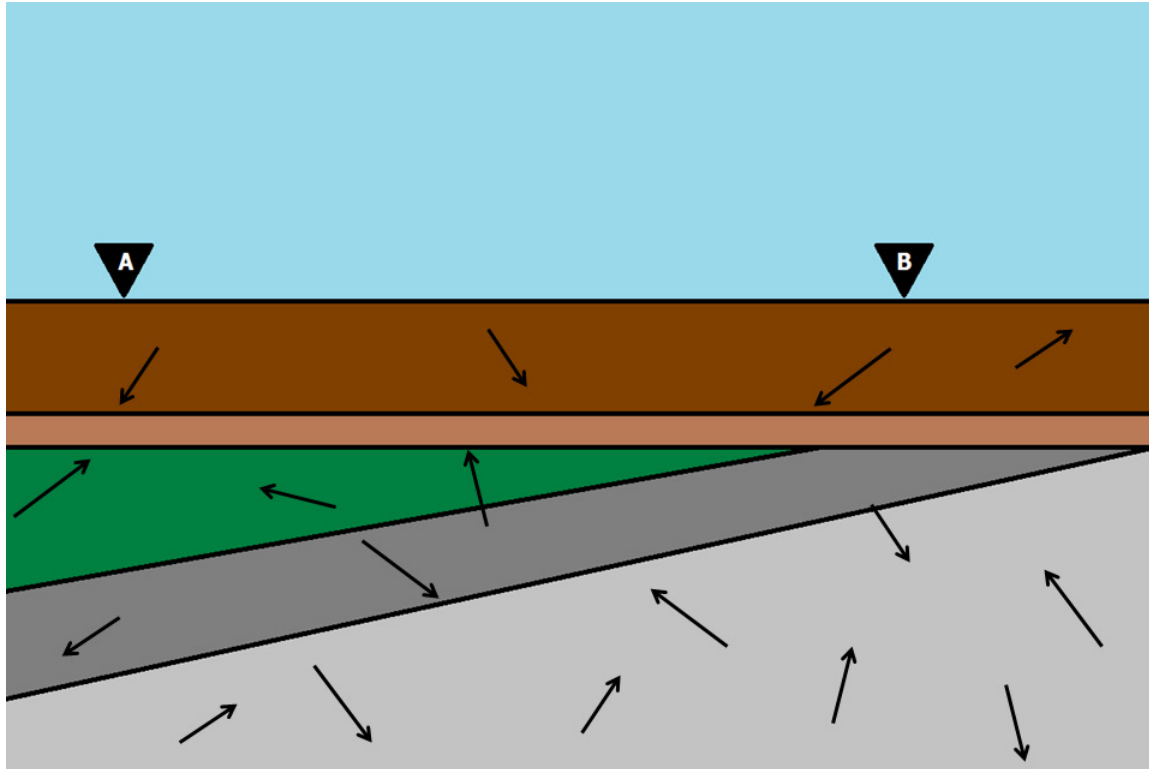


Figure 1.1 Cross-correlation of seismic noise, arrows indicate randomly scattered noise

A positive pulse correlated with a positive pulse translates to positive correlation. Equally, a negative with a negative pulse is a positive correlation, while a negative with a positive pulse and vice versa is a negative correlation. In turn, the correlation is zero when one or both signals are zero. In practice, cross-correlation is done from stations A to B and from B to A; with well scattered noise, the cross-correlation function (CCF) will be symmetric about zero time lag. The negative lag is the correlation from A to B, and positive lag from B to A. Since the CCF is an approximation to a Green's function, the lag time in the CCF is equal to travel time. Therefore, p-waves, s-waves and surface waves are present in the CCF.

The significance of the use of ambient noise is that a distinct source, such as an earthquake, volcanic explosion, or chemical explosion, is not necessary to gain information about the subsurface structure. However, many weeks to months of ambient noise data are needed to improve the signal to noise ratio in the CCF, the signal showing the correlation of the two seismograms. With the Green's functions from many pairs of receivers, tomographic studies are conducted to image volumes of high and low-velocity zones; low-velocity zones are often interpreted as magma chambers in volcanic systems, as in Masterlark et al. (2010).

Cross-correlation functions are also used in interferometry studies. In this case changes in the arrival time of well correlated signal, as in Figure 1.2, are computed. These variations can be interpreted as changes in velocity structure over time through the studied time period based on the relationship, $\Delta t/t = -\Delta v/v$, (Minato et al., 2012).

Changes in arrival time of the Green's function indicate changes in structure; at a volcano this could be due to magma and/or gas migration.

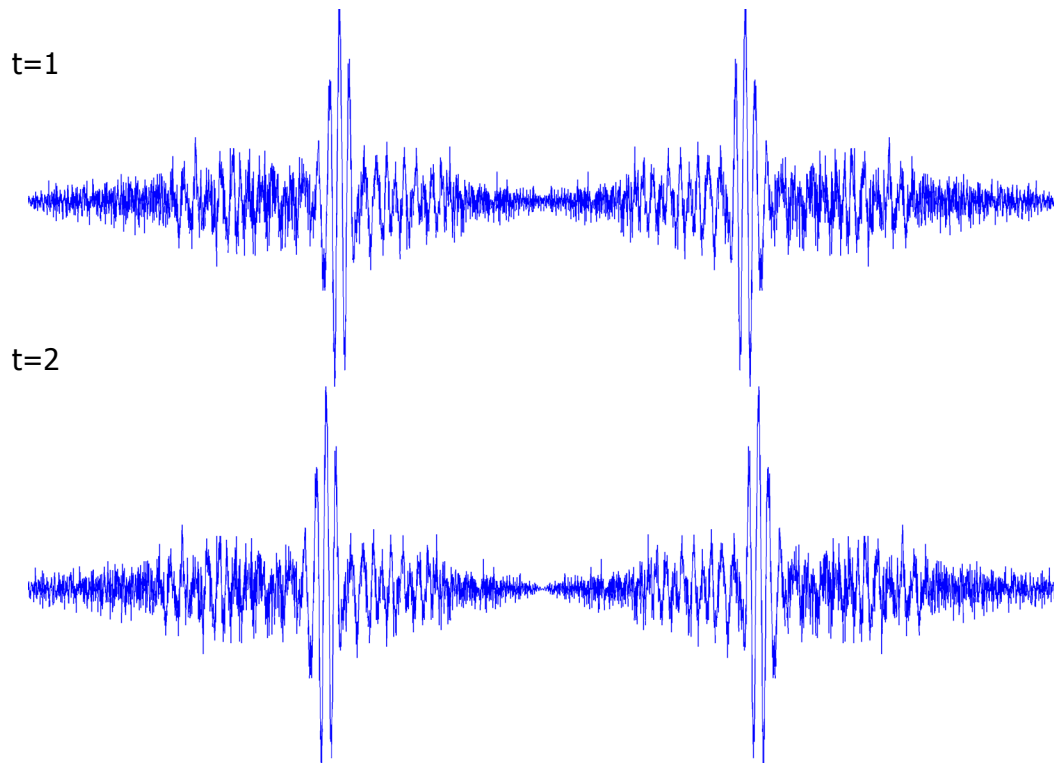


Figure 1.2 Cross-correlation functions from two time periods showing an increase in arrival time of prominent signal.

In this study, we employ the method used by Minato et al. (2012) to measure the changes in the CCFs and auto-correlation functions (ACFs), described next. For this method a CCF is cross-correlated with a reference CCF. To describe this method the first CCF from Figure 1.2 at $t=1$ is the reference, referred to as such, and the CCF at $t=2$ will be compared to it, referred to as CCF. First, the CCF is stretched and shrunk to various percentages, then each of those are cross-correlated with the reference. The percentage to which it is stretched is $\Delta t/t$. In the example, if the CCF is positively stretched the cross-correlation with the reference would decrease, whereas if the CCF is negatively stretched (shrunk), then the cross-correlation would increase. Since $\Delta t/t$ is inversely related to $\Delta v/v$ an increase in $\Delta t/t$ results in a decrease in $\Delta v/v$. Based on $\Delta t/t = -\Delta v/v$ and $v = d/t$, an increase (decrease) in $\Delta t/t$ could be due to a change in the subsurface properties that would decrease (increase) $\Delta v/v$, such a heating (cooling) of rock or opening (closing) micro-cracks. The $\Delta t/t$ could also change due to a change in the distance the wave travels such that an increase (decrease) in the distance would increase (decrease) $\Delta t/t$.

Auto-correlation, correlating a seismogram with itself, can also be used to study structure and also changes in the medium over time. The auto-correlation of ambient seismic noise produces an approximation to the seismic record from a source at the surface and reflected off layers within the earth. For example, if we auto-correlate a

vertical channel, we get an approximation of the vertical record of a vertical source at the surface at the location of the station. Thus, the area to which the auto-correlation is sensitive is the subsurface around the sensor as opposed to between two sensors. Similarly, we can correlate an east channel with a vertical or north with east, etc., to estimate other components. The time in the ACF is two-way travel time compared to the travel time from sensor A to sensor B in the CCF. ACFs have strong correlation at time zero, whereas CCFs have stronger correlation at positive and negative time lag as long as the stations are separated by more than a wavelength. Due to the strong correlation at time zero, changes in ACF are tracked from a time greater than zero. Also, ACFs are symmetric about zero time but cross-correlations may not be if the noise is not randomly scattered. What makes this potentially valuable for volcano monitoring is the ability to detect very small changes in the velocity structure through variations in the delay times for different features in the auto- (or cross-) correlations.

This study, like the others mentioned, relies on Green's function (GF),

$$G(x_A, x_B, t) = \Re \left(\sum_n \frac{\phi_n(x_A)\phi_n(x_B)}{-i\omega_n} e^{-i\omega_n t} \right), \quad (1)$$

(where x_A and x_B are locations, t is time, ϕ_n are eigenfunctions, and ω_n are eigenfrequencies (Campillo, 2006)), which is the response from an impulsive point source (Snieder and Wapenaar, 2010). It has been shown that in a diffuse wavefield cross- (and auto-) correlation of ambient seismic noise between points A and B,

$$C_{AB}(\tau) = \frac{1}{T} \int_0^T \langle v(x_A, t + \tau) v(x_B, t) \rangle dt, \quad (2)$$

where τ is lag time and T is the integration time (Snieder and Wapenaar, 2010) yields the same GF which would be gleaned at A if B were a receiver (Gou  ard et al., 2008; Sabra et al., 2006; Shapiro and Campillo, 2004; Shen et al., 2012; Wapenaar et al., 2005; Weaver, 2005). The extraction of GF from cross-correlation extends beyond seismology, but within the field it has enabled imaging of magma chambers (Bren  guier et al., 2007; Chaput et al., 2012), observation of subsurface velocity changes (Bren  guier et al., 2011), and more.

Here, we use the GF calculated from auto- and cross-correlations of seismic ambient noise to observe temporal changes in the subsurface of Villarrica volcano. Villarrica, located in the southern Andes of Chile, is an alpine glaciated stratovolcano with strombolian activity (Curilem et al., 2009; Ortiz et al., 2003; Palma et al., 2008; Witter et al., 2004). Through this work we observed short and long-term temporal changes and discuss likely sources for them, which include seasonal snow loading (Christiansen et al., 2005; Heki, 2003; Sens-Sch  nfelder and Wegler, 2006), regional earthquakes (Battaglia et al., 2012; Hill et al., 2002; Manga and Brodsky, 2006) and volcanic activity (Duputel et al., 2009).

2 Background

Villarrica (Chile) is an active stratovolcano located in the southern Andes (39.42°S, 71.93°W) in the sub-volcanic chain Villarrica-Quetrupillán-Lanín (VQL) (Curilem et al., 2009; Ortiz et al., 2003; Palma et al., 2008; Witter et al., 2004), which runs NW-SE and obliquely intersects the regional Liquiñe-Ofqui Fault Zone. Today, Villarrica (2847masl) is a symmetrical cone with a summit crater and lava lake situated on the northwest side of the late Pleistocene formed elliptical caldera (Palma et al., 2008). Recent eruptive activity at Villarrica has been strombolian, while the historic record also includes hawaiian, phreatomagmatic, and vulcanian (Ortiz et al., 2003). Prehistoric eruption intensities ranged from hawaiian to plinian (VEI 0 – 6). According to Ortiz et al. (2003) Villarrica is comprised of basaltic to basaltic-andesitic lava and pyroclasts.

Since the eruption in 1984-1985, seismic activity at Villarrica has been dominated by tremor associated with persistent magmatic degassing and some long-period events (Palma et al., 2008). Palma et al. (2008) found the concentration of seismic energy to range from 1 to 7.2Hz; similarly Ripepe et al. (2010) found the spectra of the tremor to focus around the 0.6 – 3Hz and 5 – 10Hz bands. While they constitute less than 10% of the seismic energy, volcano-tectonic earthquakes, hybrid signals, and explosion events are present (Palma et al., 2008).



Figure 2.1 Villarrica Volcano with plume from degassing (Taken: March 4, 2011)

3 Methods & Analysis

3.1 Data Collection

In 2010, eight seismic stations, V01 to V08, were installed around Villarrica volcano, Chile in a circular array with one located at the summit, see Figure 3.1. The following year two stations were removed: V05 and V07. Güralp 30 second CMG 40T 3-component, broadband sensors were used in 2010, while CMG 3T ESPc 60 second and L22 2Hz sensors were used in 2011. Both campaigns used RefTek 130 data acquisition systems (DAS) to sample data at 50Hz. Data were collected from late March to early November 2010 and late February to late April 2011, Table 3.1.1 and Table 3.1.2 respectively. In 2010 stations V02 and V06 experienced clock timing problems and the DAS at V04 failed after day 119. From the 2010 to 2011 campaign, the sensors were changed because the CMG 40T sensors were no longer available.

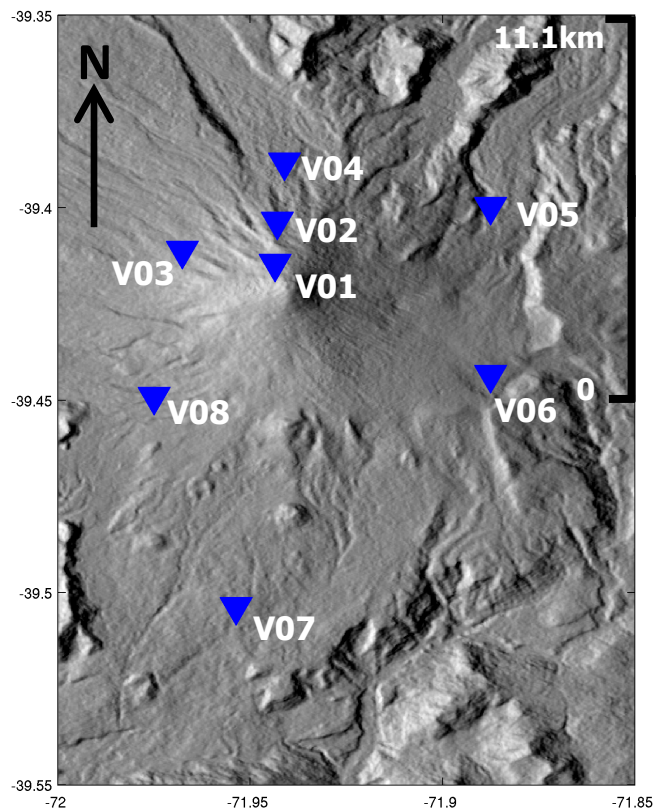


Figure 3.1 Villarrica hill-shade with stations V01 through V08

Table 3.1.1 2010 Station names, sensor type, dates used in Julian Days, and latitude/longitude

Station	Sensor	Start used	End used	Latitude	Longitude
V01	40T	96	188	-39.414490	-71.943470
V02	40T	98	261	-39.403638	-71.942937
V03	40T	94	262	-39.411170	-71.967570
V04	40T	100	119	-39.388206	-71.941100
V05	40T	94	182	-39.399740	-71.887450
V06	40T	100	300	-39.443460	-71.887450
V07	40T	99	300	-39.503680	-71.953631
V08	40T	98	283	-39.449160	-71.974960

Table 3.1.2 2011 Station names, sensor type, dates used in Julian Days, and latitude/longitude

Station	Sensor	Start used	End used	Latitude	Longitude
V01	L22	71	78	-39.414490	-71.943470
V02	ESPc	58	72	-39.403638	-71.942937
V03	ESPc	53	72	-39.411170	-71.967570
V04	L22	53	71	-39.388206	-71.941100
V06	L22	62	99	-39.443460	-71.887450
V08	L22	55	110	-39.449160	-71.974960

3.2 Preparation of Data

The data were prepared in concurrence with other similar studies (Bensen et al., 2007; Masterlark et al., 2010) to reduce the effects of transient events (e.g. earthquakes) and enhance the ambient noise. The data were prepared by first de-convolving the instrument response for each station in order to compare data collected with different instruments. The 40T, ESPc and L22 sensors used have sensitivities of approximately 800V/m/s, 1500V/m/s, and 88V/m/s, respectively. Then the traces were broadband filtered between 32 seconds and 24Hz and the means were removed. We temporally normalized the data using the running root mean square (RMS) normalization method with a 10 second window in order to prevent high amplitude signal from dominating the ambient noise. As discussed by Masterlark et al. (2010), we also found the running RMS normalization to be better than bit (Brennguier et al., 2007) or absolute mean normalization (Bensen et al., 2007). After normalizing in the time domain, we whitened in the frequency domain by first using a Butterworth filter from 1 to 10Hz and then normalized the spectra with a Hanning window of 1000 samples (20 seconds). Different window lengths were tried, but none gave as clear an image of the data as the 20 second window. As a quality control measure we filtered out noise with wavelengths greater than the interstation distance hence the low corner of 1Hz. The station pair distance ranges from 1.2km to 12.9km.

3.3 Auto and Cross Correlation and Stacking

Hour long, vertical, east and north channel auto-correlations were performed for all eight stations, but cross-correlations were only conducted between stations V01, V03, V05, V07 and V08 with the 2010 data. That year stations V02 and V06 had GPS clock errors and the DAS at V04 failed after Julian day 119. We used a maximum lag time of 20 seconds and 10 seconds for the auto- and cross correlations, respectively. For the 2011 data, only auto-correlations were processed, because the dataset was not as extensive and the periods in which the stations ran, on average, did not overlap for more than 15 days. The lag time was reduced to 10 seconds. The hour long correlation functions (CF) were then stacked by day and total time to observe temporal changes and improve signal to noise ratio. Figure 3.2 shows the daily cross correlation functions (CCF) between stations V01 and V03 with the total stack and Figure 3.3 through Figure 3.5 are examples of the auto-correlation functions (ACF) for station V01 with its corresponding total stack for the vertical, east and north channels.

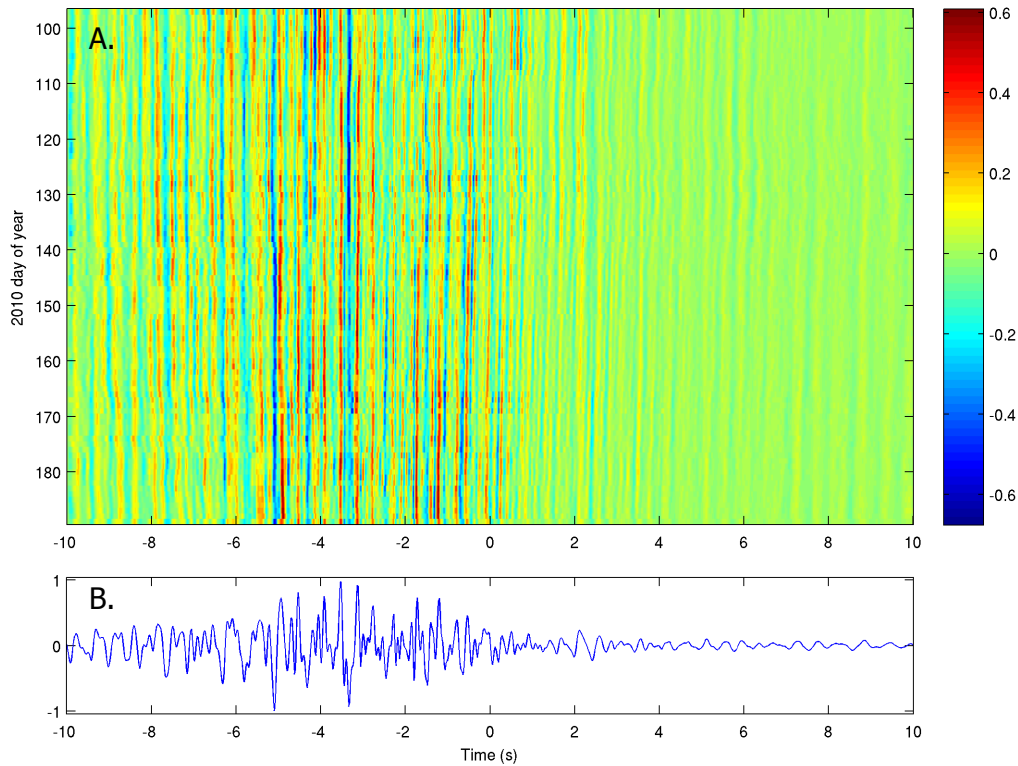


Figure 3.2 Station V01 to V03 2010 CCFs and total stack, A. Daily stacks of CCFs where red is positive correlation and blue is negative to the degree indicated in color bar to right, B. is the total stack of CCFs normalized by the number of CCFs. Positive time (+lag) is the CCF from V03 to V01 and negative time (-lag) is the CCF from V01 to V03.

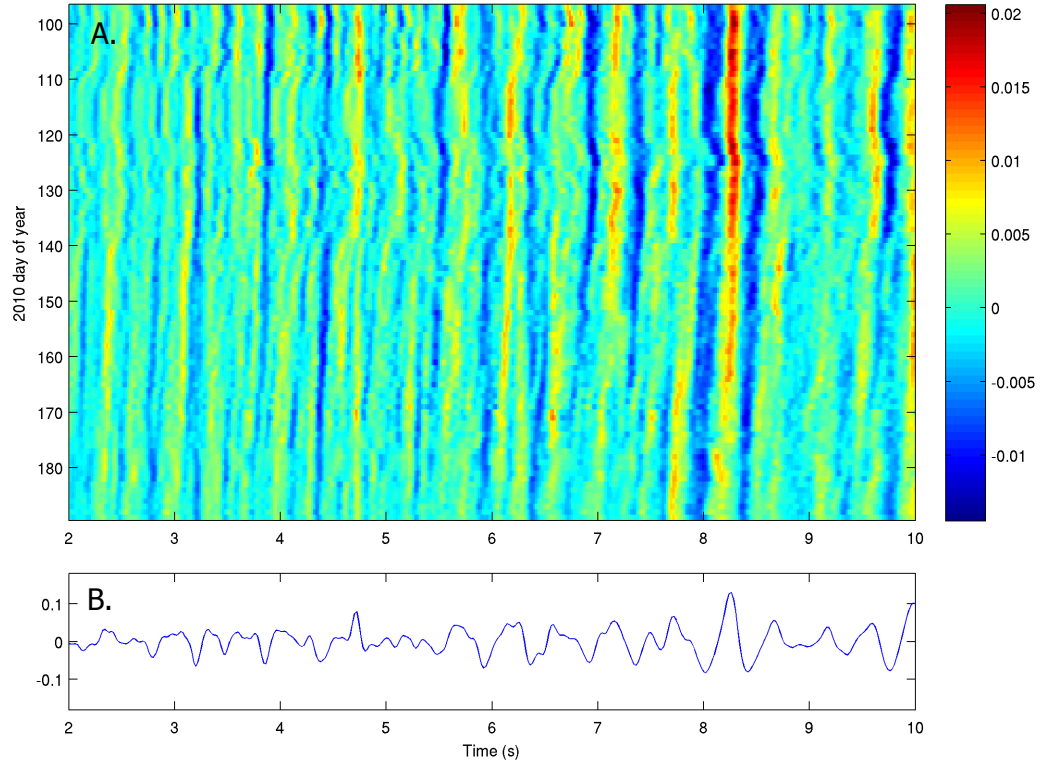


Figure 3.3 Station V01 2010 vertical channel ACFs and total stack, A. Daily stacks of ACFs where red is positive correlation and blue is negative to the degree indicated in color bar to right, B. is the total stack of ACFs normalized by the number of ACFs. Here only positive time (+lag) from 2 to 10 seconds of the ACF is displayed because the time lag closer to zero is dominated by the positive correlation at zero and negative time (-lag) is the mirror image of +lag.

For the auto-correlations we examined the positive lag from 2 to 10 seconds, because the ACF is symmetrical about zero lag and below 2s is dominated by maximum correlation at time zero. In visual review of the daily and weekly stacks of ACFs, we observed long and short term temporal changes in the 2010 array; stations V01, V02, V03, V04, V06 and V08 had visible decreases in arrival time, an example is shown in Figure 3.3. This decrease in arrival time is also present in the east and north channels. The 2011 ACF dataset shows little to no change in arrival time, Figure 3.6. As a quantitative assessment of the changes, the stretching technique used by Minato et al. (2012) was employed and will be discussed in the next section.

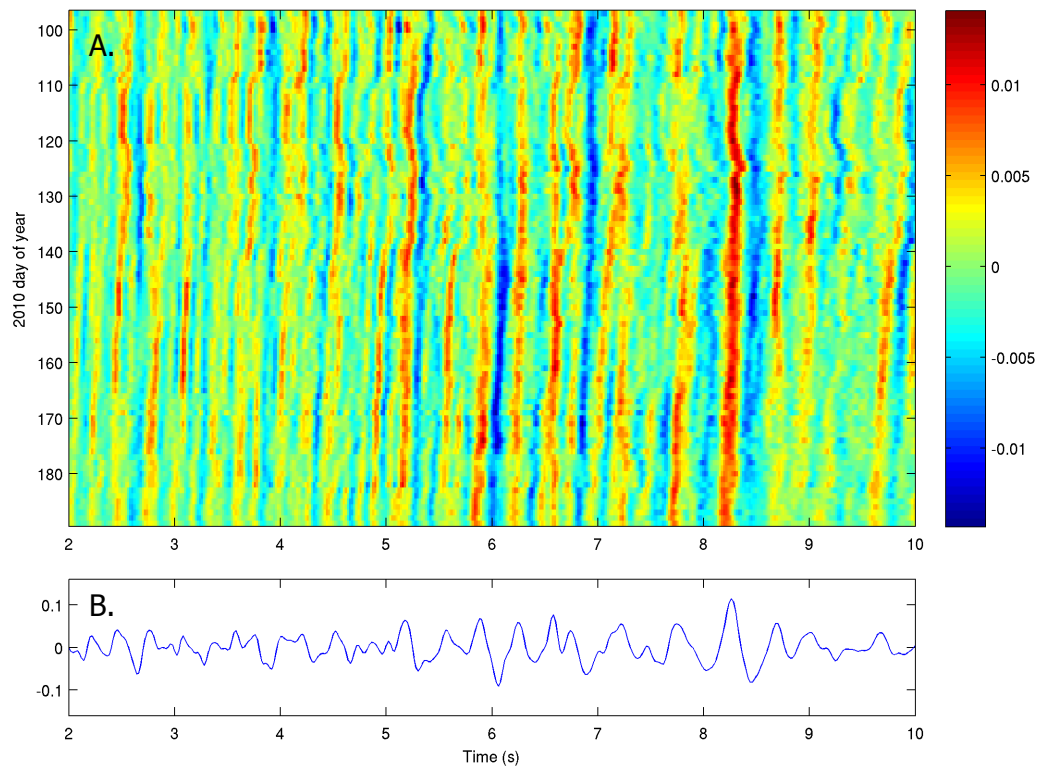


Figure 3.4 A. Station V01 east channel ACF and B. normalized total stack

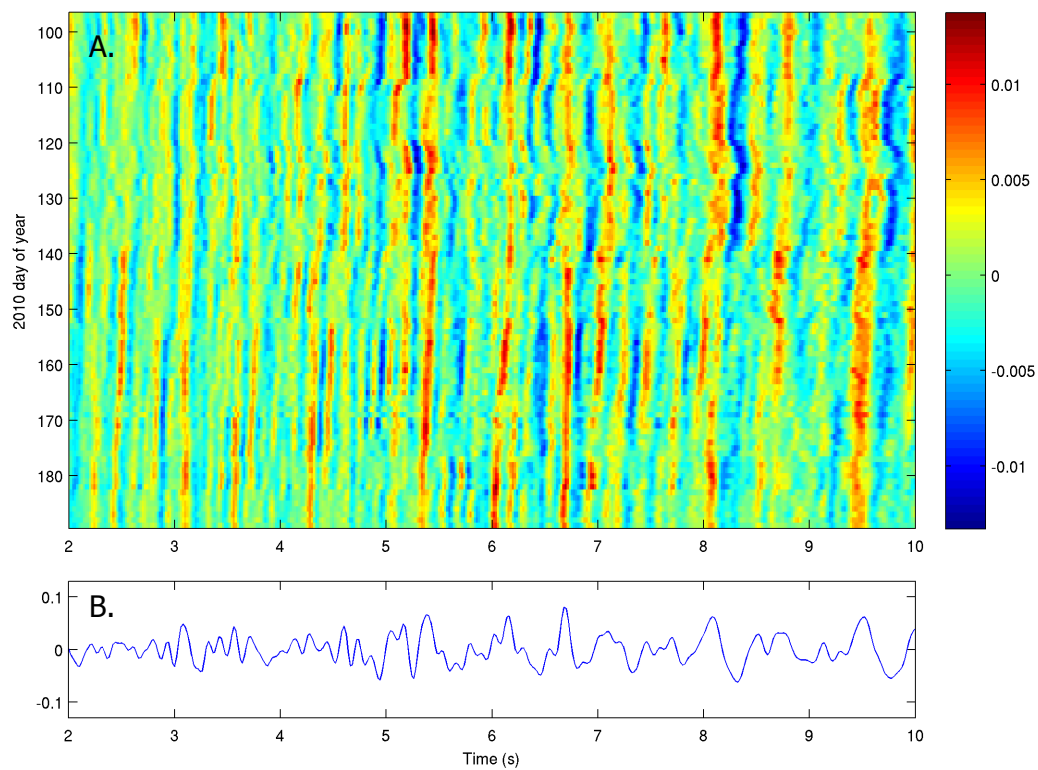


Figure 3.5 A. Station V01 north channel ACF and B. normalized total stack

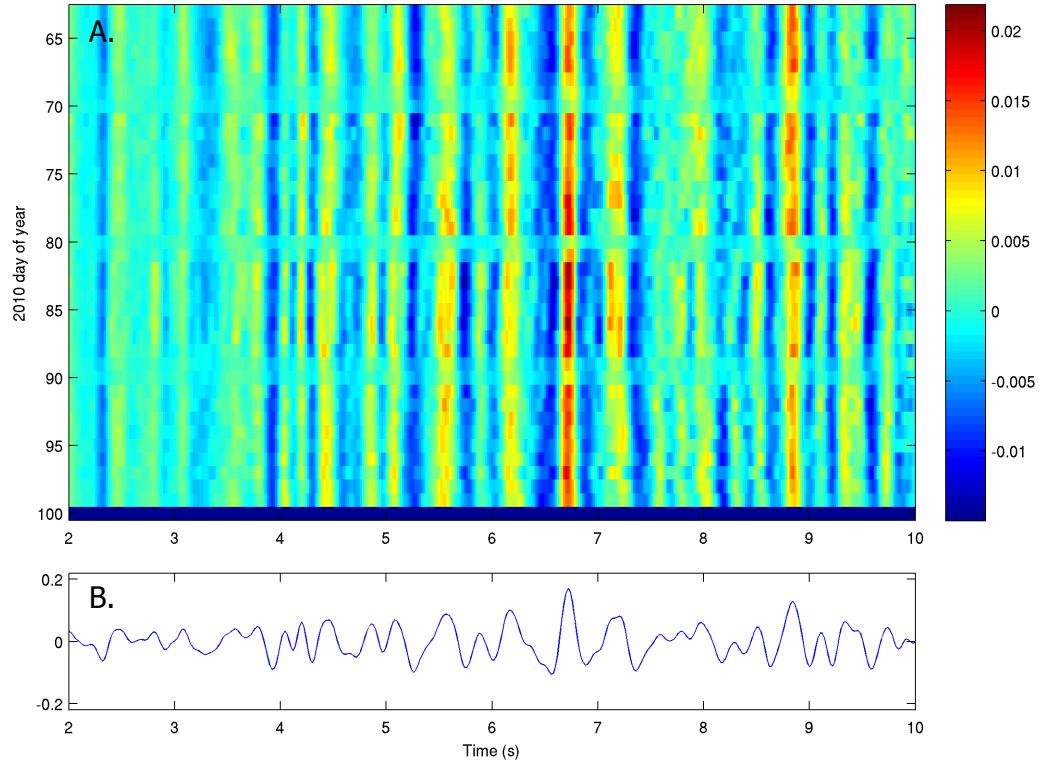


Figure 3.6 A. Station V06 2011 ACFs stacked daily and B. normalized total stack

Our catalog of CCFs is limited due to GPS clock errors at stations V02 and V06 and the failure of the DAS at V04. Ten vertical-to-vertical channels and 4 vertical-to-radial channel station pairs were cross-correlated. The vertical-to-radial channel cross-correlations were conducted to check that the vertical-to-vertical channel correlation findings were believable. More vertical-to-radial CCFs or the inverses were not cross-correlated because there was no new information provided by the 4 conducted. The comparison of Figure 3.2 and Figure 3.7 shows that the stacked CCFs from the vertical channels of V01 to V03 and the vertical to radial channels of the same station pair have little difference between them. The common trends among the CCFs are gradual decreasing in arrival time, short term excursions from the general trend and asymmetrical CCFs. The temporal changes are quantitatively accessed using the stretching method described in section 3.4. The cross-correlations from station V01 to V03, V05, V07 and V08 are heavily weighted in the negative lag time, as in Figure 3.8. Figure 3.8 and Figure 3.9 show the ten vertical to vertical channels, stacked cross-correlation functions and the asymmetry in all the station pairs. As an example, in comparison of the correlations computed between station V01 and others and station V07 and others it is apparent that in the first case the CCFs are weighted in the negative lag while in the second they are weighted in the positive lag. Station V01 is the closest to the vent and V07 is farthest. Therefore, if the first station is closer to the vent then the CCF will be weighted in the negative lag and vice versa. With Villarrica as a dominant local source of seismic noise and without a heavily scattering medium, the volcanic noise dominated the signal and explains the asymmetry to the CCFs.

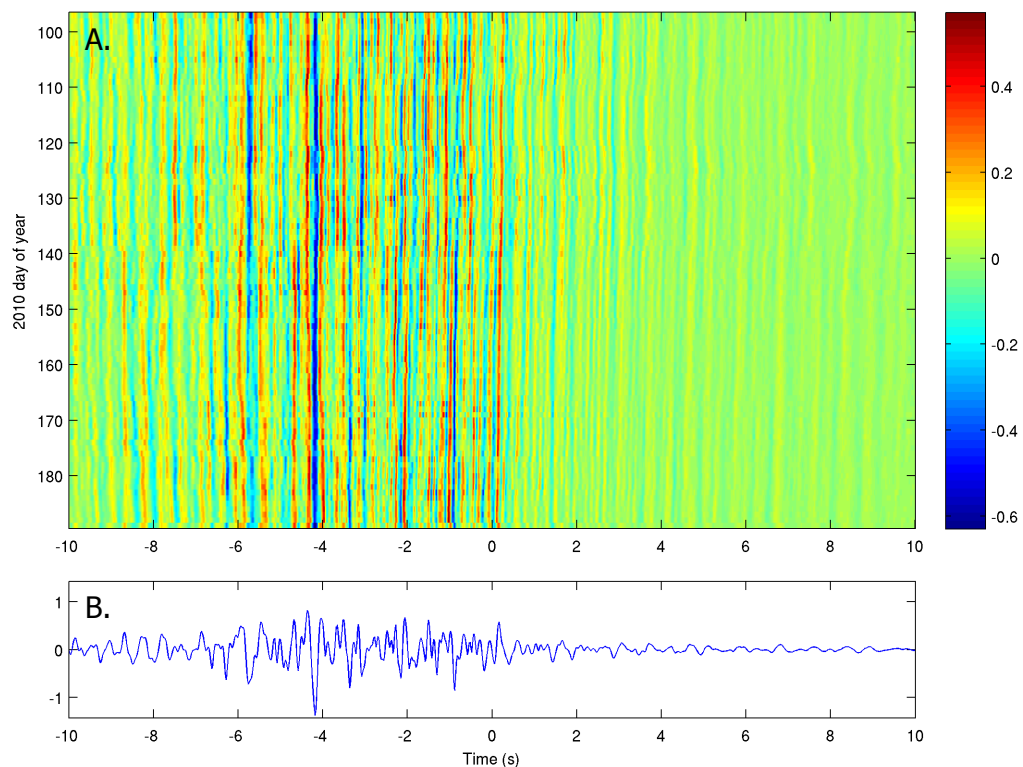


Figure 3.7 CCFs from V01Z to V03R, daily stacks and normalized total stack

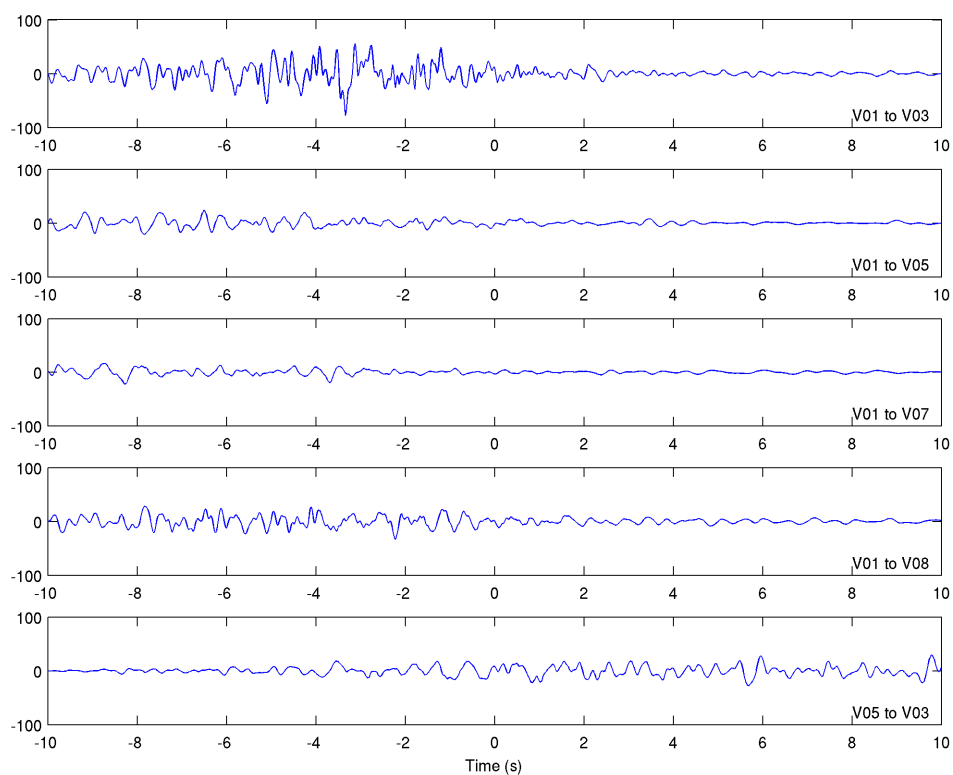


Figure 3.8 Vertical to vertical channel cross-correlation total stacks

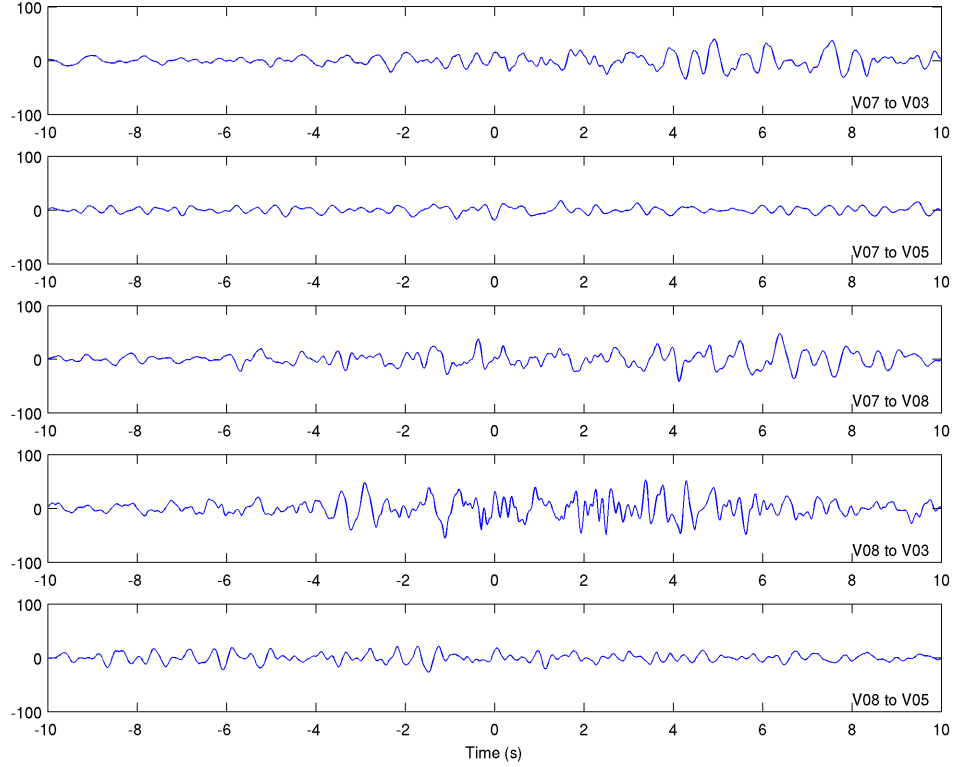


Figure 3.9 Vertical to vertical channel cross-correlation total stacks continued

3.4 Stretching

In order to measure the temporal variation of the ACFs and CCFs we used a method in which one signal is compressed or elongated and then compared to a reference signal by cross-correlation (Minato et al., 2012). We took 24 hour stacks of CFs, filtered from 1 to 10Hz, and stretched them in increments of 0.1% from 90% to 110% of the original. With these elongated CFs we cross-correlated them against the total stack of CFs and stepped through the dataset by one hour (23 hour overlap) for each station. We found the 24 hour window with a one hour step to smooth the data such that the changes were easily tracked without losing resolution, Figure 3.10 and Figure 3.11. The percentage of stretch that best fit the total stack was recorded. We interpret changes in stretching as changes in velocity (Minato et al., 2012),

$$\epsilon = \frac{\Delta t}{t} = -\frac{\Delta v}{v}, \quad (3)$$

where $\Delta t/t$ is the relative time shift and $\Delta v/v$ is relative velocity change. Positive percent stretching indicates an increase in velocity because the 24 hour window of data had to be lengthened to match the stack, meaning the waves arrived faster than the total. The opposite applies to negative percent stretching. To compare the velocity changes in the CCF and ACF from each station we fit a line to the highest correlating stretching percentage, Figure 3.12.

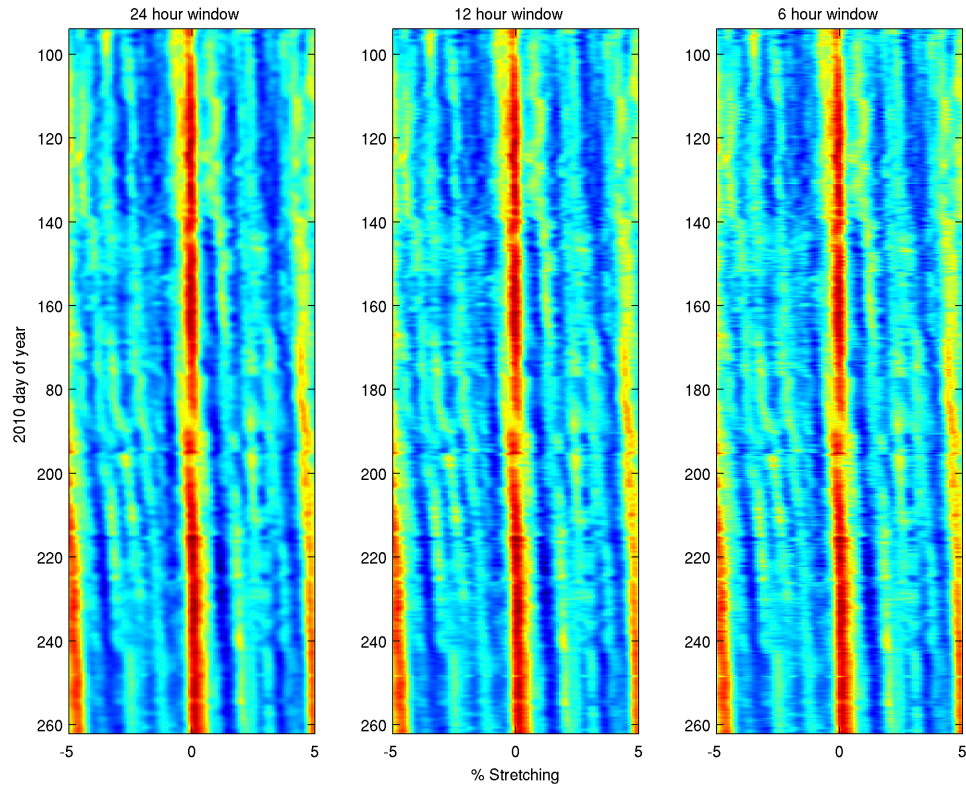


Figure 3.10 Examples of different stretching windows

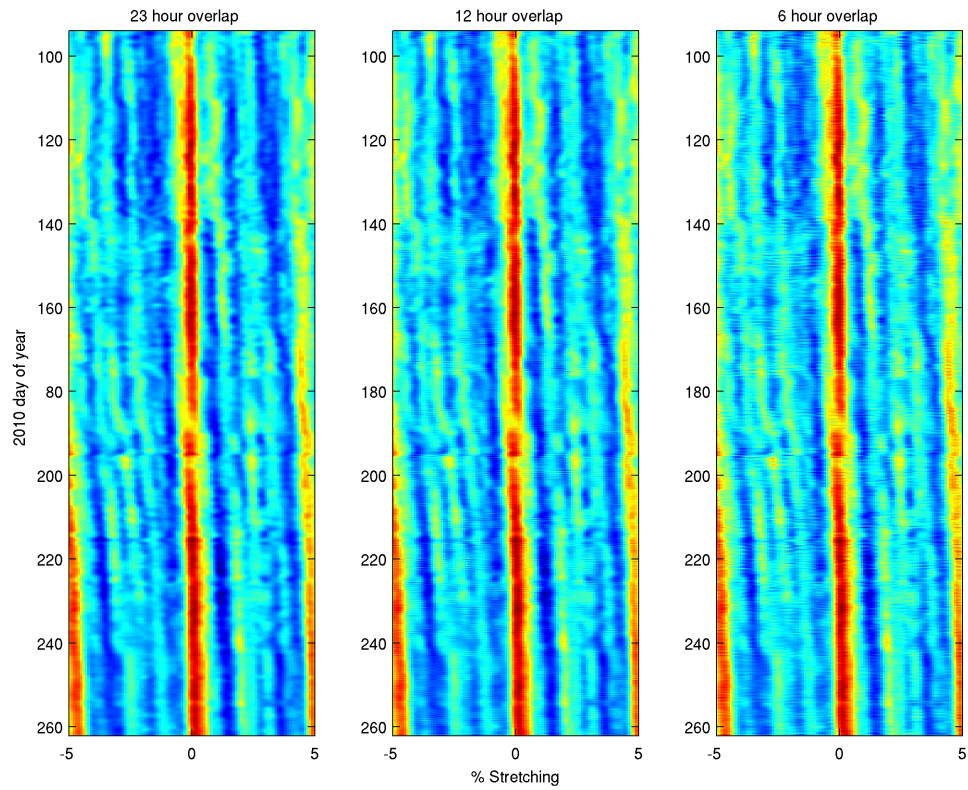


Figure 3.11 Examples of different overlap window

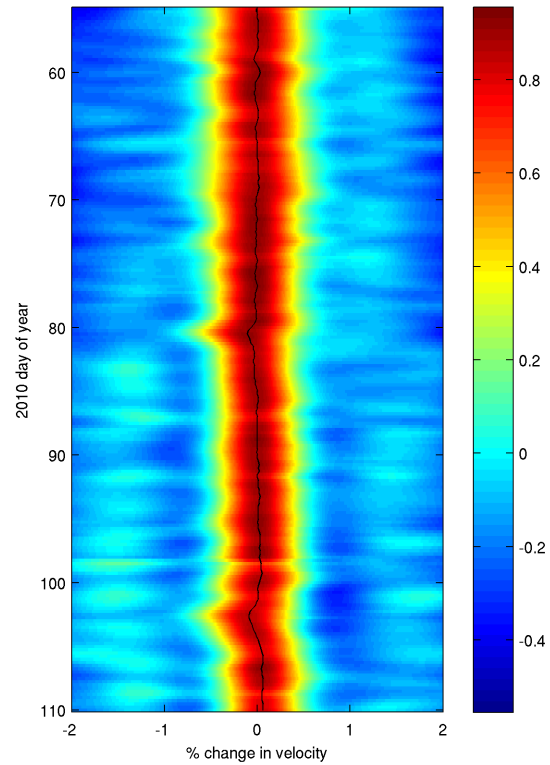


Figure 3.12 Station V08 stretching function with best-fit line

Appendices 7.1, 7.2 and 7.3 are catalogs of figures of the ACFs and CCFs with their corresponding stretching and its best-fit line. Then we plotted the stretching function from each station on a single graph to compare trends. Figure 3.13 to Figure 3.20 show the stretching functions for 2010 ACF vertical, east and north, positive lag CCF, negative lag CCF and 2011 ACF, respectively.

In 2010 the average increase in velocity gleaned from the ACFs, except V04 due its short run time, was 0.13%. The 2011 dataset is less extensive than in 2010 therefore we averaged the percent change in velocity between stations V06 and V08, resulting in 0.09% increase in velocity. In addition to the overall increase in velocity, there are excursions from the trend that are on the same order. In Figure 3.13 two examples are highlighted from 2010 Julian days 102 to 112 and 123 to 126. The magnitude/amplitude of perturbations decreases with distance from the vent as is seen with stations V06 and V07, which suggests short-term velocity changes at Villarrica are volcanic in origin. In the stretching functions for the CCFs in Figure 3.16 to Figure 3.19, the same excursions are present that are in the ACFs. The 2011 stretching functions also have short-term velocity changes that show up on multiple stations and decrease with distance from the edifice, as seen in Figure 3.20.

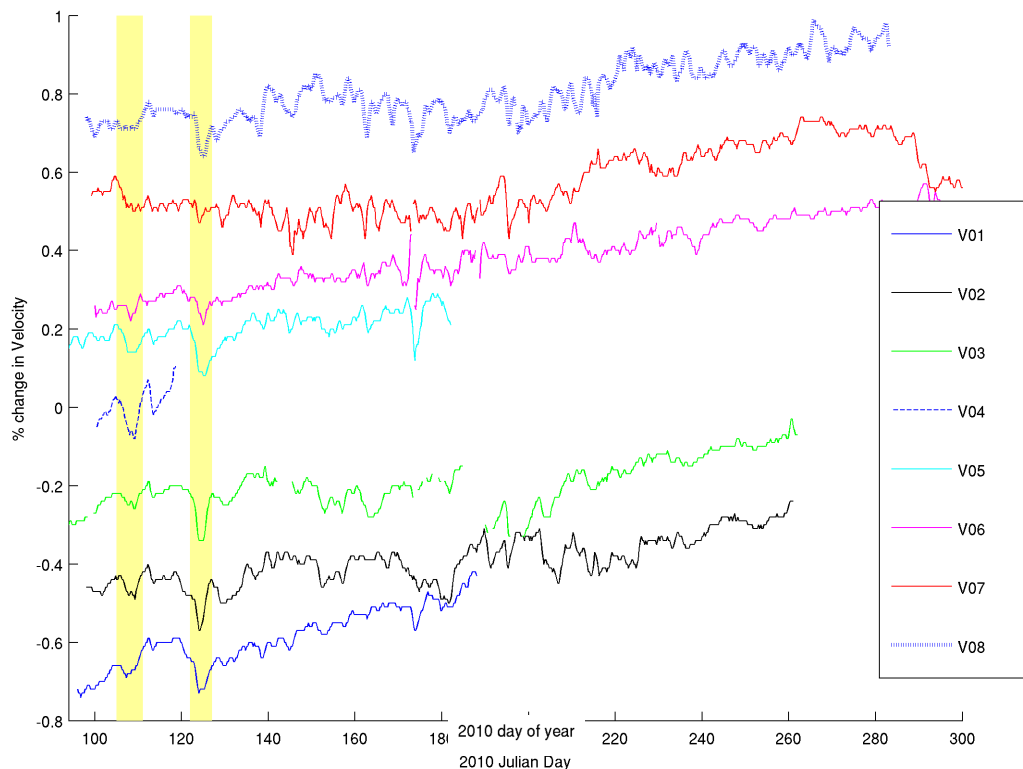


Figure 3.13 2010 ACF vertical channel velocity changes

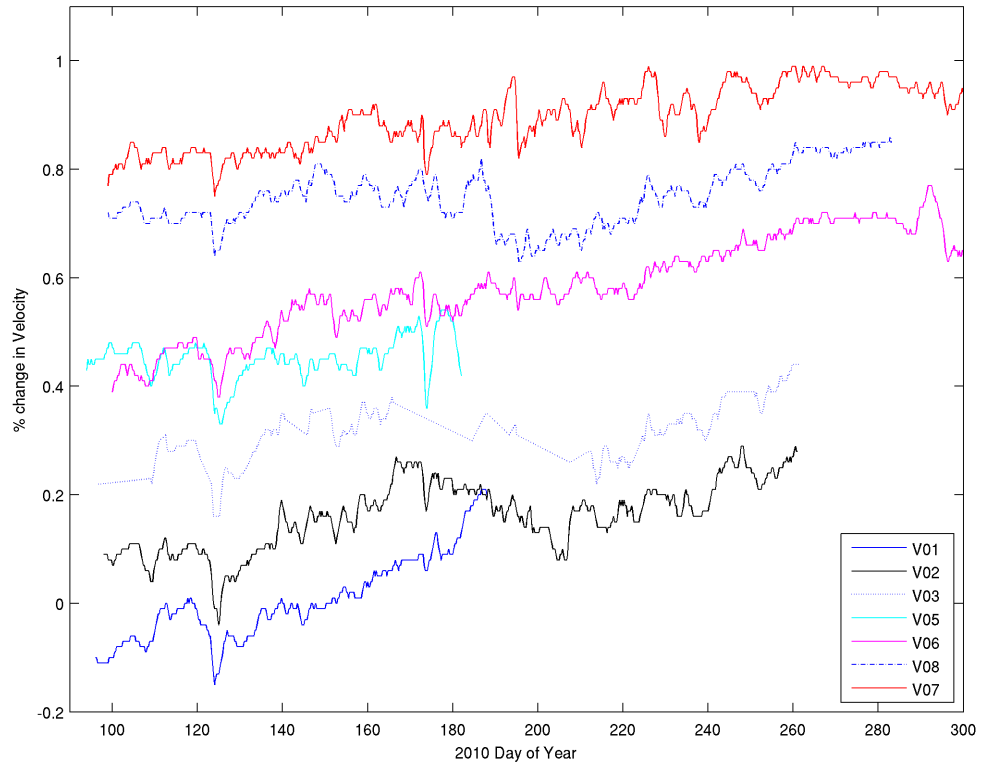


Figure 3.14 2010 ACF east channel velocity changes

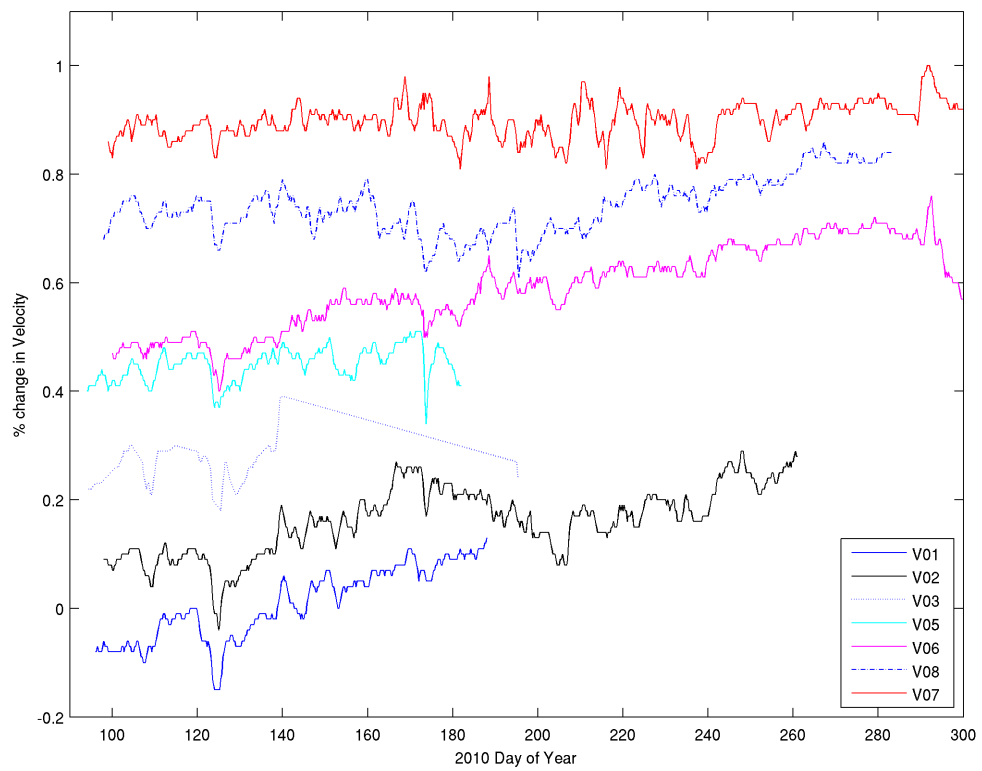


Figure 3.15 2010 ACF north channel velocity changes

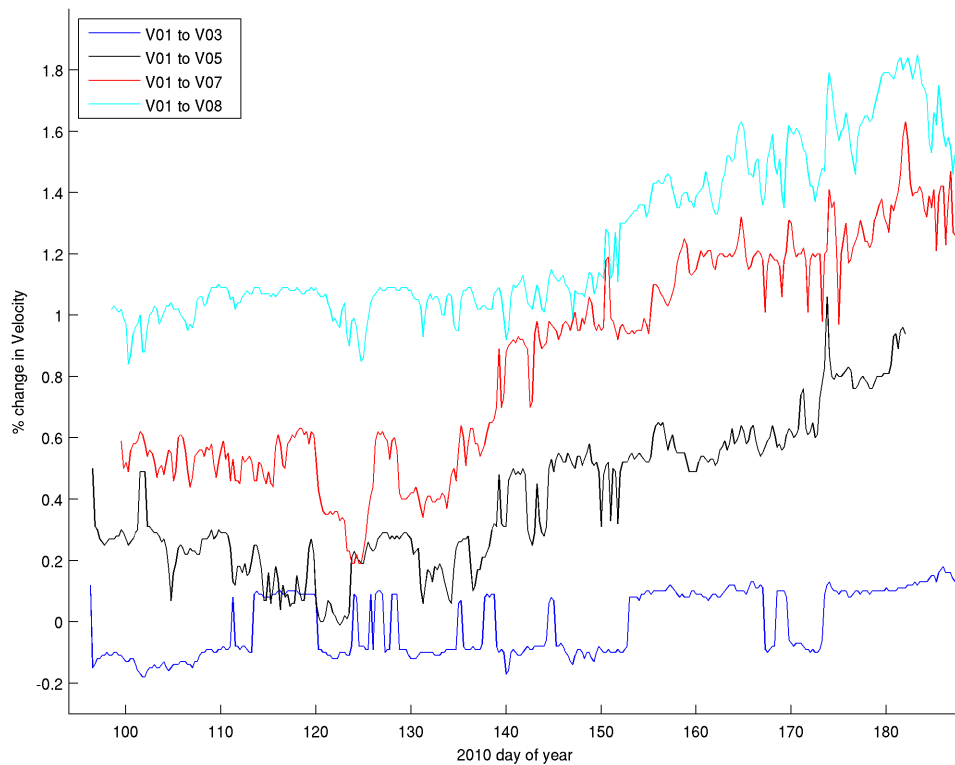


Figure 3.16 2010 CCF velocity changes from the negative lag for station pairs V01 to V03, V05, V07 and V08

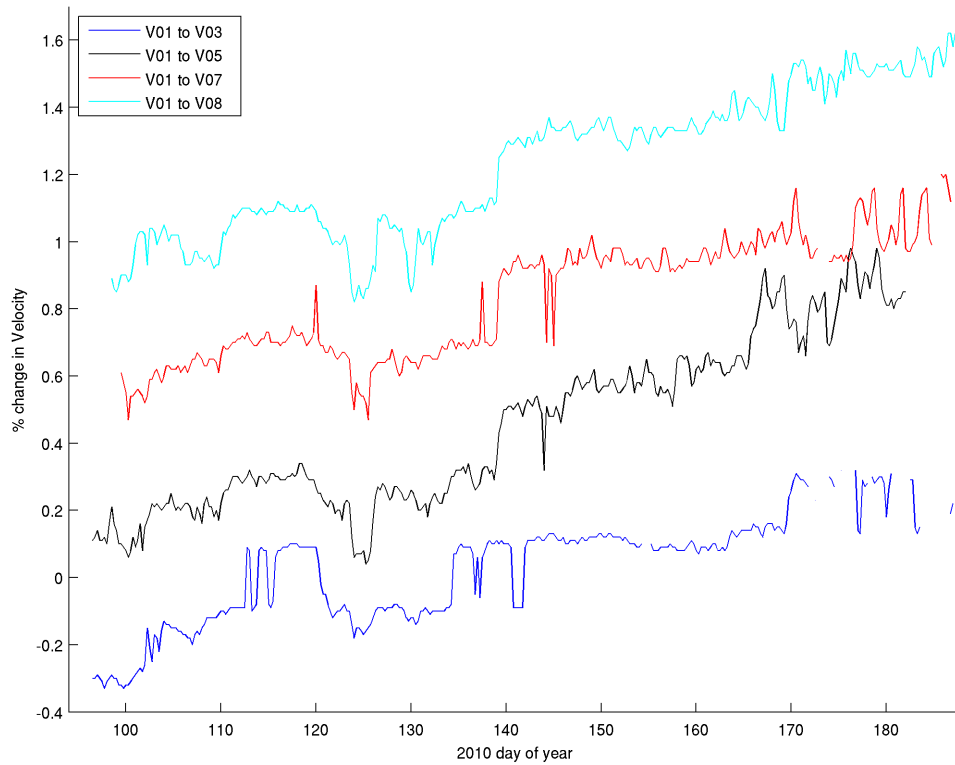


Figure 3.17 2010 CCF velocity changes from the positive lag for station pairs V01 to V03, V05, V07 and V08

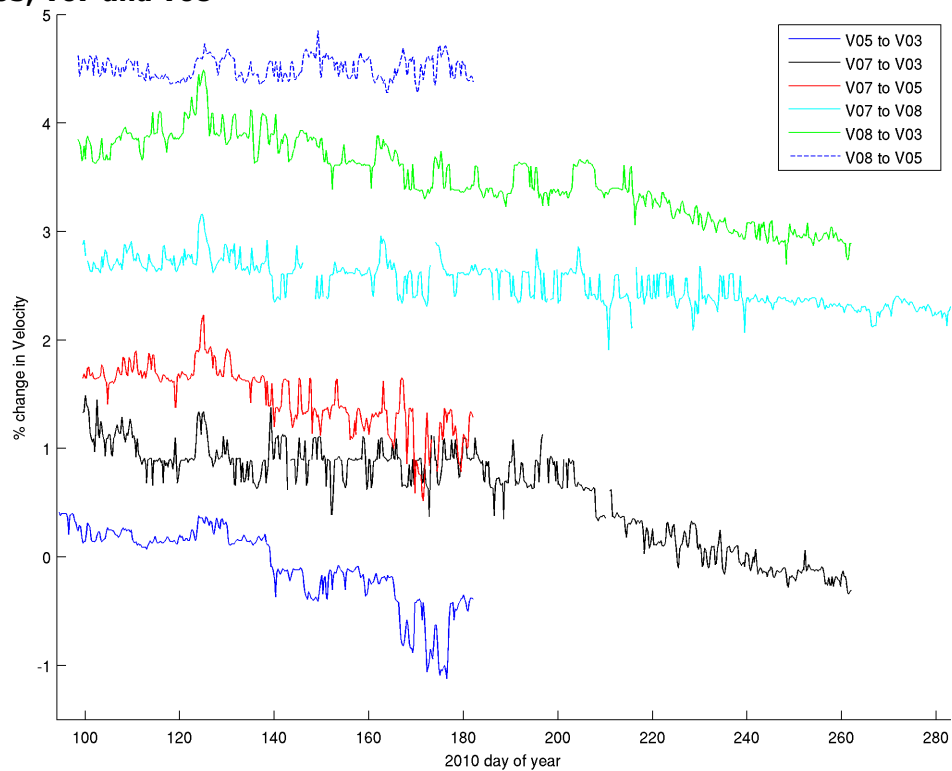


Figure 3.18 2010 CCF velocity changes from the negative lag for station pairs V05 to V03, V07 to V03, V05 and V08, and V08 to V03 and V05

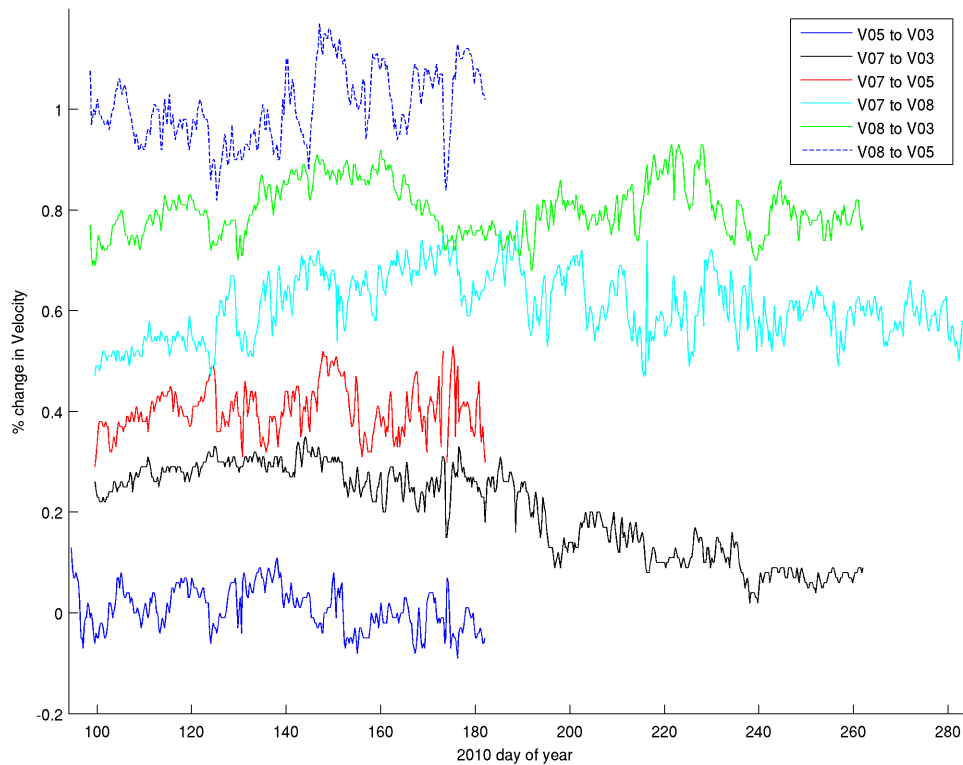


Figure 3.19 2010 CCF velocity changes from the positive lag for station pairs V05 to V03, V07 to V03, V05 and V08, and V08 to V03 and V05

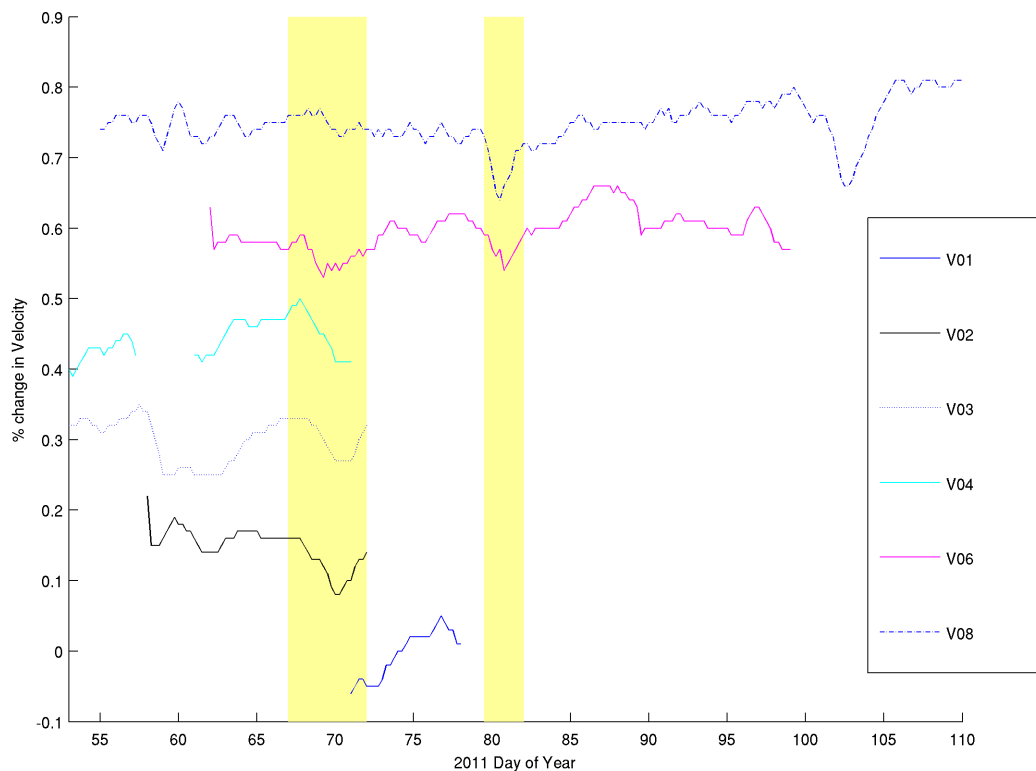


Figure 3.20 2011 ACF velocity changes from the vertical channel

4 Discussion

Through the two datasets we observe short-term and long-term velocity changes; here we discuss possible causes of these perturbations. Likely sources are seasonal snow loading and unloading, regional earthquakes, and activity at the volcano. We also include a discussion of applying the observation of velocity changes as a volcano monitoring tool.

4.1 Seasonal Variations

Recent studies show links between the change in snow load with the resulting shift in ground water level (GWL) and changes in frequency of earthquakes and in velocity. With passive image interferometry Sens-Schönfelder and Wegler (2006) observed $\sim 2\%$ decreases (increases) in velocity over a four (six) month period which correlates with the increase (decrease) in GWL through the rainy (dry) season at Merapi volcano. Christiansen et al. (2005) found increased seismic activity at Mt. St. Helens, Yellowstone and other volcanoes in the United States from a reduction in effective stress due to unloading of snow and the subsequent increase in GWL. In a similar study, Heki (2003) discerned increased occurrences of large earthquakes through the north-south, central backbone of Japan after snow unloading which decreases effective stress. In parallel, Palma et al. (2008) observed increased seismic activity at Villarrica after the snow melt. Figure 4.1 shows the percent velocity changes observed at each station at Villarrica from April through October 2010, an average increase of 0.13%. We attribute this velocity increase to snow loading over the winter months, which is comparable to changes observed at Merapi.

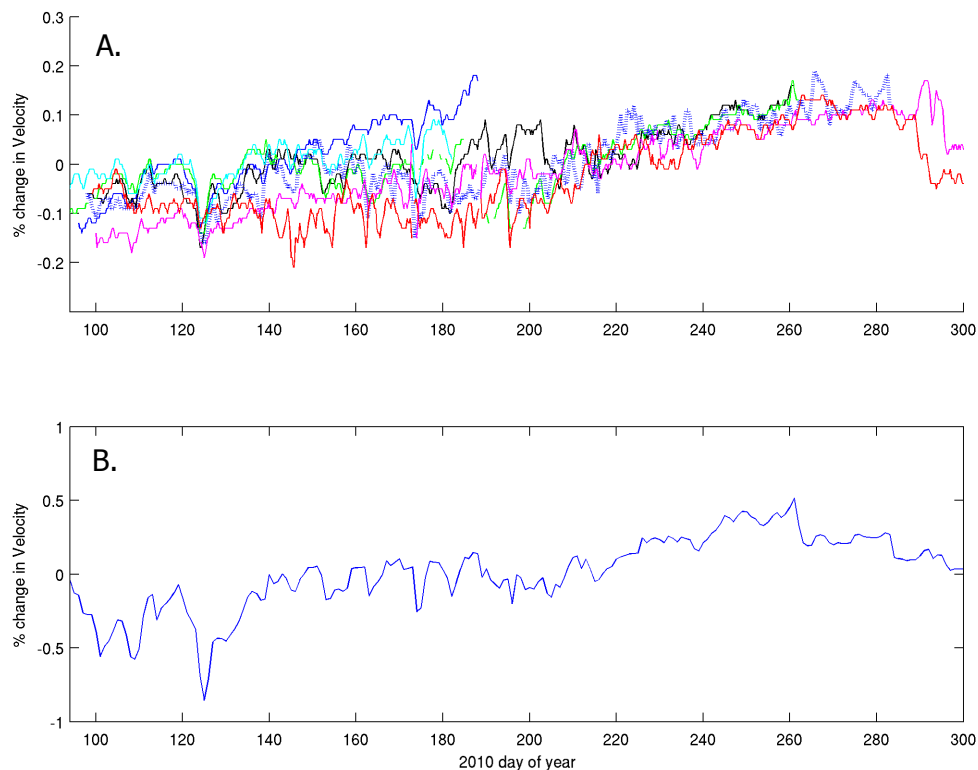


Figure 4.1 A. 2010 velocity changes and B. total stack of 2010 velocity changes

An approximate snow load was calculated as 10.9kPa based on an estimated thickness of 3m and an alpine snow density of 370kg/m^3 (Alford, 1967). We calculated the effective stress at depth to be 4.73kPa which is based on the equations used and falls within the range found by Christiansen et al. (2005). The time periods over which our data were collected are the late summer through the winter and the late summer to early fall, 2010 and 2011 respectively; in turn we do not incorporate ground water recharge, which occurs during the spring snow melt.

Meier et al. (2010) note that velocity changes can be attributed not only to changes in the stress field and water saturation, but also temperature variation. They attribute the seasonal seismic velocity variation in the Los Angeles basin to be caused by the thermo-elastic strain resulting from temperature change after comparing their findings to GPS and temperature modeling by Prawirodirdjo et al. (2006). This is plausible for the long-term velocity variation we see at Villarrica especially since our percent change in velocity, 0.13%, is on the same order as theirs, 0.125%. In considering thermo-elastic strain as the source for the velocity changes, we expect there to be a time lag to allow the seasonal temperature change to reach seismogenic depths. With a seasonal snow load, however, the stress changes are instantaneous with the start of snow fall, which is more in line with our data.

4.2 Regional Tectonics

In addition to the long-term apparent increase in velocity described above, we also observe short-term velocity changes, up to a week, that are likely caused by either regional tectonic activity, i.e. earthquakes, or activity from Villarrica; the latter is discussed in section 4.3. Earthquakes can cause static, quasi-static and dynamic stress changes (Hill et al., 2002). Static stress changes in the stress field from before to after an earthquake have been shown to trigger other earthquakes (King et al., 1994; Stein et al., 1997; Stein et al., 1994) and volcanic eruptions (Harris and Ripepe, 2007; Hill et al., 2002; Manga and Brodsky, 2006). There is evidence from Villarrica and other volcanoes that regional earthquakes trigger increased volcano activity observed through MODIS thermal data (Harris and Ripepe, 2007) and SO_2 gas emission (Hansteen et al., 2011).

We find static stress changes from regional earthquakes an unlikely source for the short-term velocity changes found at Villarrica because there are no earthquakes large enough or close enough to affect significant static stress changes. The rapid rate of decay, approximately $1/r^3$, where r is the distance from the epicenter (Hill et al., 2002) of static stress changes means that the effects are insignificant beyond about one or two fault lengths from the source. In addition, the velocity changes we observe are elastic in that they rebound to their starting point in a matter of days. Those described are plastic, such that there is an increase in the relative time shift that does not return to its starting point as Battaglia et al. (2012) found with the interaction of a magnitude 7.3 earthquake and Yasur volcano. Quasi-static stress change is described by Hill et al. (2002) as the "slow viscous relaxation of the lower crust and upper mantle beneath the epicenter of a large earthquake". These effects would not be seen as abrupt changes in the velocity beneath Villarrica unless they were coupled with, or triggered, some other change in the system.

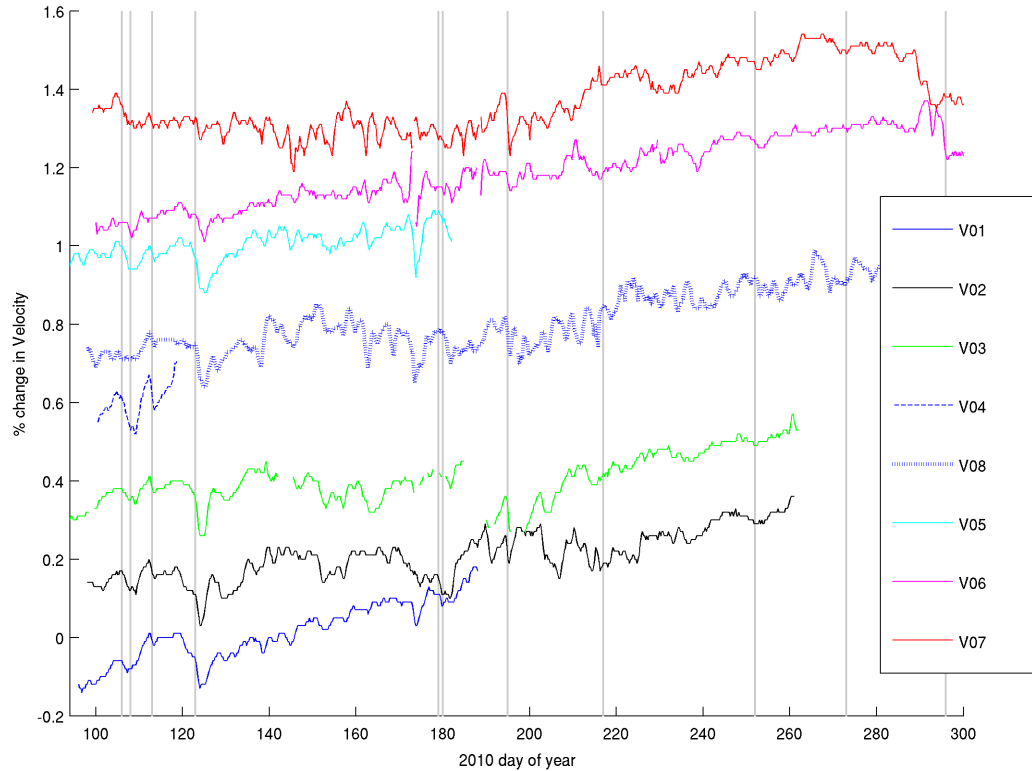


Figure 4.2 2010 Velocity changes with regional earthquakes (gray lines), $6.5 > M > 5.4$

Table 4.2.1 Date, location, depth, magnitude and distance to Villarrica of the earthquakes displayed in Figure 4.2.1

Magnitude	Depth (km)	Time	Julian Day	Latitude	Longitude	distance (km)
5.6	6	04/16/2010 10:41:34 PM	106	-37.460	-73.7320	268.9
5.7	24	04/16/2010 11:15:36 PM	106	-37.420	-73.6690	269.4
5.6	29.9	04/18/2010 01:49:38 AM	108	-37.159	-73.7530	297.8
6	32	04/23/2010 10:03:06 AM	113	-37.529	-72.9690	229.1
6.4	23	05/03/2010 11:09:38 PM	123	-38.271	-74.3090	242.7
6.3	19	05/03/2010 11:09:45 PM	123	-38.072	-73.4540	200.1
5.8	28.2	06/28/2010 12:59:47 AM	179	-37.910	-75.0380	318.1
5.5	17	06/29/2010 01:40:01 AM	180	-37.836	-73.2780	211.7
5.9	22	07/14/2010 08:32:21 AM	195	-38.067	-73.3100	192.5
5.8	35	07/14/2010 03:05:50 PM	195	-38.224	-73.2300	174.5
5.8	18	08/05/2010 06:01:47 AM	217	-37.443	-73.2810	249.6
6.2	16	09/09/2010 07:28:02 AM	252	-37.034	-73.4120	295.5
5.8	37	09/30/2010 12:26:23 AM	273	-36.347	-73.0210	355.2
5.7	15	10/23/2010 05:58:28 AM	296	-37.743	-73.3620	224.4

Dynamic stress change, the change in stress due to body and especially surface waves from an earthquake, affect volcanic systems at greater distances from the epicenter due to their slower rate of decay, $1/r$ (Hill et al., 2002; Manga and Brodsky, 2006). A challenge arises in attributing the observed velocity changes to earthquakes; that is the occurrence of an earthquake near the time of velocity change with a large magnitude, $M \geq 7$. There were not any earthquakes that fit the criterion in the catalog. Figure 4.2 shows the occurrence of regional earthquakes in relation to the velocity changes and Table 4.2.1 provides more detailed information of magnitude, location, and distance from Villarrica, etc. While there is some correlation of events and velocity change, the distance between earthquakes and Villarrica combined with the smaller magnitude suggests that they are not the source. However, the apparent correlation of the two earthquakes, seconds apart, on May 3, 2010, day 123, of magnitudes 6.4 and 6.3 prompts further investigation.

We broadened our search of earthquakes to include all earthquakes of magnitude 6 and greater globally and those of M5.5 to 5.9 within the latitudes of -64.09 and 51.07 and the longitudes -157.15 to 31.82, referred to as regional. Tables of the magnitude, depth, time, location and distance to Villarrica of these earthquakes can be found in Appendix 7.4 2010 Earthquakes and peak surface wave amplitudes. Then we filtered the V07 data between 32 and 12 seconds to highlight the surface waves from the earthquakes and picked their peak amplitudes. Figure 4.3 compares the vertical channel peak surface wave amplitude from V07 with the stacked percent change in velocity. The radial and tangential channels can also be found in Appendix 7.4. Here again the May 3, 2010 earthquakes stand out as positively correlating, which suggests they influence Villarrica. There have been cases in which earthquakes at distances greater than a thousand kilometers have triggered activity in volcanic systems due to directivity, as was observed at Yellowstone and other systems in 2002 from the rupture of the Denali fault, M7.9 (Husen et al., 2004a; Husen et al., 2004b). Since the rupture history is unknown for the faults of the M6.3 and M6.4 earthquakes at 200.1km and 242.7km distance, respectively, we cannot attribute the changes to directivity, but it could be a contributing factor. These earthquakes could have caused this decrease in velocity by shaking the edifice and enabling bubble nucleation. However, the decrease in velocity at day 252 is not on the same order. These differences may be due to a variety of factors such as directivity, distance and fault geometry. The comparison of peak surface wave amplitude and velocity change suggests there are earthquakes that influence the Villarrica volcanic system, but it also leaves open the possibility that the velocity variations are due to activity within Villarrica.

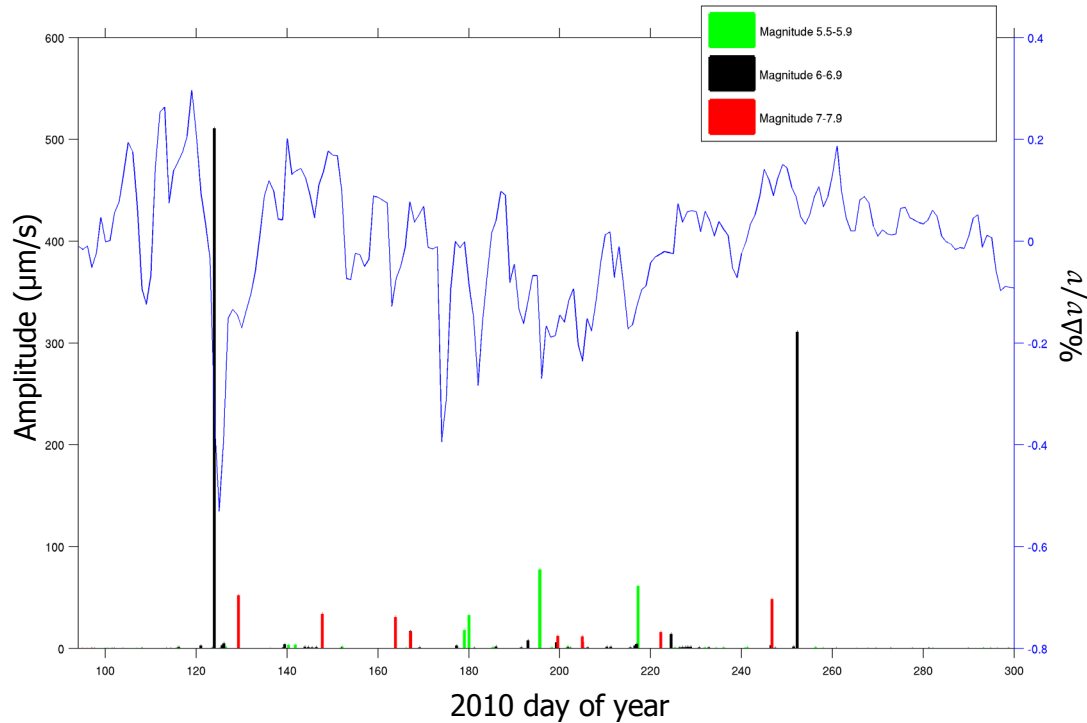


Figure 4.3 V07 vertical channel surface wave amplitude versus stacked $\% \Delta v/v$

4.3 Volcanic

As discussed previously, the short-term velocity changes observed could be caused by earthquakes, but due to Villarrica's distance from and the smaller magnitude of the earthquakes during data collections they are a less plausible source compared with volcanic activity, aside from the May 3 example. The velocity perturbations on day 108 (18 April) and 123 (3 May) decreased and increased over a few days. The change that began on day 123 also diminished in magnitude with distance from the edifice (Figure 4.4), suggesting the source may be volcanic. In consideration of the activity at Villarrica, degassing with tremor (Palma et al., 2008), and the smaller magnitude velocity change compared to Piton de la Fournaise, it is unlikely that the dilation and relaxation of the subsurface is due to magma migration.

We examined other available observations of volcanic activity for comparison with the apparent short-term velocity changes. Long-period (LP) events, also known as volcanic earthquakes, are associated with the location of eruption at volcanos (McNutt, 1996). Since the sources of the noise recorded are likely scattered long-period (LP) events at the surface of the lava lake, a correlation with their frequency of occurrence and the velocity changes would indicate that these changes are the result of LP event influences. The LP events were identified using a waveform similarity algorithm and then compared with the velocity changes (Figure 4.5). Unfortunately, the frequency of LP events and velocity changes do not seem to correlate which could indicate that the noise and LP events are unrelated.

Next, the velocity changes were compared with the Moderate Resolution Imaging Spectroradiometer (MODIS) radiant heat output (Figure 4.6). MODIS has been applied

to monitor global volcanic hotspots through imaging radiant heat emitted in the short wave infrared (SWIR) region of the electromagnetic spectrum, specifically in the 4- (bands 21 and 22) and 11 μ m (band 32) regions (Wright et al., 2002). Changes in ground temperature by 500 K translate to large increases in the radiance in the 4 μ m region and small changes in the 11 μ m, by orders of magnitude, as described by Wright et al. (2002). An increase in radiant heat indicates an increase in temperature which suggests a change in activity at the volcano being monitored. An increase in temperature could be due to an influx of hot magma to a lava lake or a fresh lava flow. MODIS images are taken twice a day, sometimes more depending on the overlap of the satellite path, of an area about 1354 X 2030 km. Unfortunately, clouds scatter the waves resulting in poor images when clouds are present. Over the time period of the seismic array there are gaps in the MODIS data probably due to cloud cover in the winter resulting in less than one image a day in some cases. This poor dataset results in poor correlation with our velocity change data.

Real-time Seismic Amplitude Measurement (RSAM) is employed as a monitoring tool at volcanoes such that an increase in the average amplitude of ground shaking and/or frequency of seismic events results in an increase in RSAM without taking into account the location or magnitude of the seismicity (Endo and Murray, 1991; Ewert et al., 1993). We compared the RSAM at Villarrica with the velocity changes to try to detect surface wave influence (Figure 4.7). The seismograms from station V03 were filtered from 12 to 30 seconds and then the average amplitude was summed and stored in 60 minute intervals, because our data are in hour long records. Here again there is little correlation between the velocity changes and RSAM.

Lastly we compared the velocity changes to the Ozone Monitoring Instrument (OMI) SO₂ mass data (Figure 4.8). OMI is a space-based, ultraviolet/visible sensor that maps global SO₂, but also measures passive volcanic degassing (Carn et al., 2008). The SO₂ mass and velocity changes do not correlate because all but two of the SO₂ data points fall within background levels.

The comparison of the observed velocity changes with frequency of long period events (Figure 4.5), MODIS radiant heat output (Figure 4.6), RSAM (Figure 4.7) and OMI SO₂ mass (Figure 4.8) showed little to no correlation. In turn, we suggest that quick depressurization and subsequent gas exsolution and pore fluid migration in response to slow pressurization from within the conduit causes these small velocity decreases which then re-pressurize, equilibrating the system.

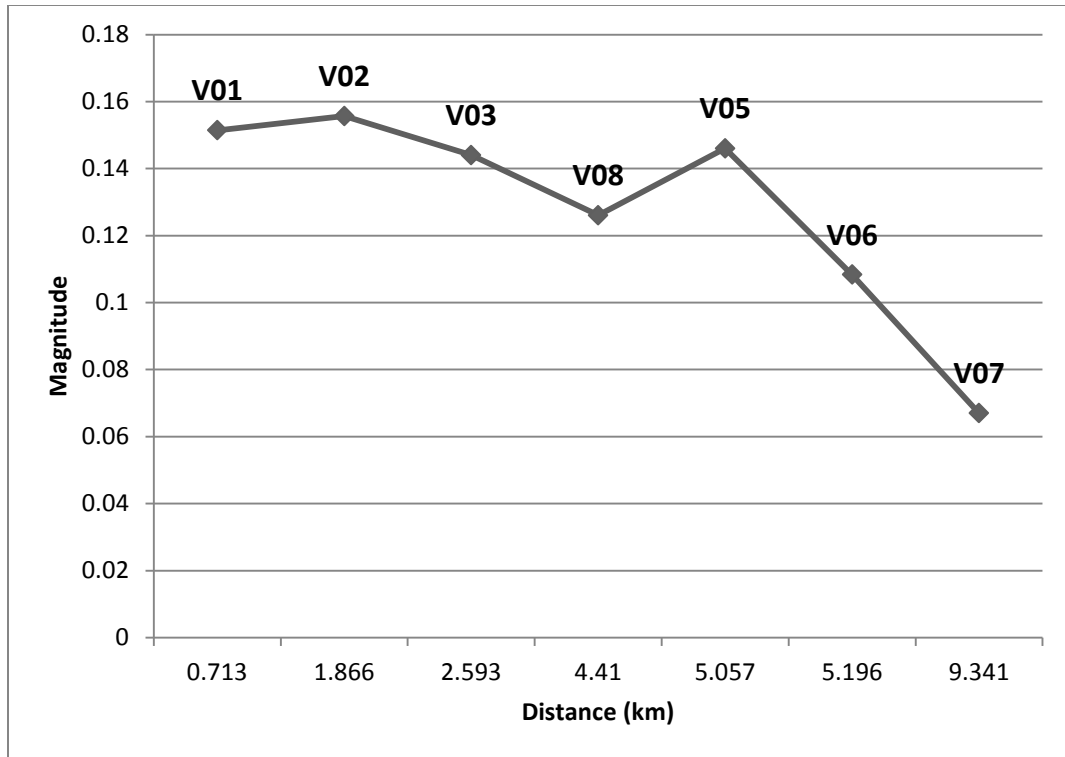


Figure 4.4 Distance from the edifice in kilometers versus magnitude of velocity change at each station during the perturbation that starts on day 123 of 2010.

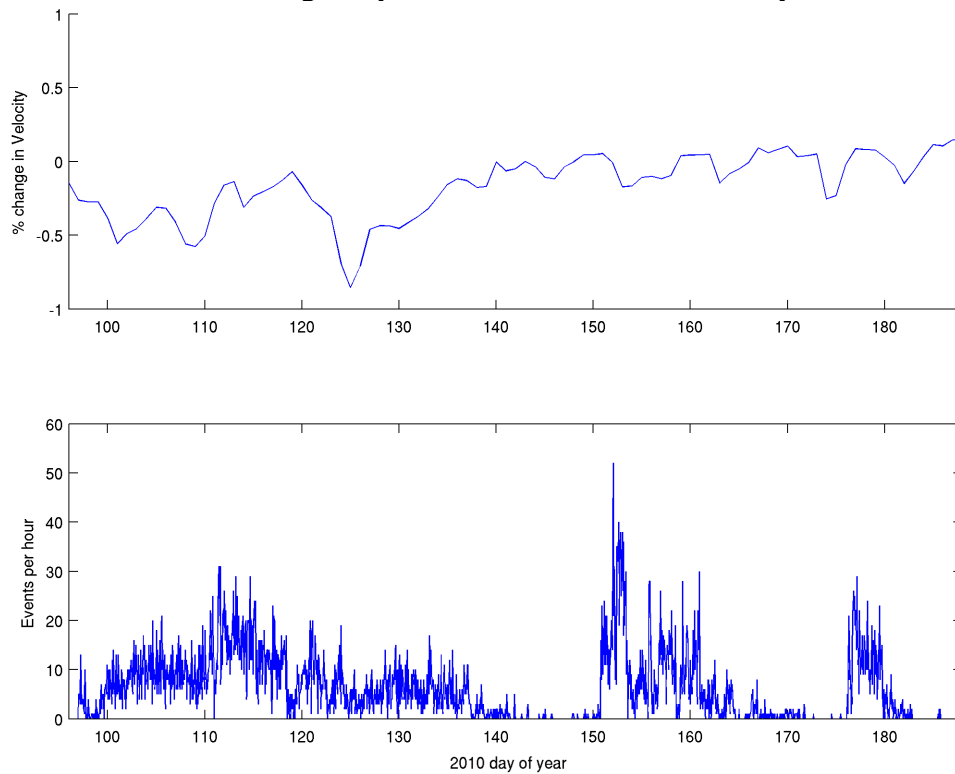


Figure 4.5 2010 stacked velocity change compared to frequency of long-period events

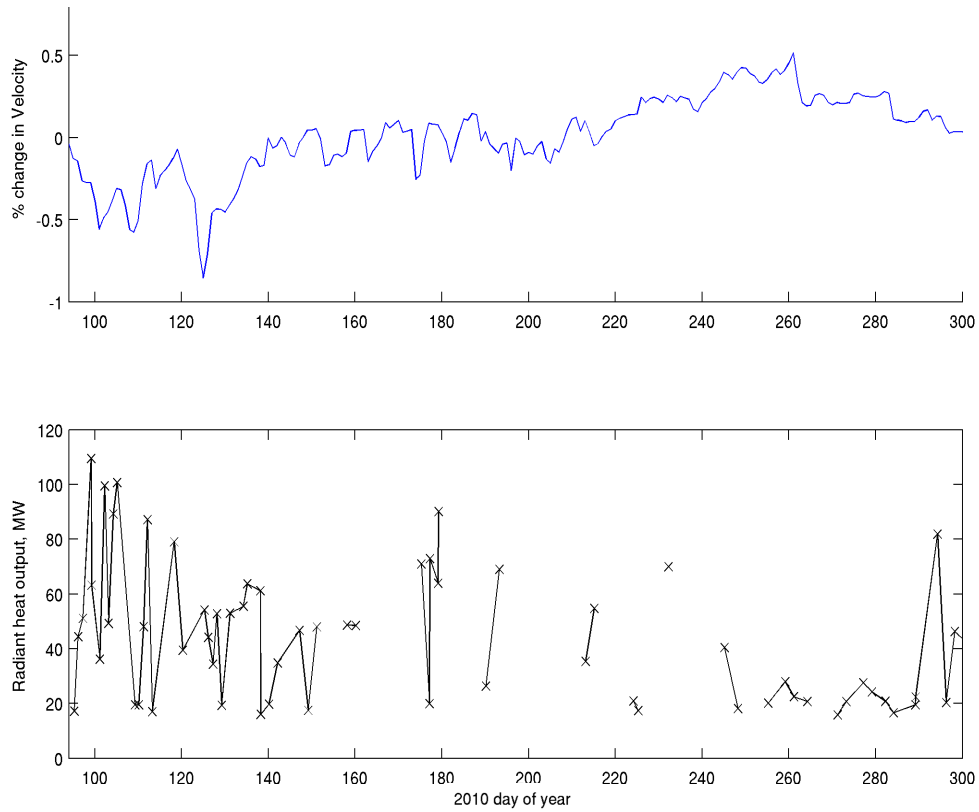


Figure 4.6 2010 stacked velocity change compared to MODIS radiant heat output data from MODVOLC <http://modis.higp.hawaii.edu/>

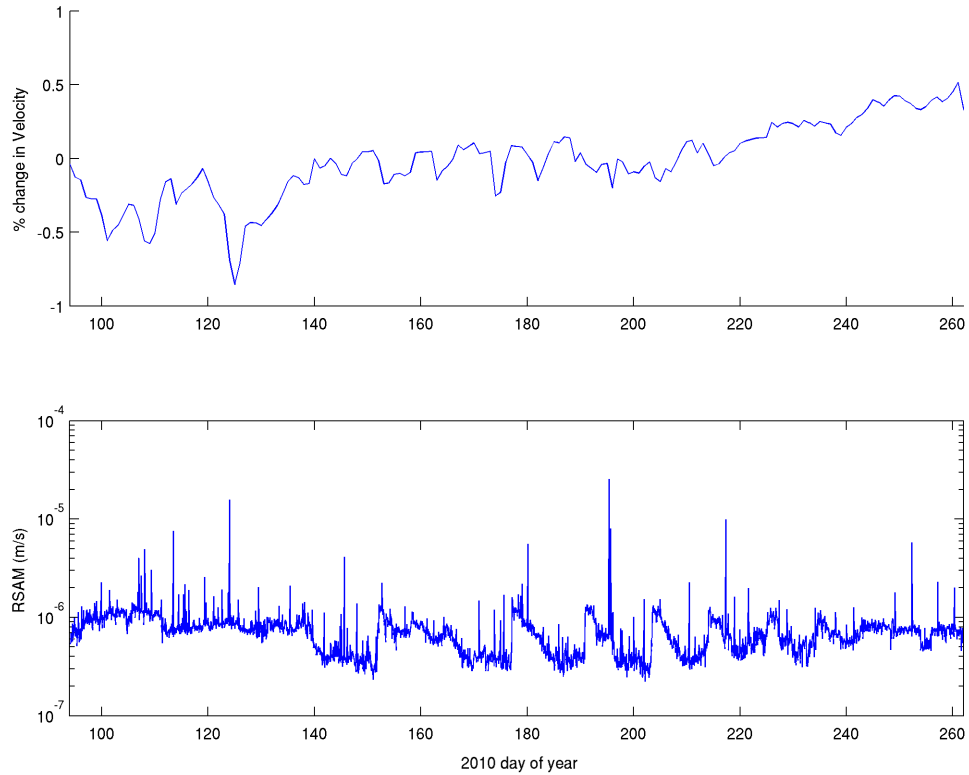


Figure 4.7 2010 stacked velocity change compared to 60min RSAM from station V03

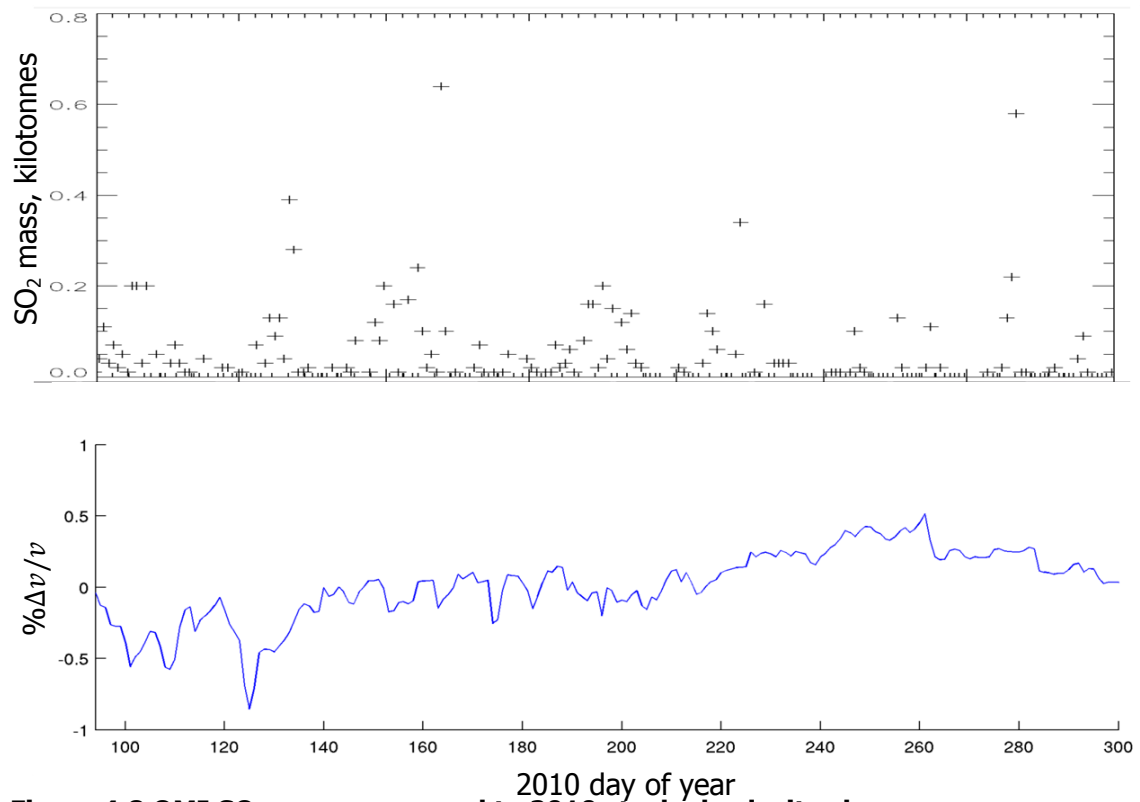


Figure 4.8 OMI SO₂ mass compared to 2010 stacked velocity change

5 Conclusions

Villarrica volcano, of the southern Chilean Andes, is an actively degassing stratovolcano and part of the VQL volcanic chain (Curilem et al., 2009; Ortiz et al., 2003; Palma et al., 2008). Through this seismic ambient noise study we observed a long-term velocity increase during 2010 and short term velocity perturbations in 2010 and 2011. We attribute the long term velocity increase to seasonal snow loading which is why it is not present in 2011 because the data are from the summer (Christiansen et al., 2005; Heki, 2003; Sens-Schönfelder and Wegler, 2006). Thermo-elastic strain is also considered but without a time delay in the velocity change to allow for heat change to reach seismogenic depths it is an unlikely candidate for the source (Meier et al., 2010).

In the case of short-term velocity perturbations, earthquakes (Hill et al., 2002; Manga and Brodsky, 2006) or volcanic activity (Brenguier et al., 2011; Brenguier et al., 2008; Duputel et al., 2009) are the likely sources. At this point the data suggest that the perturbations are due to changes within the edifice, such as changing level of the lava lake, thus changing the source and path or gas exsolution and related pore fluid movement either due to rising of volatile rich magma or shaking the system with earthquakes enabling bubble nucleation. Rising fresh magma as a source of the changes fits the data better than shaking due to earthquakes for several reasons 1) the regional earthquakes are smaller in magnitude compared to other cases (Hill et al., 2002; King et al., 1994; Stein et al., 1997; Stein et al., 1994), 2) the earthquakes are at a distance of at least 200km and 3) the amplitude of the perturbations decreases with distance from the edifice (Brenguier et al., 2011; Brenguier et al., 2008; Duputel et al., 2009). The correlation of the peak surface wave amplitude of the earthquakes on May 3, 2010 suggests they influence Villarrica.

To better determine the source of the velocity changes at Villarrica other observables are necessary, but are unavailable for the periods for which we have data. This study of Villarrica volcano encourages continued research of cross- and auto-correlations from seismic ambient noise that delves into the subtle intricacies and their meaning. This is particularly important since they could be used to monitor volcanoes (Brenguier et al., 2011).

6 References

- Alford, D., 1967. Density Variations in Alpine Snow. *Journal of Glaciology*, 6(46): 495-503.
- Battaglia, J., Métaxian, J.-P. and Garaebiti, E., 2012. Earthquake-volcano interaction imaged by coda wave interferometry. *Geophysical Research Letters*, 39(11).
- Bensen, G.D., Ritzwoller, M.H., Barmin, M.P., Levshin, A.L., Lin, F., Moschetti, M.P., Shapiro, N.M. and Yang, Y., 2007. Processing seismic ambient noise data to obtain reliable broad-band surface wave dispersion measurements. *Geophysical Journal International*, 169(3): 1239-1260.
- Brenguier, F., Clarke, D., Aoki, Y., Shapiro, N.M., Campillo, M. and Ferrazzini, V., 2011. Monitoring volcanoes using seismic noise correlations. *Comptes Rendus Geoscience*, 343(8-9): 633-638.
- Brenguier, F., Shapiro, N.M., Campillo, M., Ferrazzini, V., Duputel, Z., Coutant, O. and Nercessian, A., 2008. Towards forecasting volcanic eruptions using seismic noise. *Nature Geoscience*, 1: 5.
- Brenguier, F., Shapiro, N.M., Campillo, M., Nercessian, A. and Ferrazzini, V., 2007. 3-D surface wave tomography of the Piton de la Fournaise volcano using seismic noise correlations. *Geophysical Research Letters*, 34(2).
- Campillo, M., 2006. Phase and correlation in 'Random' seismic fields and the reconstruction of the green function. *Pure and Applied Geophysics*, 163(2-3): 475-502.
- Carn, S.A., Krueger, A.J., Arellano, S., Krotkov, N.A. and Yang, K., 2008. Daily monitoring of Ecuadorian volcanic degassing from space. *Journal of Volcanology and Geothermal Research*, 176(1): 141-150.
- Chaput, J.A., Zandomenighi, D., Aster, R.C., Knox, H. and Kyle, P.R., 2012. Imaging of Erebus volcano using body wave seismic interferometry of Strombolian eruption coda. *Geophysical Research Letters*, 39(7).
- Christiansen, L., Hurwitz, S., Saar, M.O., Ingebritsen, S.E. and Hsieh, P.A., 2005. Seasonal seismicity at western United States volcanic centers. *Earth and Planetary Science Letters*, 240: 307-321.
- Curilem, G., Vergara, J., Fuentealba, G., Acuña, G. and Chacón, M., 2009. Classification of seismic signals at Villarrica volcano (Chile) using neural networks and genetic algorithms. *Journal of Volcanology and Geothermal Research*, 180(1): 1-8.
- Draganov, D., Wapenaar, K. and Thorbecke, J., 2006. Seismic interferometry: Reconstructing the earth's reflection response. *Geophysics*, 71(4): 10.
- Duputel, Z., Ferrazzini, V., Brenguier, F., Shapiro, N., Campillo, M. and Nercessian, A., 2009. Real time monitoring of relative velocity changes using ambient seismic noise at the Piton de la Fournaise volcano (La Réunion) from January 2006 to June 2007. *Journal of Volcanology and Geothermal Research*, 184(1-2): 164-173.
- Endo, E.T. and Murray, T., 1991. Real-time Seismic Amplitude Measurement (RSAM): a volcano monitoring and prediction tool. *Bulletin of Volcanology*, 53: 13.
- Ewert, J.W., Murray, T.L., Lockhart, A.B. and Miller, C.D., 1993. Report: Preventing Volcanic Catastrophe: The U.S. International Volcano Disaster Assistance Program. *Earth and Volcanoes Bulletin*, 24(6): 22.
- Gouédard, P., Stehly, L., Brenguier, F., Campillo, M., Colin de Verdière, Y., Larose, E., Margerin, L., Roux, P., Sánchez-Sesma, F.J., Shapiro, N.M. and Weaver, R.L.,

2008. Cross-correlation of random fields: mathematical approach and applications. *Geophysical Prospecting*, 56(3): 375-393.
- Hansteen, T.H., Bredemeyer, S., Garofalo, K., Pena, P., Rupke, L., Mora Stock, C., Dzierma, Y., Rabbel, W., Bataille, K. and Gil Cruz, F., 2011. The Influence Of Earthquakes On Degassing At Villarrica Volcano, Chile. American Geophysical Union, Fall Meeting 2011, abstract #V53E-2681.
- Harris, A.J.L. and Ripepe, M., 2007. Regional earthquake as a trigger for enhanced volcanic activity: Evidence from MODIS thermal data. *Geophysical Research Letters*, 34(2).
- Heki, K., 2003. Snow load and seasonal variation of earthquake occurrence in Japan. *Earth and Planetary Science Letters*, 207(1-4): 159-164.
- Hill, D.P., Pollitz, F.F. and Newhall, C., 2002. Earthquake-Volcano Interactions. *Physics Today*, 55(11): 7.
- Husen, S., Taylor, R., Smith, R.B. and Healy, H., 2004a. Changes in geyser eruption behavior and remotely triggered seismicity in Yellowstone National Park produced by the 2002 M 7.9 Denali fault earthquake, Alaska. *Geology*, 32(6): 537.
- Husen, S., Wiemer, S. and Smith, R.B., 2004b. Remotely Triggered Seismicity in the Yellowstone National Park Region by the 2002 Mw 7.9 Denali Fault Earthquake, Alaska. *Bulletin of the Seismological Society of America*, 94(6B): S317-S331.
- King, G.C.P., Stein, R.S. and Lin, J., 1994. Static Stress Changes and the Triggering of Earthquakes. *Bulletin of the Seismological Society of America*, 84(3): 935-953.
- Manga, M. and Brodsky, E., 2006. Seismic triggering of eruptions in the far field: Volcanoes and geysers. *Annual Review of Earth and Planetary Sciences*, 34: 263-291.
- Masterlark, T., Haney, M., Dickinson, H., Fournier, T. and Searcy, C., 2010. Rheologic and structural controls on the deformation of Okmok volcano, Alaska: FEMs, InSAR, and ambient noise tomography. *Journal of Geophysical Research*, 115(B2).
- McNutt, S.R., 1996. Seismic Monitoring and Eruption Forecasting of Volcanoes: A Review of the State-of-the-Art and Case Histories. *Monitoring and Mitigation of Volcano Hazards*: 48.
- Meier, U., Shapiro, N.M. and Brenguier, F., 2010. Detecting seasonal variations in seismic velocities within Los Angeles basin from correlations of ambient seismic noise. *Geophysical Journal International*.
- Minato, S., Tsuji, T., Ohmi, S. and Matsuoka, T., 2012. Monitoring seismic velocity change caused by the 2011 Tohoku-oki earthquake using ambient noise records. *Geophysical Research Letters*, 39(9).
- Nagaoka, Y., Nishida, K., Aoki, Y., Takeo, M. and Ohminato, T., 2012. Seismic imaging of magma chamber beneath an active volcano. *Earth and Planetary Science Letters*, 333-334: 1-8.
- Ortiz, R., Moreno, H., Garcia, A., Fuentealba, G., Astiz, M., Pena, P., Sanchez, N. and Tarraga, M., 2003. Villarrica volcano (Chile): characteristics of the volcanic tremor and forecasting of small explosions by means of a material failure method. *Journal of Volcanology and Geothermal Research*, 128(1-3): 247-259.
- Palma, J.L., Calder, E.S., Basualto, D., Blake, S. and Rothery, D.A., 2008. Correlations between SO₂ flux, seismicity, and outgassing activity at the open vent of

- Villarrica volcano, Chile. *Journal of Geophysical Research-Solid Earth*, 113(B10): 23.
- Prawirodirdjo, L., Ben-Zion, Y. and Bock, Y., 2006. Observation and modeling of thermoelastic strain in Southern California Integrated GPS Network daily position time series. *Journal of Geophysical Research-Solid Earth*, 111(B2).
- Ripepe, M., Marchetti, E., Bonadonna, C., Harris, A.J.L., Pioli, L. and Ulivieri, G., 2010. Monochromatic infrasonic tremor driven by persistent degassing and convection at Villarrica Volcano, Chile. *Geophysical Research Letters*, 37(15).
- Sabra, K.G., Roux, P., Gerstoft, P., Kuperman, W.A. and Fehler, M.C., 2006. Extracting coherent coda arrivals from cross-correlations of long period seismic waves during the Mount St. Helens 2004 eruption. *Geophysical Research Letters*, 33(6).
- Sens-Schönfelder, C. and Wegler, U., 2006. Passive image interferometry and seasonal variations of seismic velocities at Merapi Volcano, Indonesia. *Geophysical Research Letters*, 33(21).
- Shapiro, N.M. and Campillo, M., 2004. Emergence of broadband Rayleigh waves from correlations of the ambient seismic noise. *Geophysical Research Letters*, 31(7).
- Shen, Y., Ren, Y., Gao, H. and Savage, B., 2012. An Improved Method to Extract Very-Broadband Empirical Green's Functions from Ambient Seismic Noise. *Bulletin of the Seismological Society of America*, 102(4): 1872-1877.
- Snieder, R. and Wapenaar, K., 2010. Imaging with ambient noise. *Physics Today*: 6.
- Stein, R.S., Barka, A.A. and Dieterich, J.H., 1997. Progressive failure on the North Anatolian fault since 1939 by earthquake stress triggering. *Geophysical Journal International*, 128(3): 594-604.
- Stein, R.S., King, G.C.P. and Lin, J., 1994. Stress Triggering of the 1994 M=6.7 Northridge, California, Earthquake by Its Predecessors. *Science*, 265(5177): 1432-1435.
- Wapenaar, K. and Fokkema, J., 2006. Green's function representations for seismic interferometry. *Geophysics*, 71(4): 14.
- Wapenaar, K., Fokkema, J. and Snieder, R., 2005. Retrieving the Green's function in an open system by cross-correlation: A comparison of approaches. *Journal of Acoustical Society of America*: 6.
- Weaver, R. and Lobkis, O., 2001. Ultrasonics without a Source: Thermal Fluctuation Correlations at MHz Frequencies. *Physical Review Letters*, 87(13).
- Weaver, R.L., 2005. Information from Seismic Noise. *Science*, 307.
- Witter, J.B., Kress, V.C., Delmelle, P. and Stix, J., 2004. Volatile degassing, petrology, and magma dynamics of the Villarrica Lava Lake, Southern Chile. *Journal of Volcanology and Geothermal Research*, 134(4): 303-337.
- Wright, R., Flynn, L., Garbeil, H., Harris, A. and Pilger, E., 2002. Automated volcanic eruption detection using MODIS. *Remote Sensing of Environment*, 82: 21.

7 Appendices

7.1 2010 Auto-correlations with total stack and velocity change

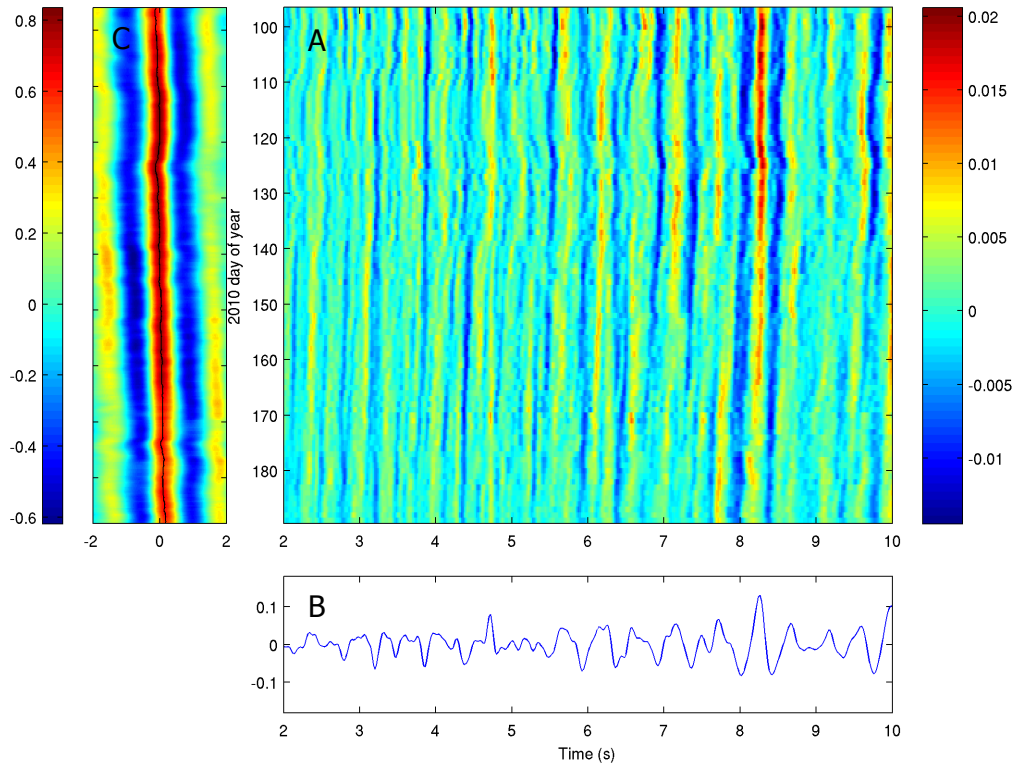


Figure 7.1 Station V01 ACFs, A. daily stacks, B. normalized total stack and C. stretching function, y-axis is the same for A and C

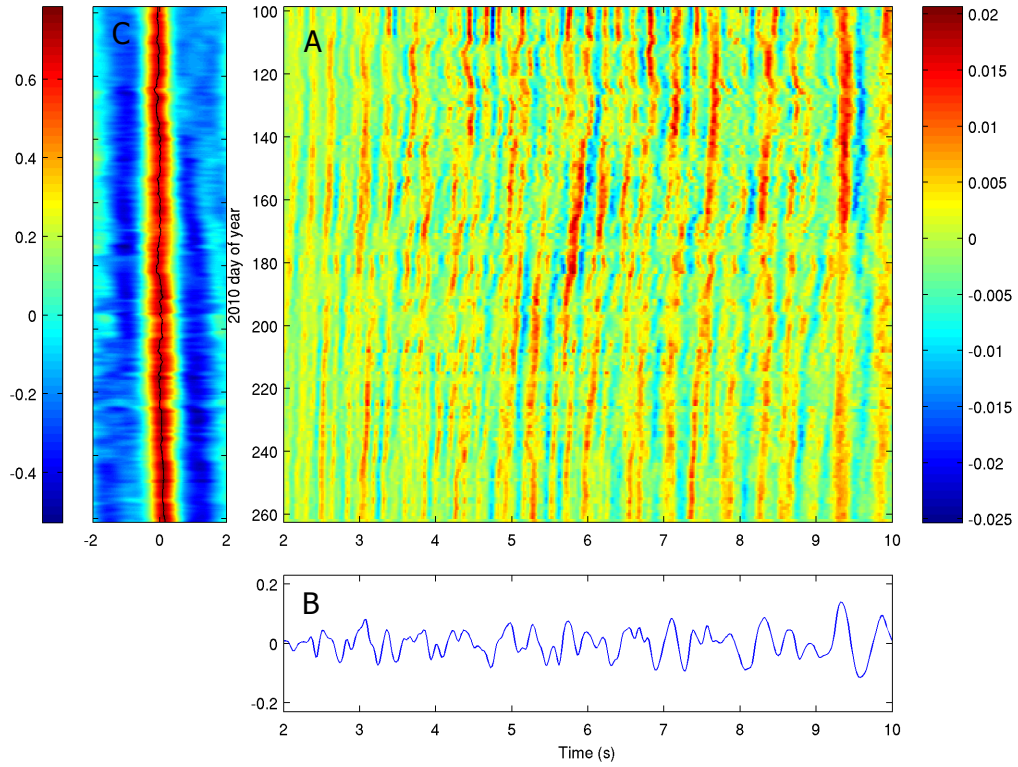


Figure 7.2 Station V02 ACFs, A. daily stacks, B. normalized total stack and C. stretching function, y-axis is the same for A and C

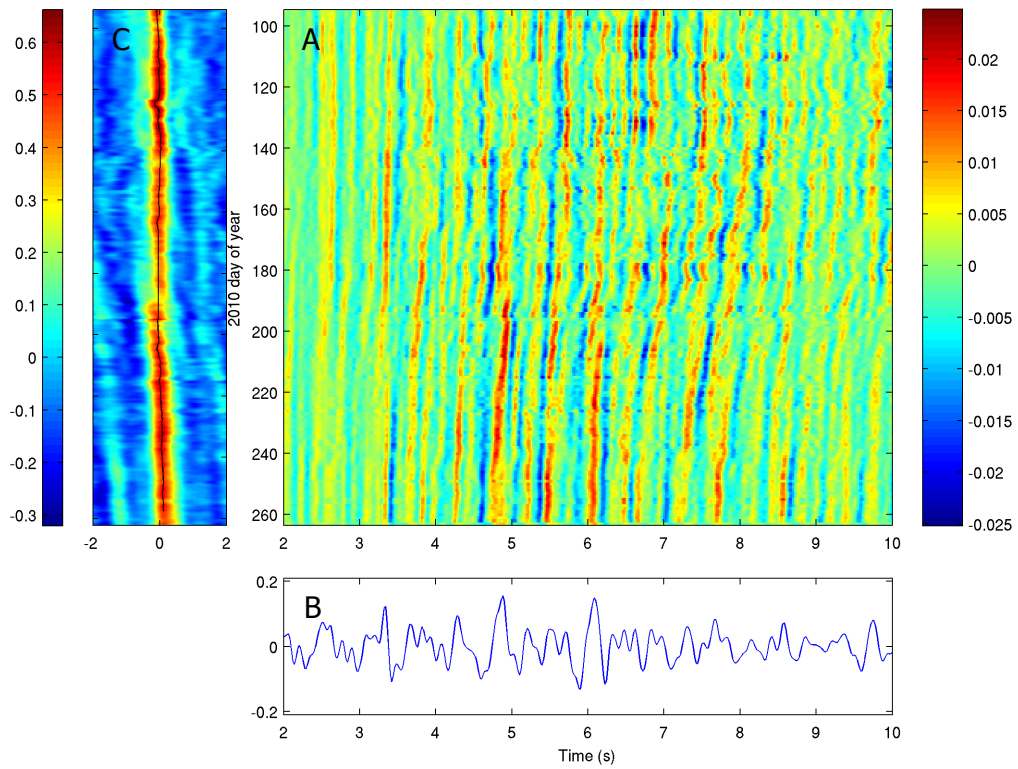


Figure 7.3 Station V03 ACFs, A. daily stacks, B. normalized total stack and C. stretching function, y-axis is the same for A and C

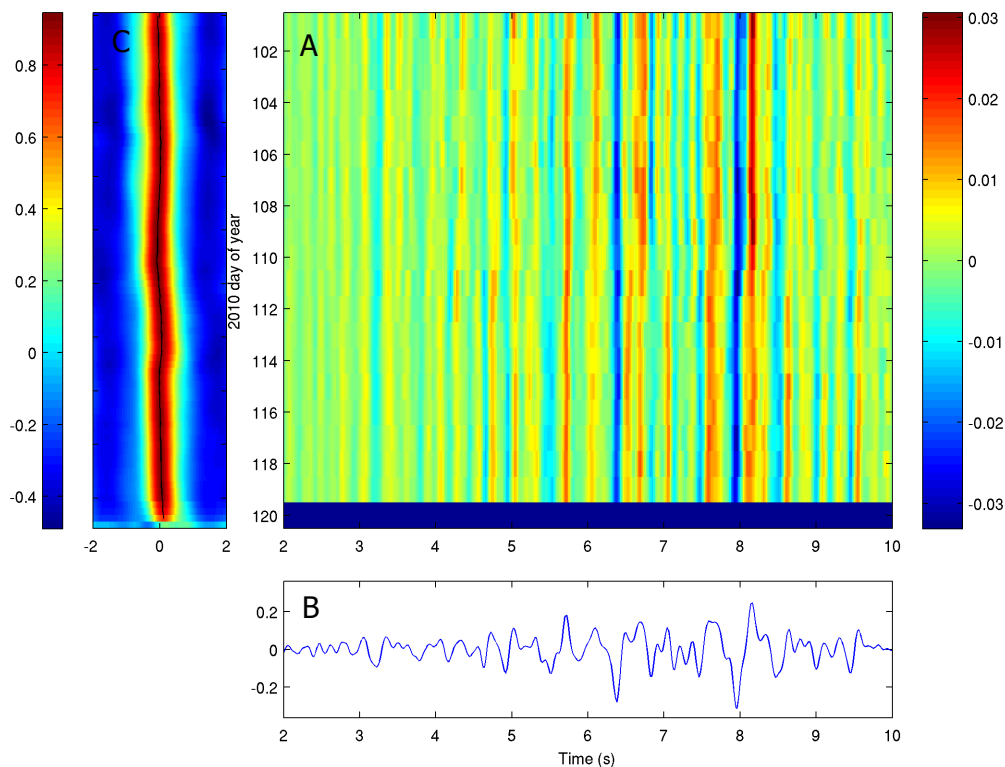


Figure 7.4 Station V04 ACFs, A. daily stacks, B. normalized total stack and C. stretching function, y-axis is the same for A and C

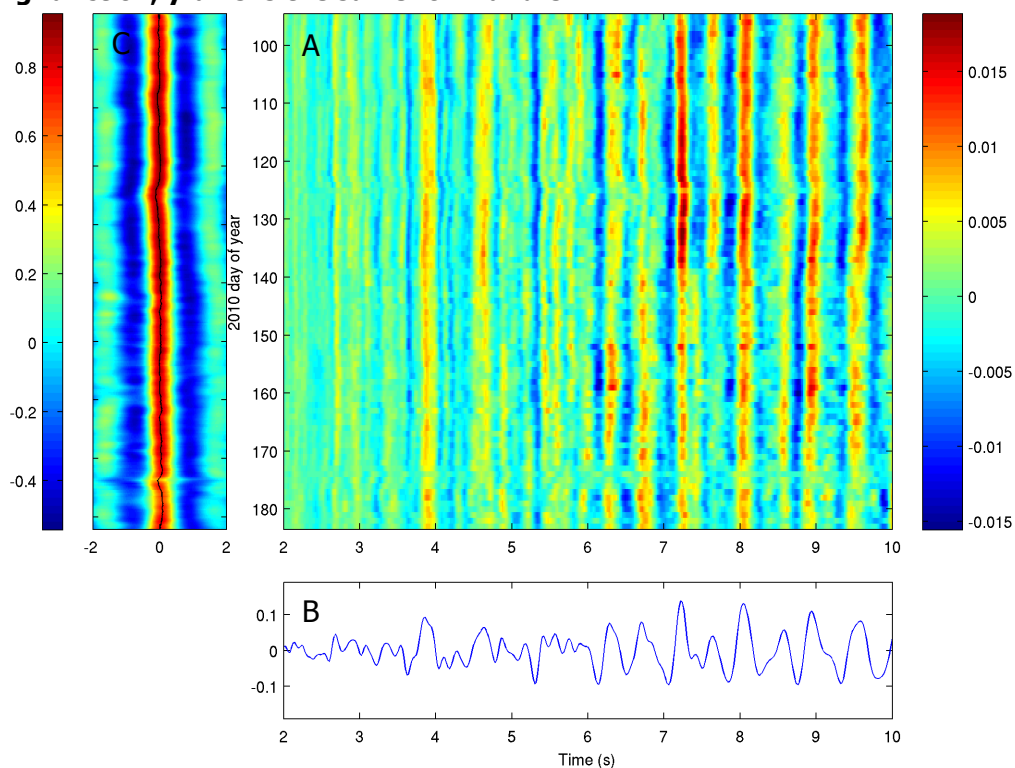


Figure 7.5 Station V05 ACFs, A. daily stacks, B. normalized total stack and C. stretching function, y-axis is the same for A and C

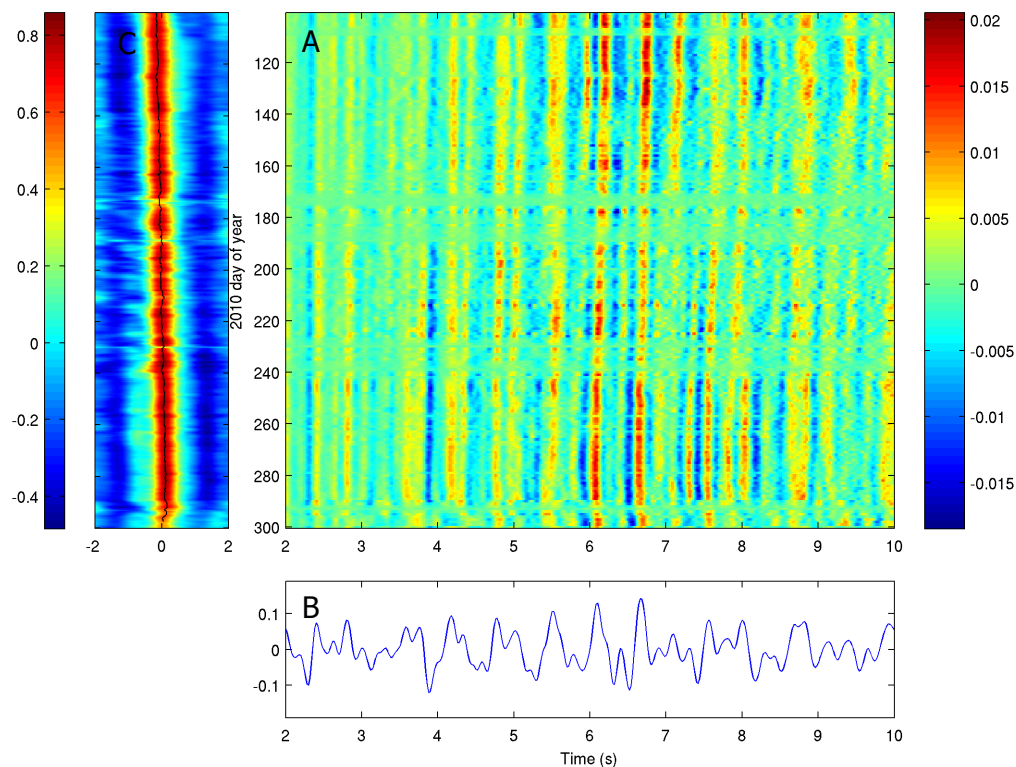


Figure 7.6 Station V06 ACFs, A. daily stacks, B. normalized total stack and C. stretching function, y-axis is the same for A and C

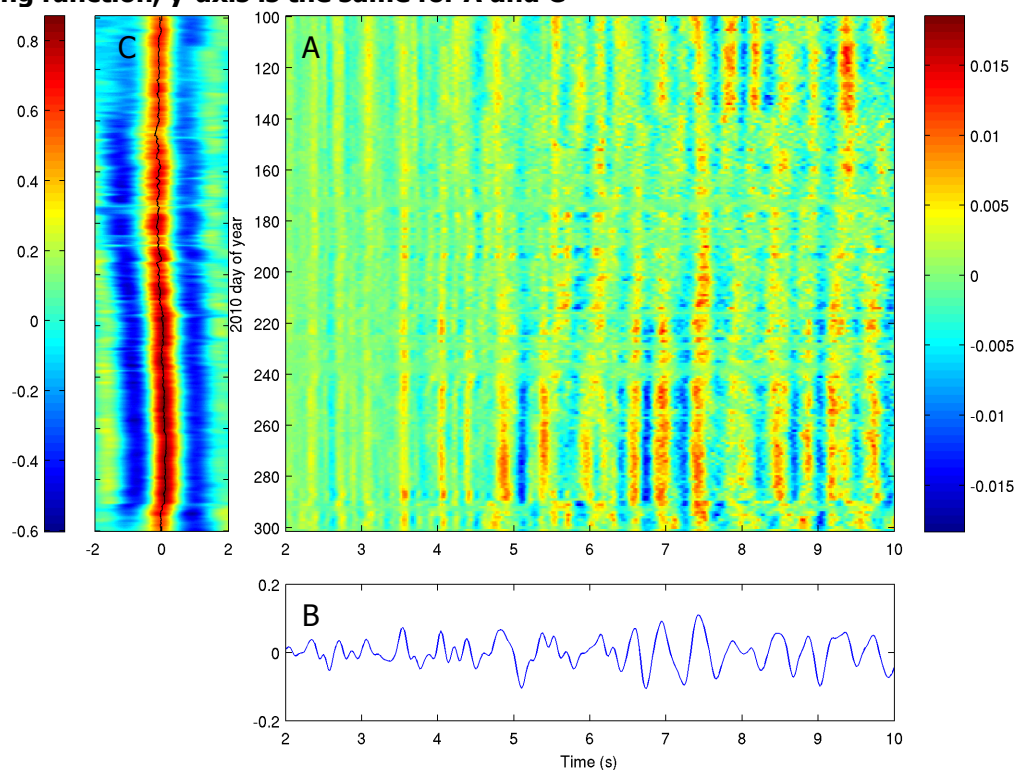


Figure 7.7 Station V07 ACFs, A. daily stacks, B. normalized total stack and C. stretching function, y-axis is the same for A and C

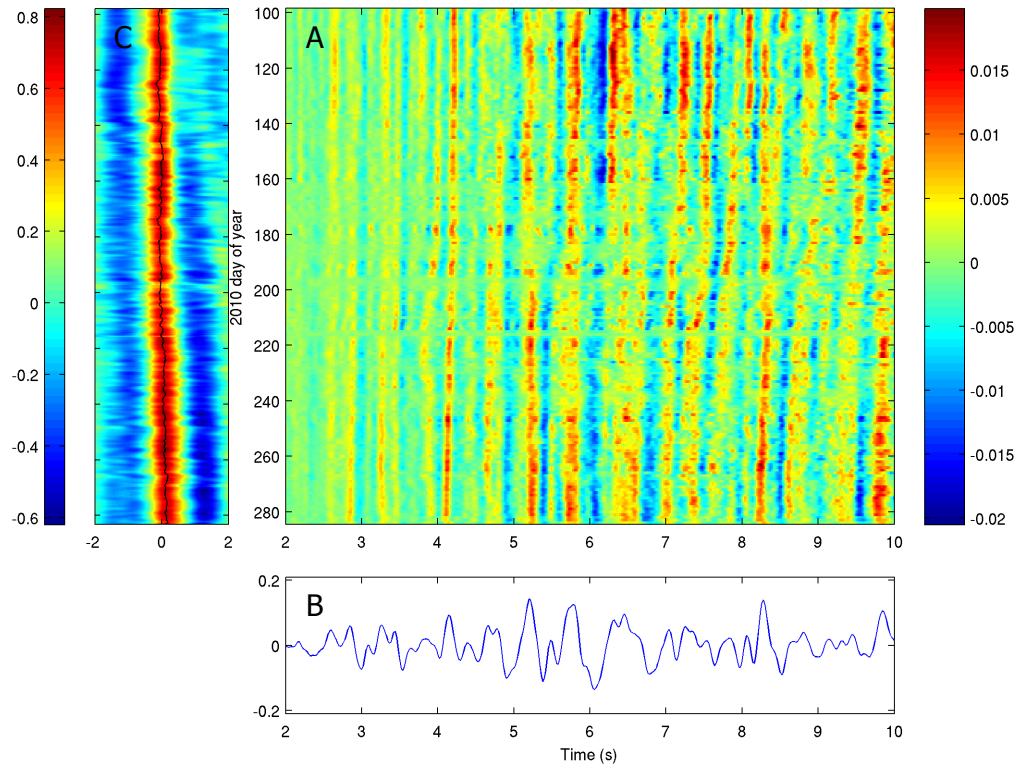


Figure 7.8 Station V08 ACFs, A. daily stacks, B. normalized total stack and C. stretching function, y-axis is the same for A and C

7.2 2010 Cross-correlations with total stack and velocity change, positive and negative lag in separate plots

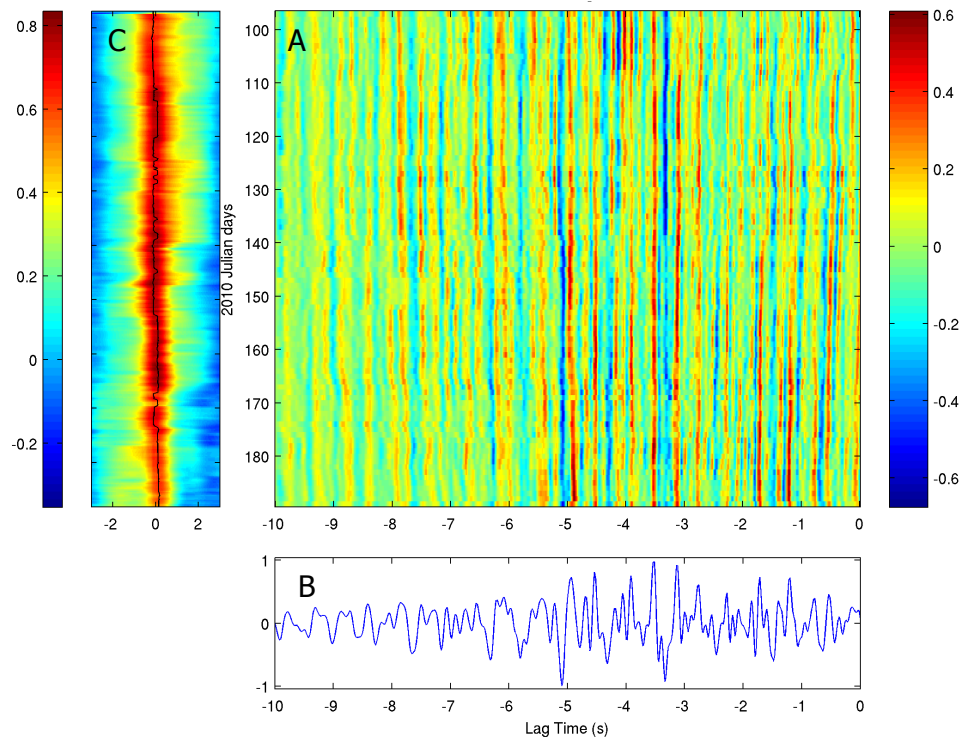


Figure 7.9 CCFs from V01 to V03, -lag, A. daily stacks, B. normalized total stack and C. stretching function, y-axis is the same for A and C

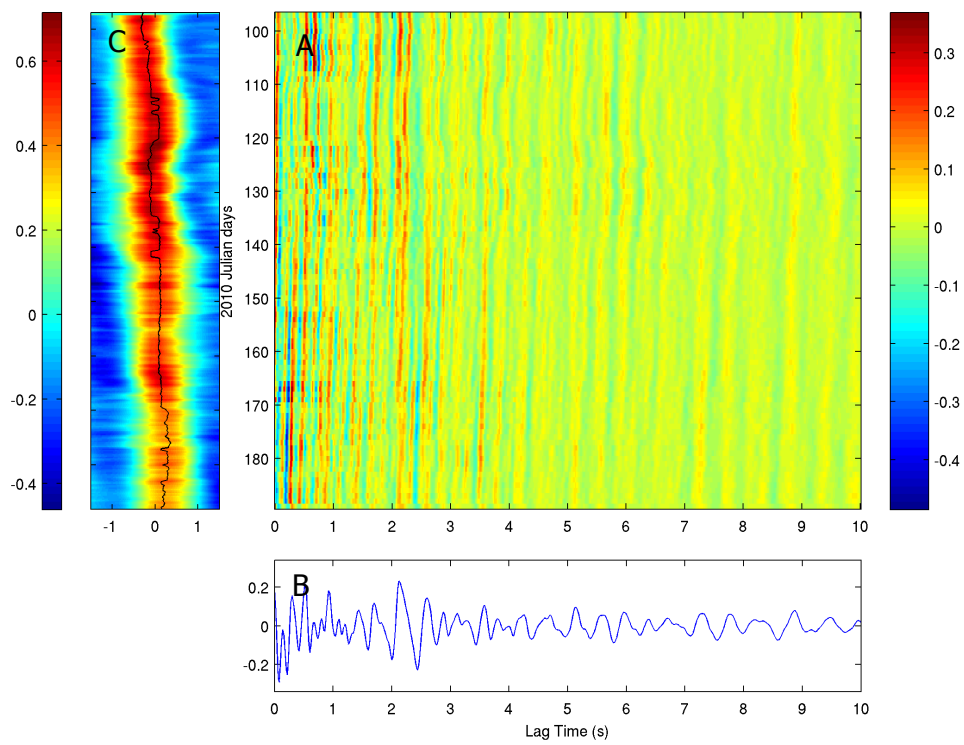


Figure 7.10 CCFs from V01 to V03, +lag, A. daily stacks, B. normalized total stack and C. stretching function, y-axis is the same for A and C

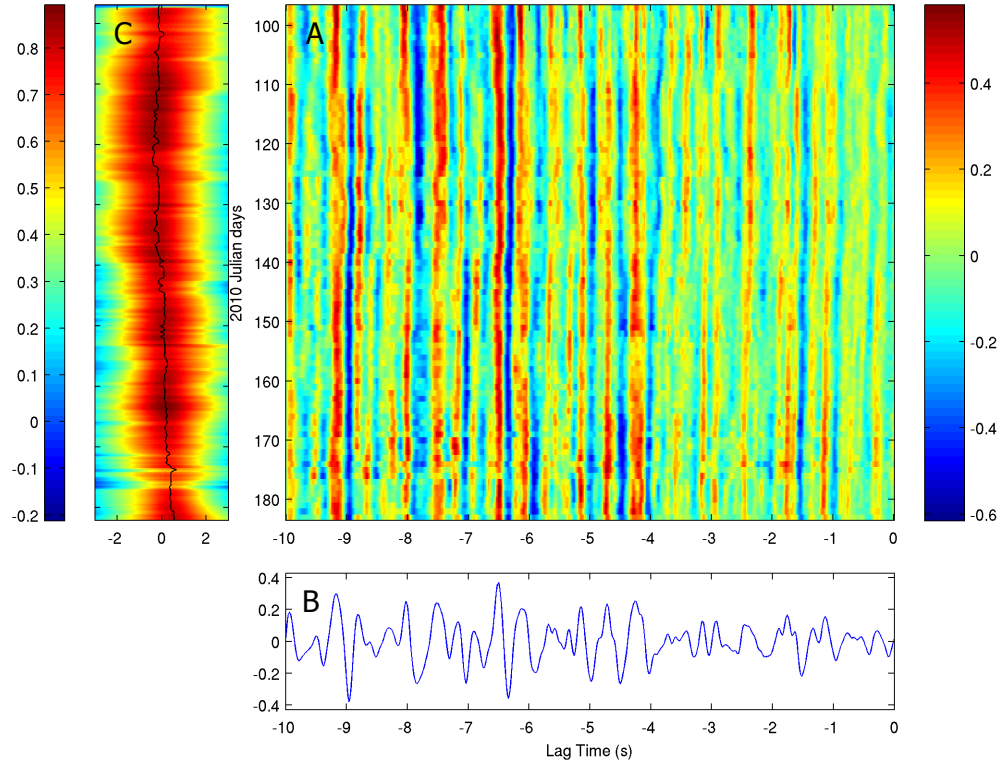


Figure 7.11 CCFs from V01 to V05, -lag, A. daily stacks, B. normalized total stack and C. stretching function, y-axis is the same for A and C

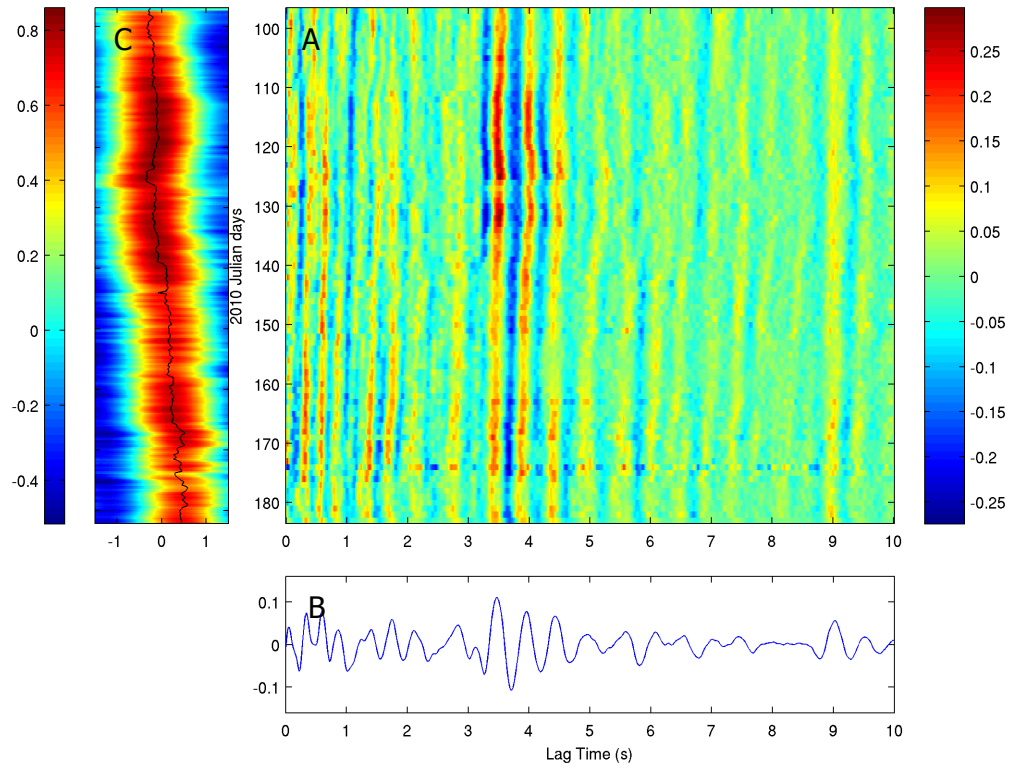


Figure 7.12 CCFs from V01 to V05, +lag, A. daily stacks, B. normalized total stack and C. stretching function, y-axis is the same for A and C

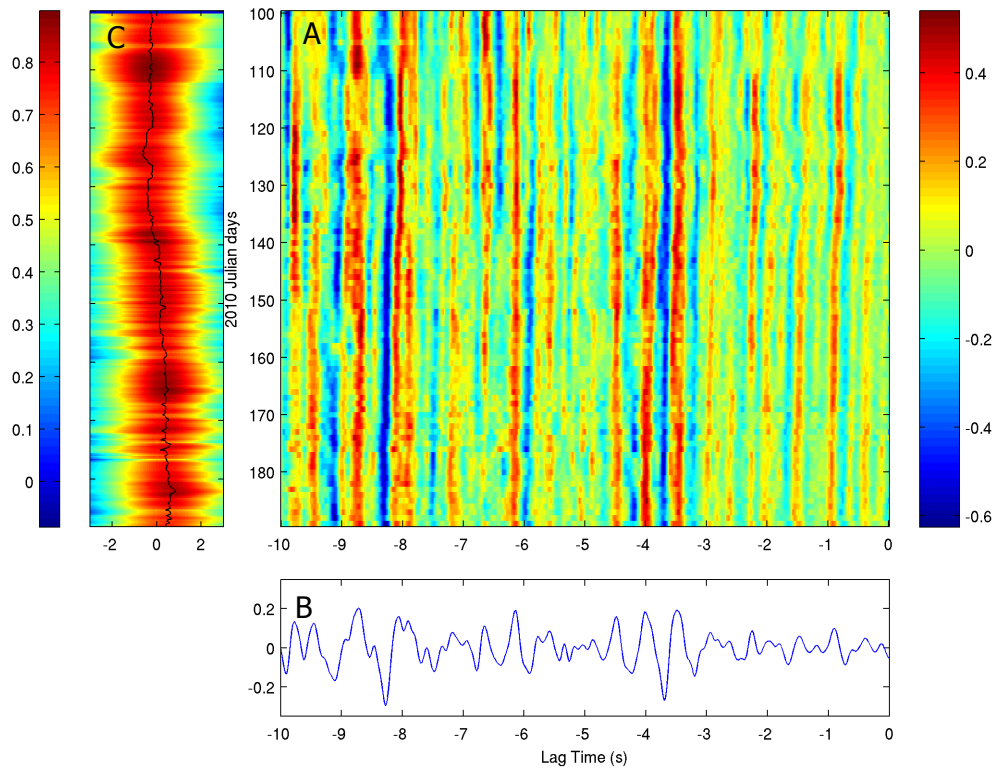


Figure 7.13 CCFs from V01 to V07, -lag, A. daily stacks, B. normalized total stack and C. stretching function, y-axis is the same for A and C

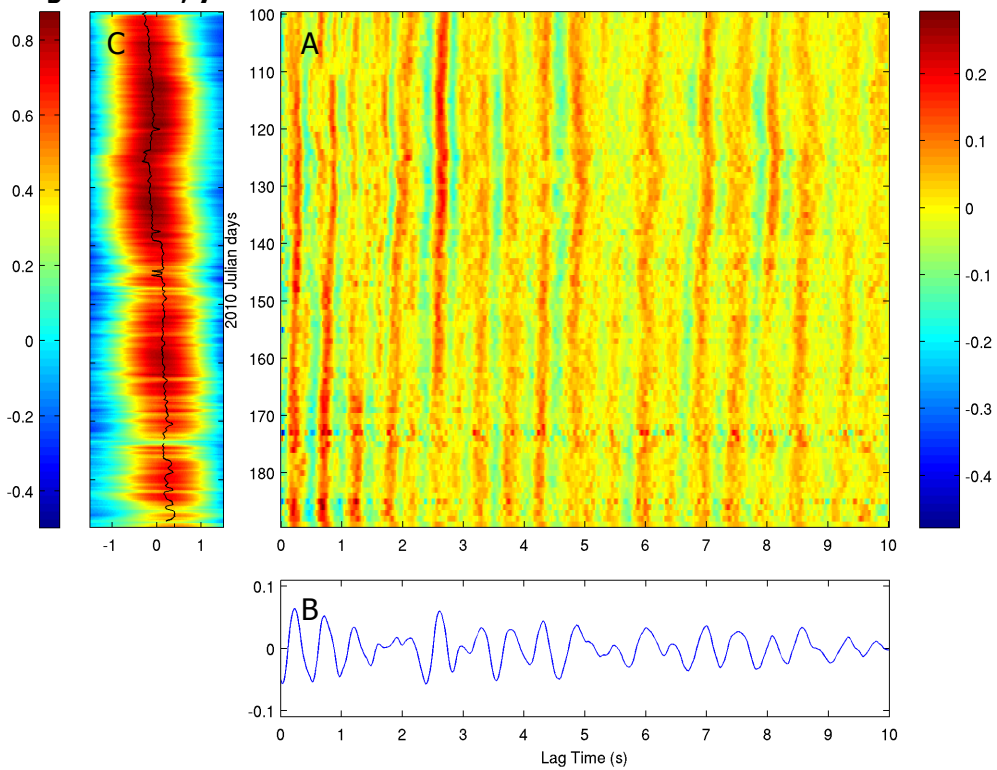


Figure 7.14 CCFs from V01 to V07, +lag, A. daily stacks, B. normalized total stack and C. stretching function, y-axis is the same for A and C

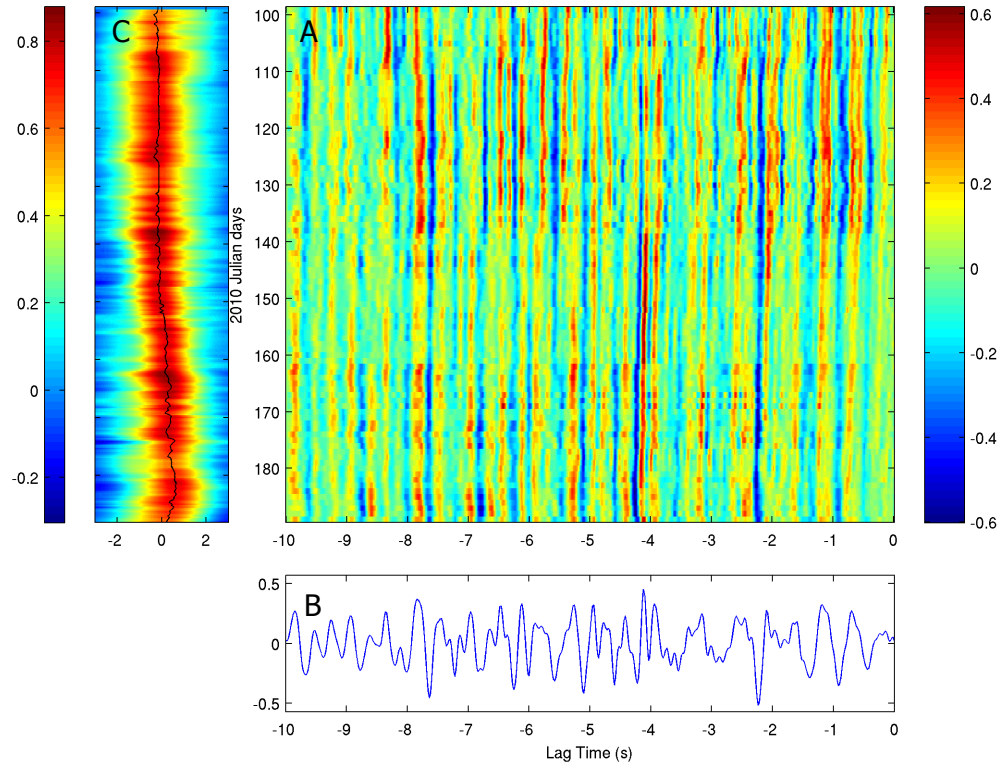


Figure 7.15 CCFs from V01 to V08, -lag, A. daily stacks, B. normalized total stack and C. stretching function, y-axis is the same for A and C

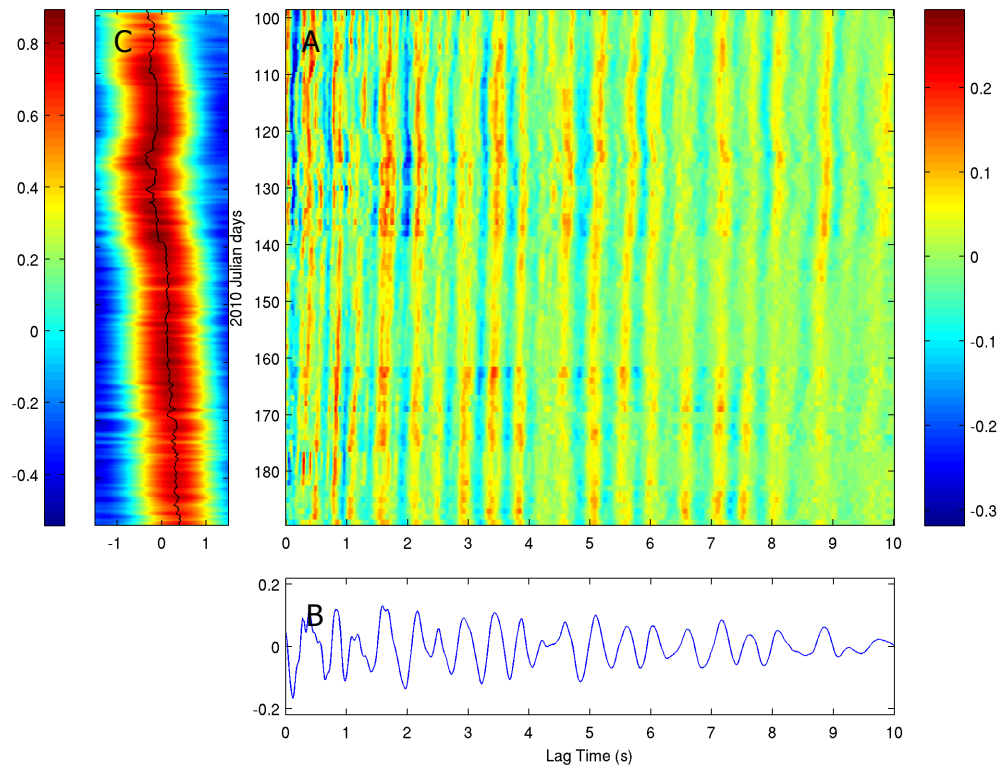


Figure 7.16 CCFs from V01 to V08, +lag, A. daily stacks, B. normalized total stack and C. stretching function, y-axis is the same for A and C

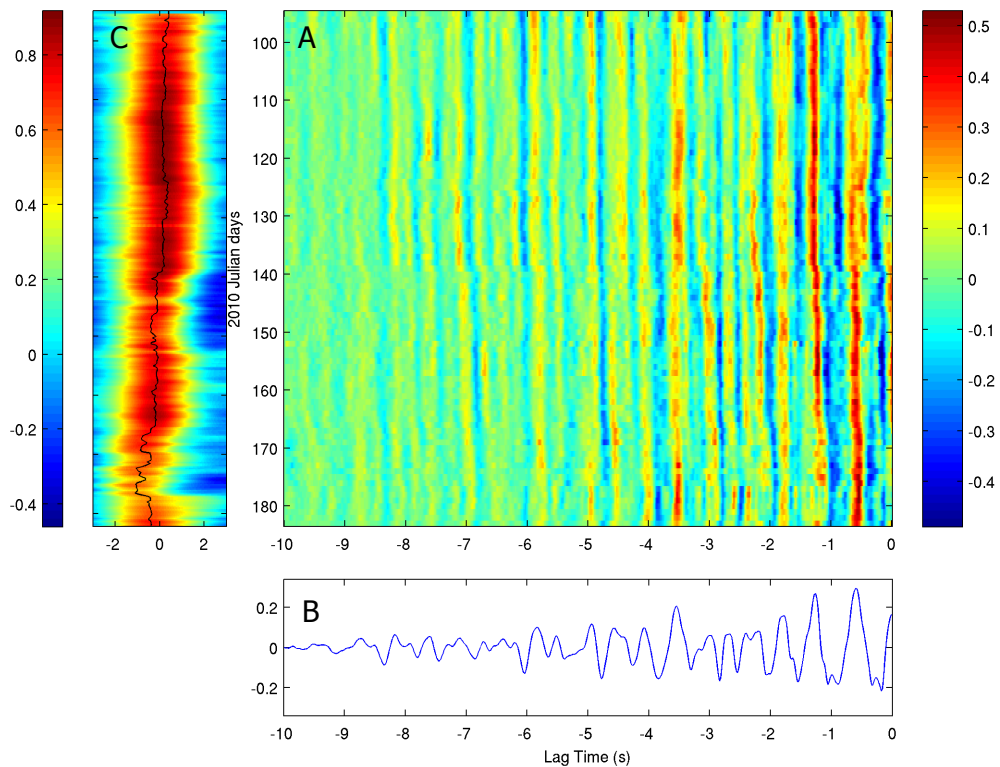


Figure 7.17 CCFs from V05 to V03, -lag, A. daily stacks, B. normalized total stack and C. stretching function, y-axis is the same for A and C

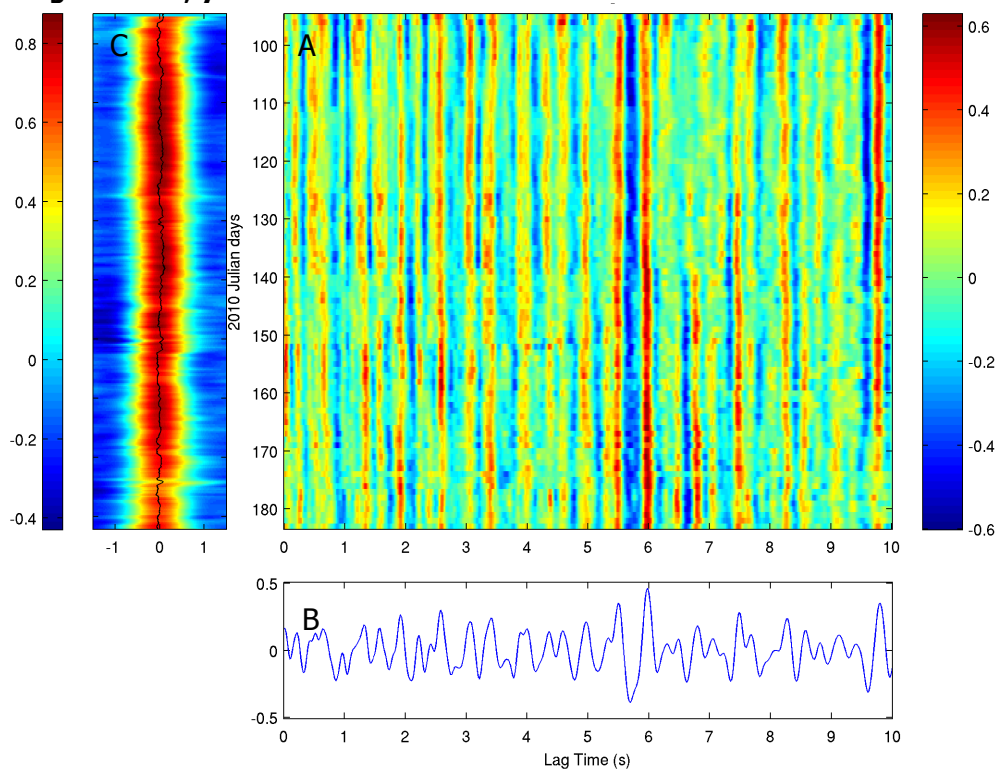


Figure 7.18 CCFs from V05 to V03, +lag, A. daily stacks, B. normalized total stack and C. stretching function, y-axis is the same for A and C

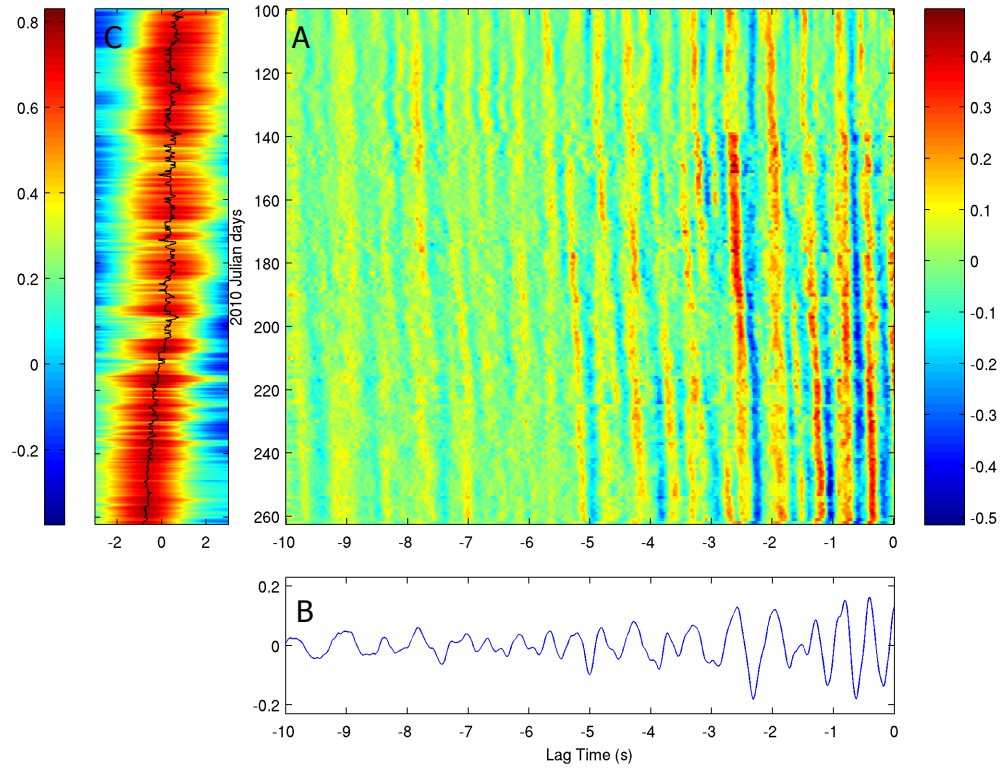


Figure 7.19 CCFs from V07 to V03, -lag, A. daily stacks, B. normalized total stack and C. stretching function, y-axis is the same for A and C

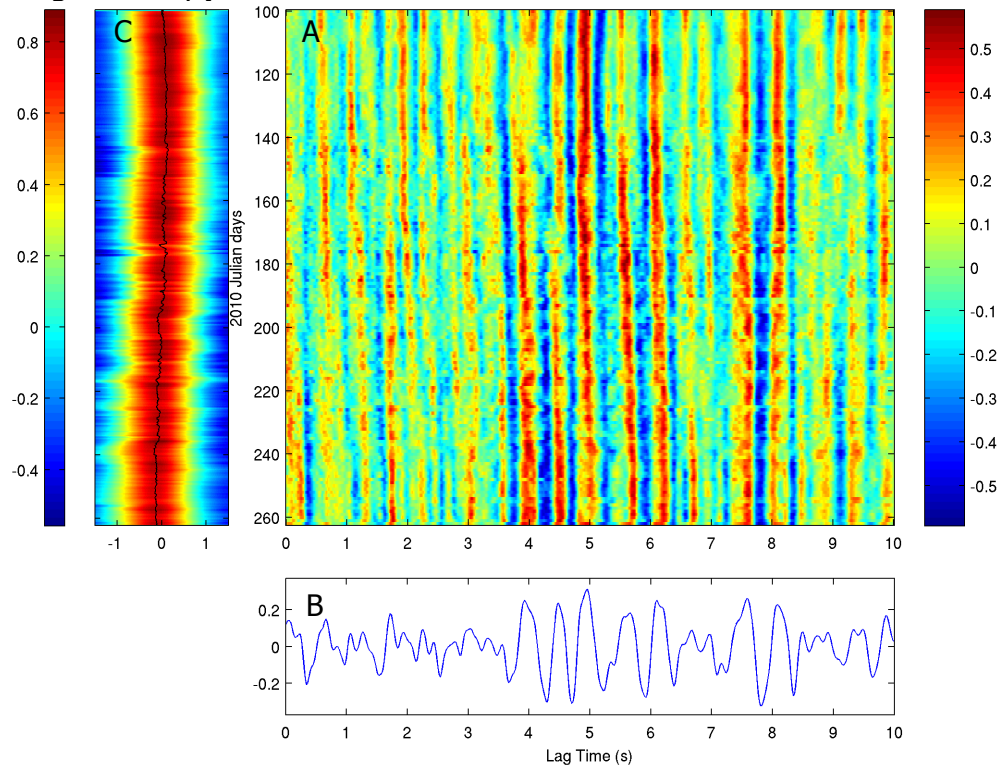


Figure 7.20 CCFs from V07 to V03, +lag, A. daily stacks, B. normalized total stack and C. stretching function, y-axis is the same for A and C

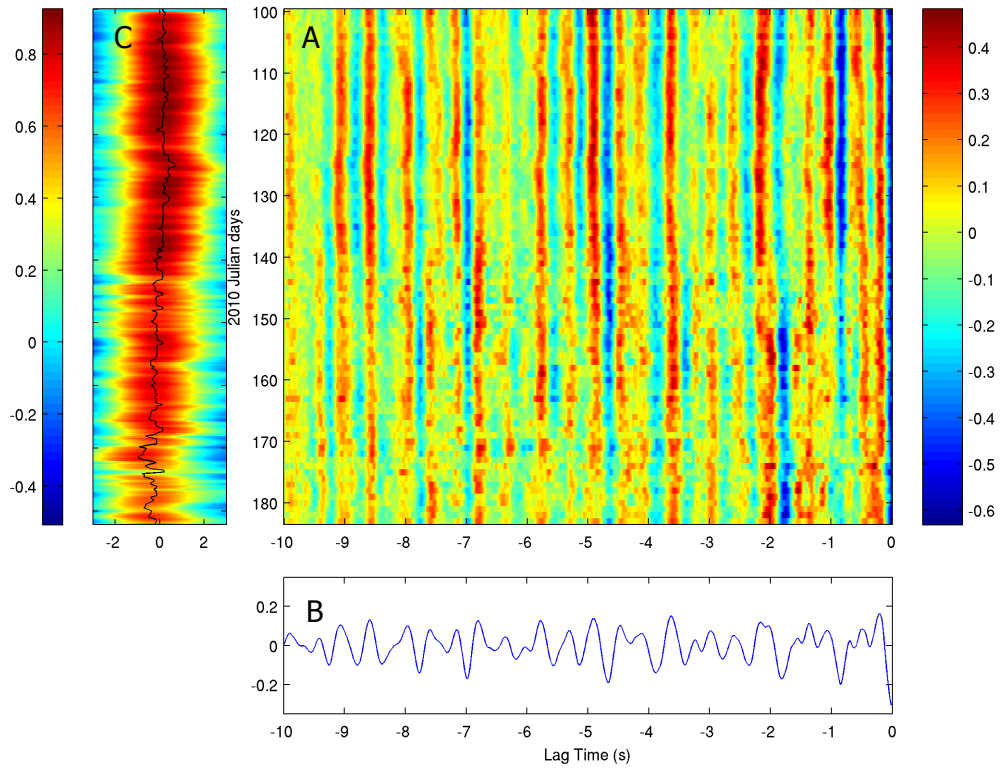


Figure 7.21 CCFs from V07 to V05, -lag, A. daily stacks, B. normalized total stack and C. stretching function, y-axis is the same for A and C

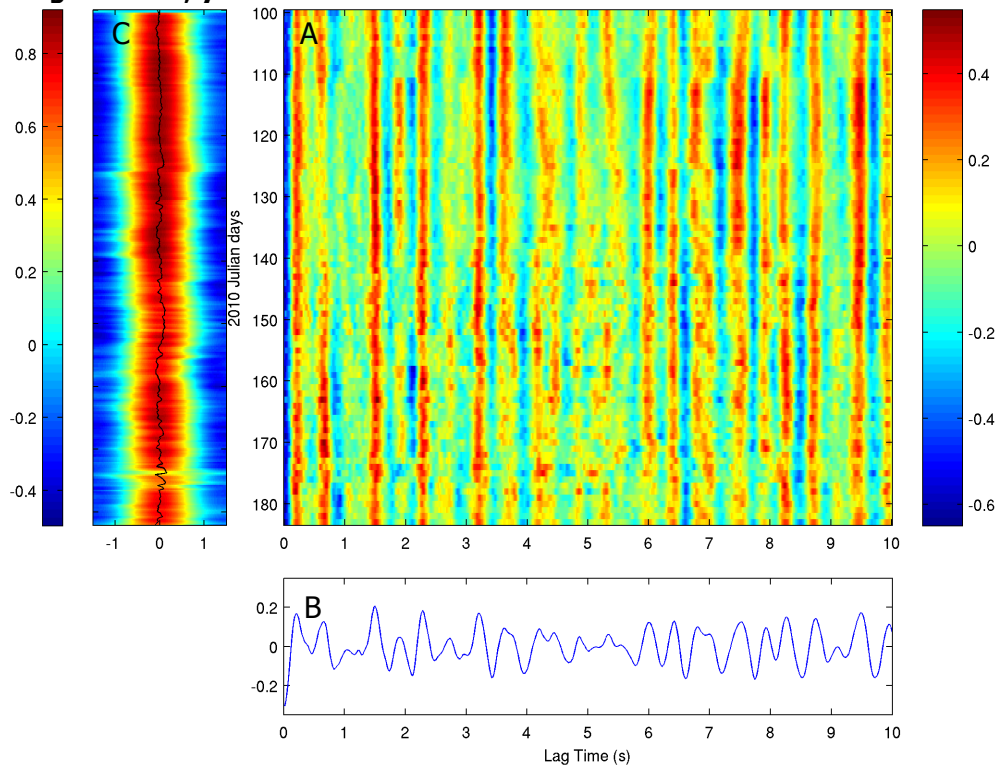


Figure 7.22 CCFs from V07 to V05, +lag, A. daily stacks, B. normalized total stack and C. stretching function, y-axis is the same for A and C

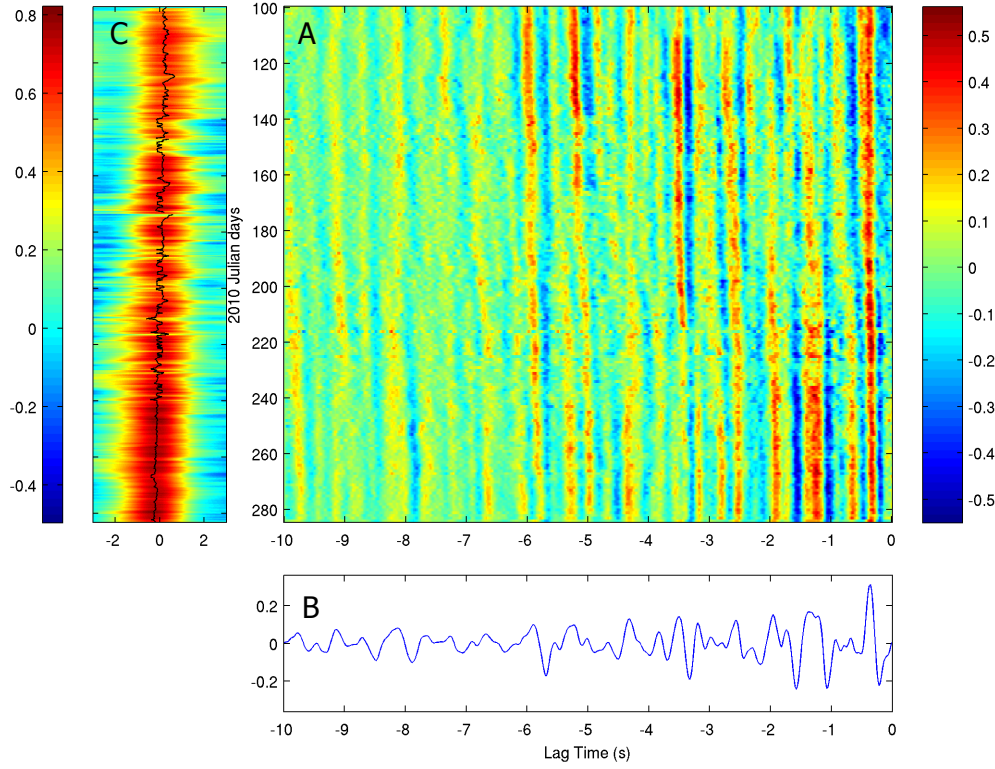


Figure 7.23 CCFs from V07 to V08, -lag, A. daily stacks, B. normalized total stack and C. stretching function, y-axis is the same for A and C

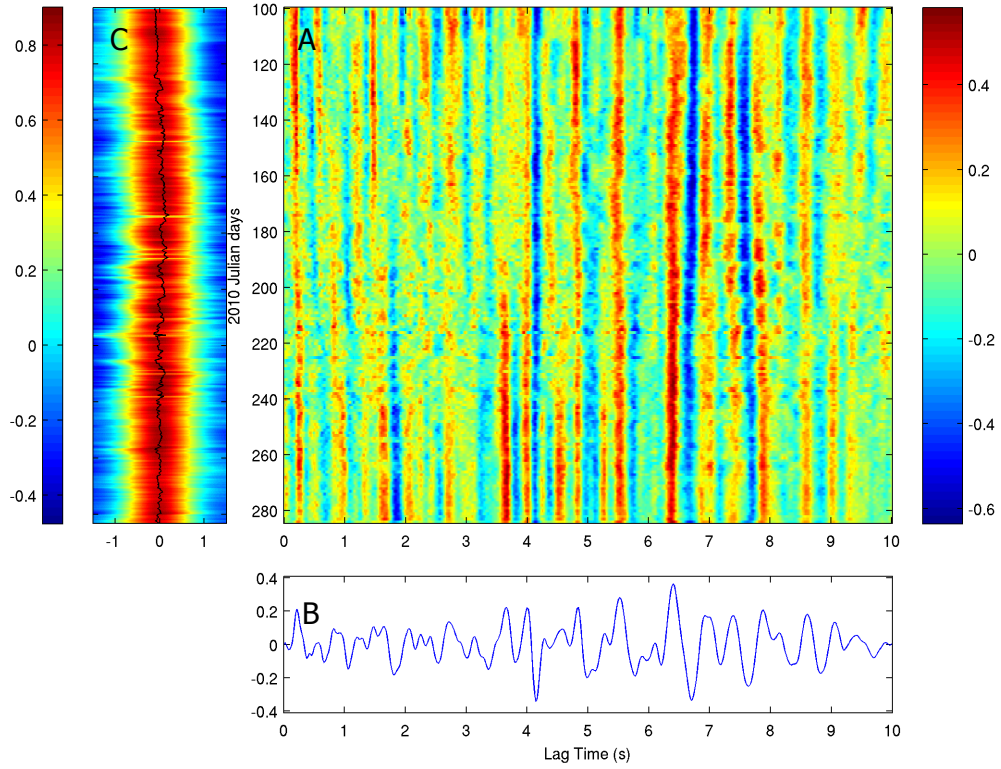


Figure 7.24 CCFs from V07 to V08, +lag, A. daily stacks, B. normalized total stack and C. stretching function, y-axis is the same for A and C

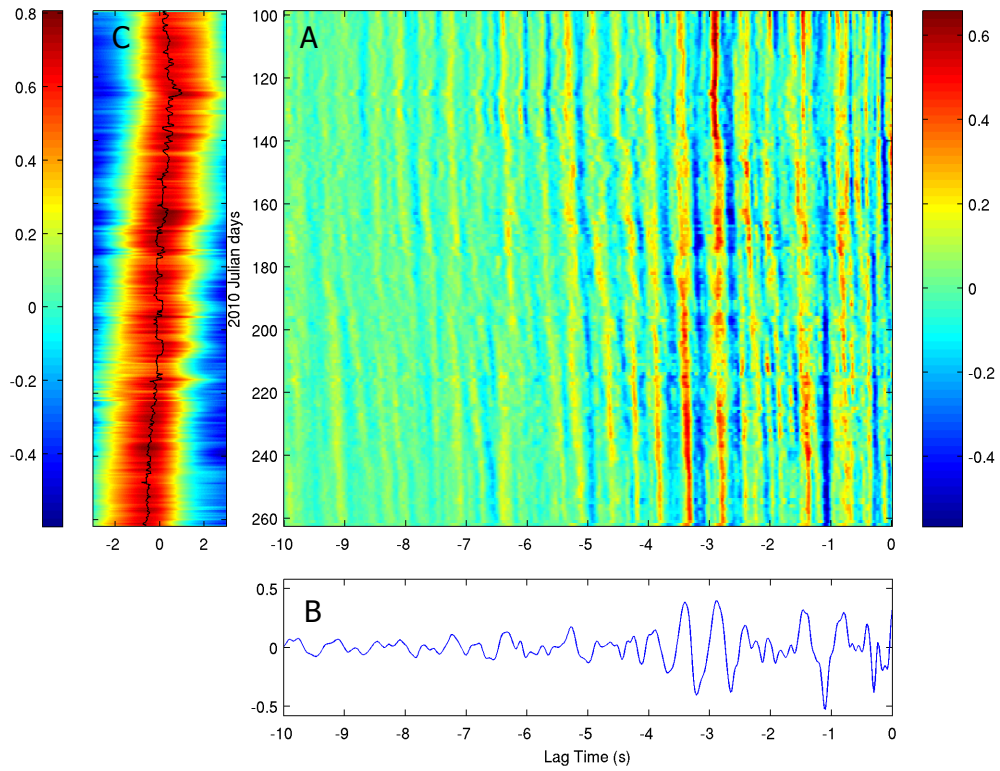


Figure 7.25 CCFs from V08 to V03, -lag, A. daily stacks, B. normalized total stack and C. stretching function, y-axis is the same for A and C

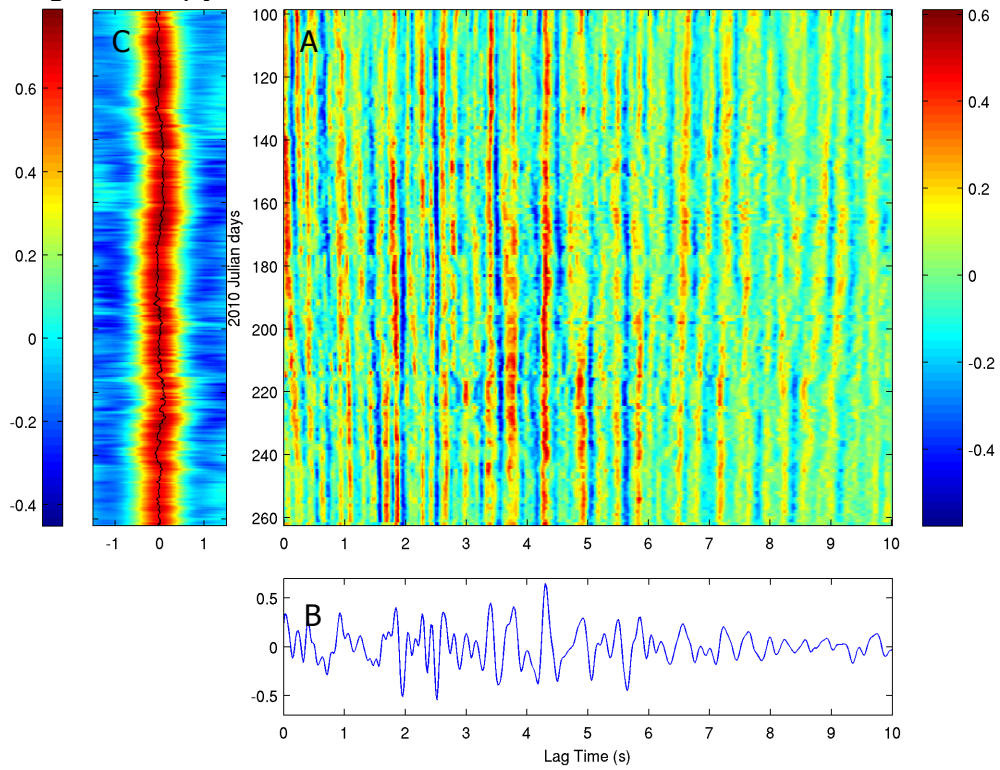


Figure 7.26 CCFs from V08 to V03, +lag, A. daily stacks, B. normalized total stack and C. stretching function, y-axis is the same for A and C

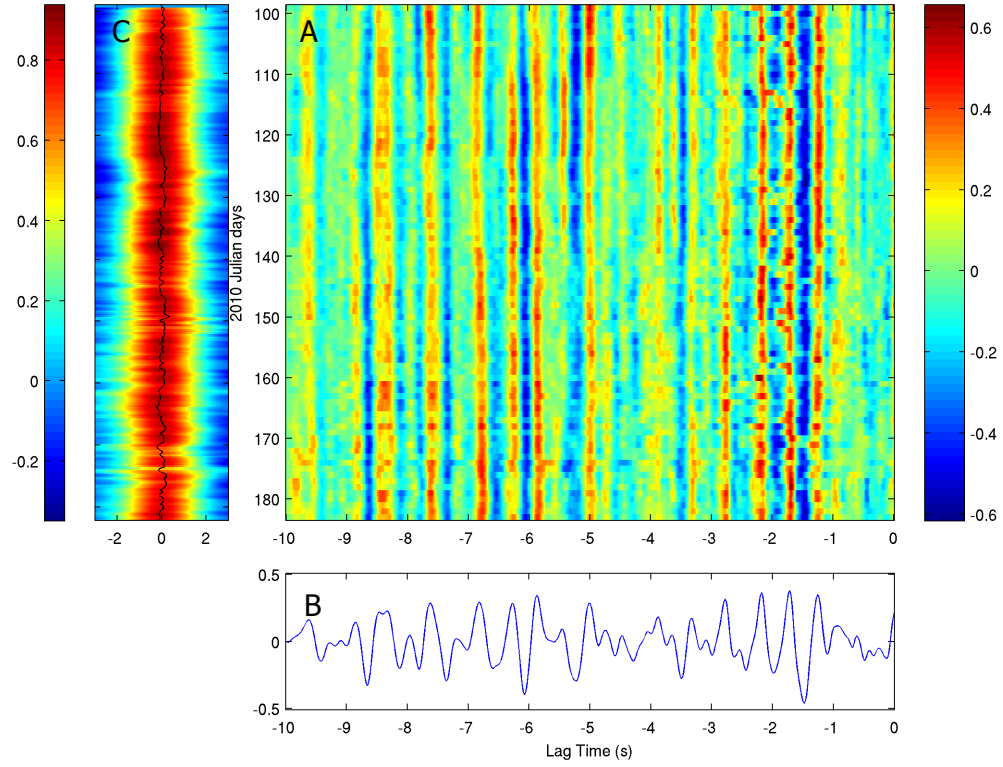


Figure 7.27 CCFs from V08 to V05, -lag, A. daily stacks, B. normalized total stack and C. stretching function, y-axis is the same for A and C

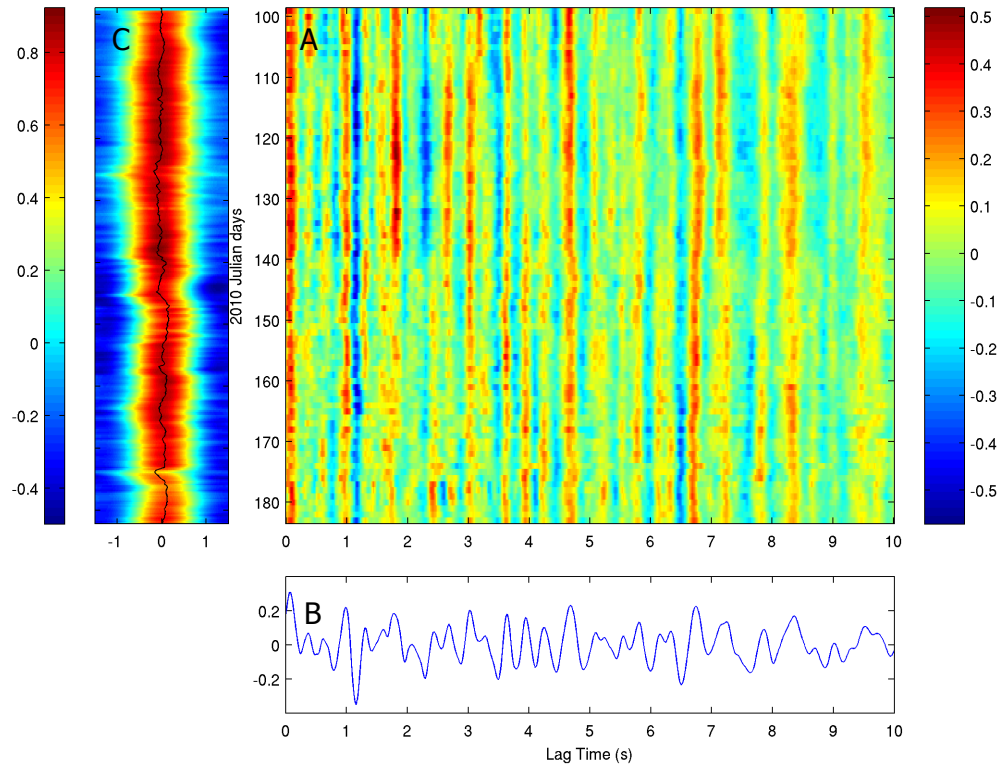


Figure 7.28 CCFs from V08 to V05, +lag, A. daily stacks, B. normalized total stack and C. stretching function, y-axis is the same for A and C

7.3 2011 Auto-correlations with total stack and velocity change

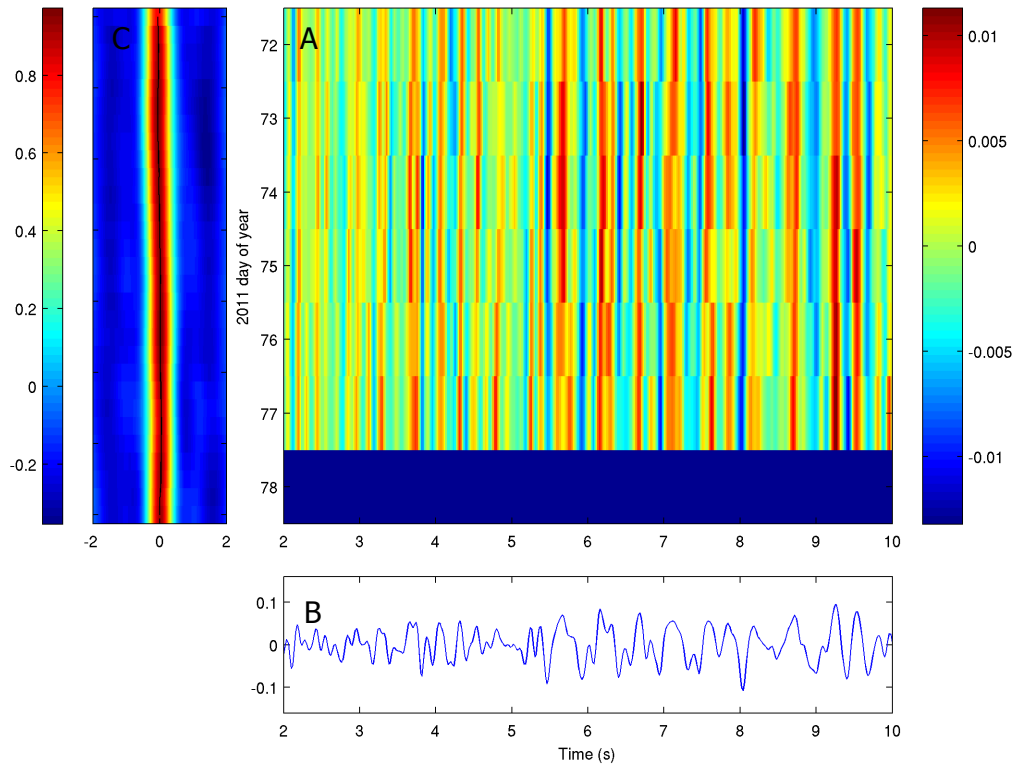


Figure 7.29 Station V01 2011 ACFs, A. 6 hour stacks, B. normalized total stack and C. stretching function, y-axis is the same for A and C

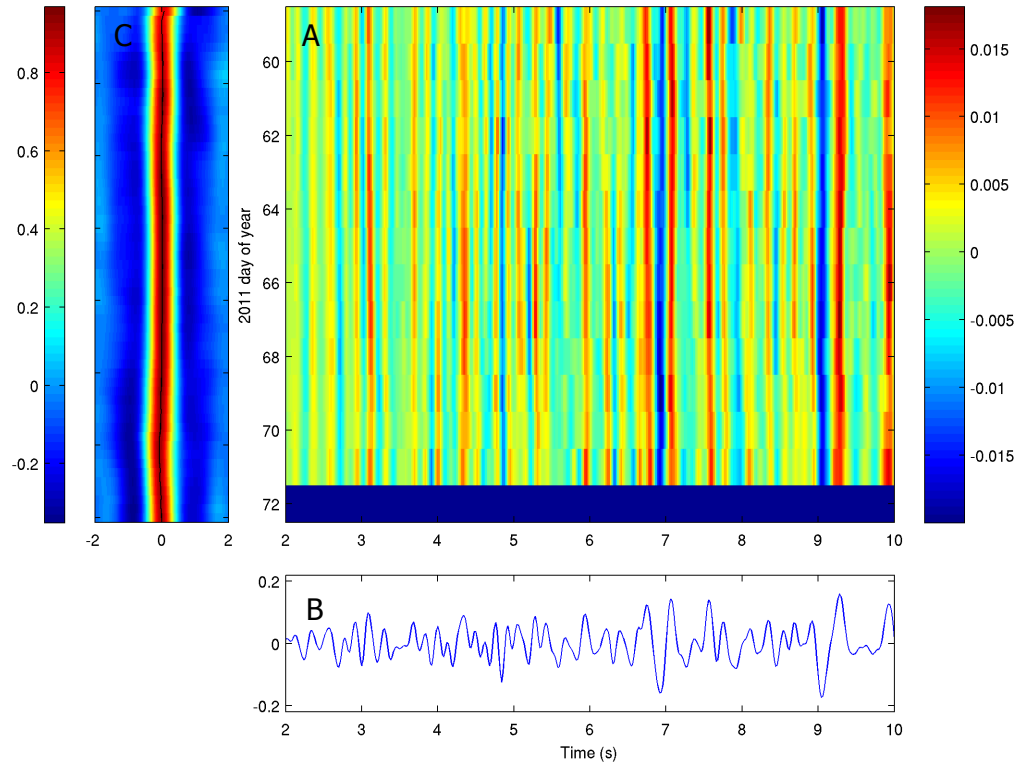


Figure 7.30 Station V02 2011 ACFs, A. daily stacks, B. normalized total stack and C. stretching function, y-axis is the same for A and C

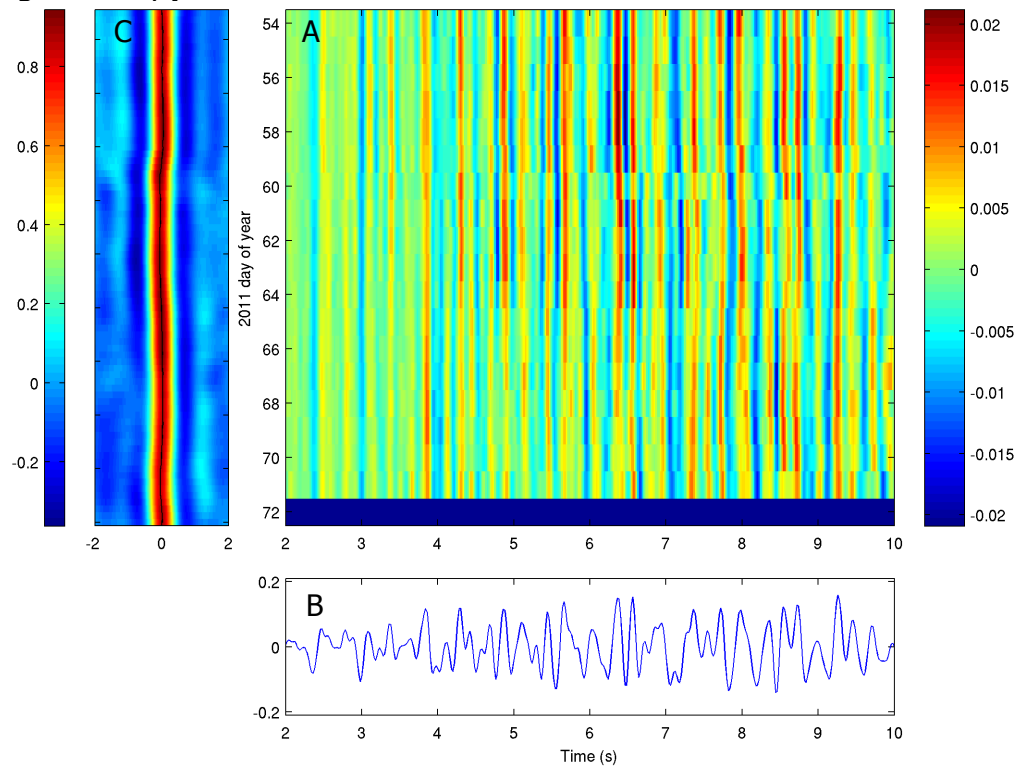


Figure 7.31 Station V03 2011 ACFs, A. daily stacks, B. normalized total stack and C. stretching function, y-axis is the same for A and C

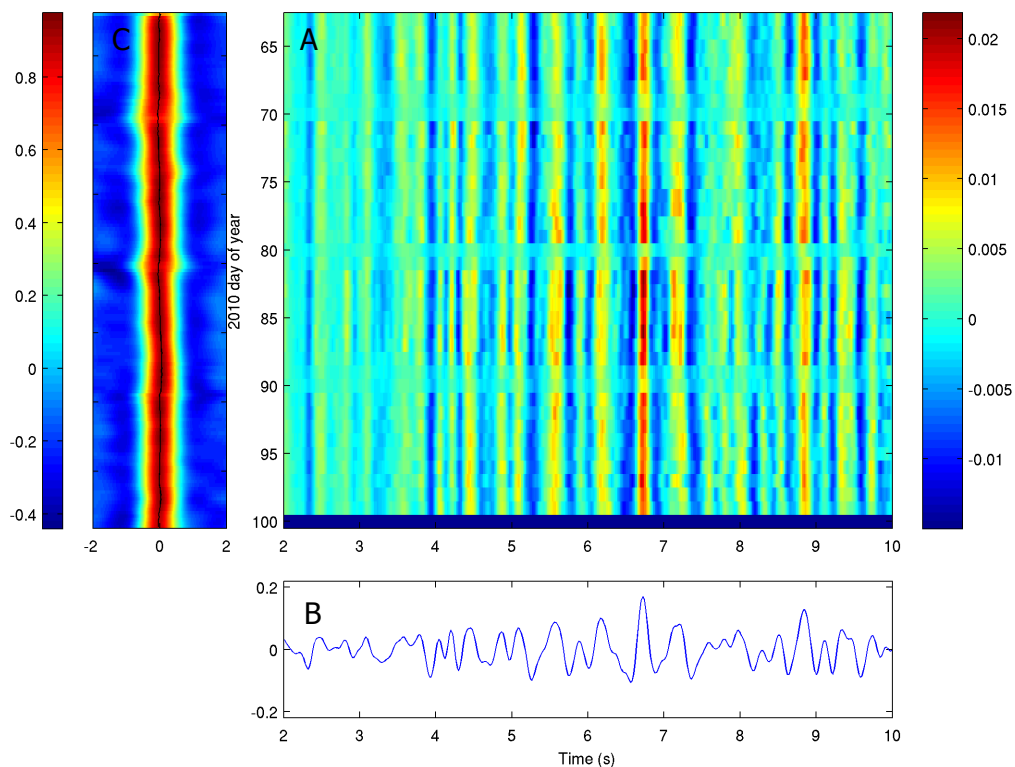


Figure 7.32 Station V06 2011 ACFs, A. daily stacks, B. normalized total stack and C. stretching function, y-axis is the same for A and C

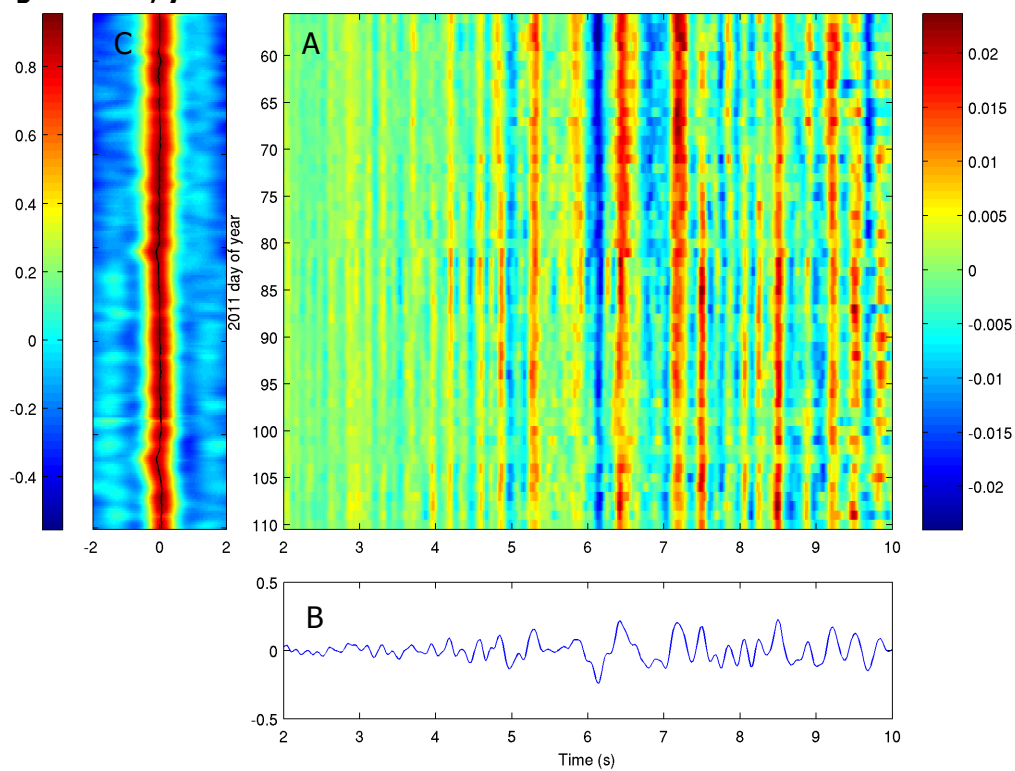


Figure 7.33 Station V08 2011 ACFs, A. daily stacks, B. normalized total stack and C. stretching function, y-axis is the same for A and C

7.4 2010 Earthquakes and peak surface wave amplitudes

Table 7.4.1 Magnitude, depth, date, location, and distance to Villarrica of the earthquakes M6 and greater displayed in Figure 4.2.2

Magnitude	Depth (km)	Time	Julian Day	Latitude	Longitude	distance (km)
7.2	4	4/4/2010 22:40:43	94	32.297	-115.278	9151.2
7	31	4/6/2010 22:15:02	96	2.383	97.048	15765.7
6	23	4/7/2010 14:33:02	97	-3.760	141.943	14109.8
6.6	21	4/11/2010 9:40:26	101	-10.878	161.116	12205.6
6.3	609.8	4/11/2010 22:08:13	101	36.965	-3.542	11007.9
6.2	53	4/17/2010 23:15:22	107	-6.669	147.291	13511.4
6	32	4/23/2010 10:03:06	113	-37.529	-72.969	229.1
6	27	4/24/2010 7:41:00	114	-1.912	128.122	15000.7
6.2	22	4/26/2010 2:59:52	116	22.180	123.623	17617.1
6.4	12	4/30/2010 23:11:43	120	60.473	-177.877	14591.6
6.3	14.9	4/30/2010 23:16:29	120	60.478	-177.650	14579.4
6.1	84	5/3/2010 10:27:45	123	29.645	140.951	16852.6
6.4	23	5/3/2010 23:09:38	123	-38.271	-74.309	242.7
6.3	19	5/3/2010 23:09:45	123	-38.072	-73.454	200.1
6.6	27	5/5/2010 16:29:03	125	-4.054	101.096	15145.1
6.2	37	5/6/2010 2:42:48	126	-18.058	-70.547	2381.7
7.2	38	5/9/2010 5:59:42	129	3.748	96.018	15883.9
6	132	5/19/2010 4:15:43	139	-5.083	-77.541	3863.8
6	10	5/19/2010 10:30:10	139	-54.800	-135.252	4902.8
6.3	101.4	5/23/2010 22:46:52	143	-13.928	-74.352	2847.6
6.5	581.2	5/24/2010 16:18:29	144	-8.087	-71.558	3488.1
6.3	10	5/25/2010 10:09:06	145	35.336	-35.924	9106.3
6.2	10	5/26/2010 8:53:08	146	25.773	129.944	17496.1
7.2	31	5/27/2010 17:14:47	147	-13.698	166.643	11570.7
6.5	112	5/31/2010 19:51:46	151	11.132	93.471	16573.1
7.5	35	6/12/2010 19:26:50	163	7.881	91.936	16174.4
6.2	13	6/16/2010 3:06:02	167	-2.386	136.635	14543.7
7	18	6/16/2010 3:16:28	167	-2.174	136.543	14569.3
6.6	10.5	6/16/2010 3:58:08	167	-2.329	136.484	14557.4
6.1	28	6/18/2010 2:23:06	169	44.448	148.689	16662.6
6.8	35	6/26/2010 5:30:19	177	-10.627	161.447	12202.9
6.4	581.4	6/30/2010 4:31:02	181	-23.307	179.116	9885.9
6.1	27	7/4/2010 21:55:52	185	39.697	142.369	17111.5
6.2	13	7/10/2010 11:43:33	191	11.143	145.999	15150.4
6.1	115	7/12/2010 0:11:21	193	-22.146	-68.216	1954.9
6.7	14	7/18/2010 5:56:45	199	52.876	-169.848	13891.0
6.7	35	7/18/2010 5:56:50	199	52.970	-169.504	13873.3

6.3	28	7/18/2010 13:04:09	199	-5.966	150.428	13371.0
7.4	35	7/18/2010 13:34:59	199	-5.931	150.590	13363.3
6.3	24	7/20/2010 19:18:20	201	-5.902	150.712	13357.7
6.1	100	7/21/2010 9:16:04	202	3.039	128.222	15503.8
7.3	607.1	7/23/2010 22:08:11	204	6.718	123.409	16085.8
7.6	578	7/23/2010 22:51:12	204	6.497	123.480	16060.0
7.5	640.6	7/23/2010 23:15:10	204	6.776	123.259	16097.7
6.6	553	7/24/2010 5:35:01	205	6.218	123.519	16029.4
6	41.2	7/25/2010 3:39:23	206	-15.032	-173.543	9926.0
6.6	618	7/29/2010 7:31:56	210	6.548	123.222	16075.3
6.3	23	7/30/2010 3:56:14	211	52.498	159.843	15877.6
6.3	41	8/3/2010 12:08:26	215	1.239	126.213	15405.0
6.5	220	8/4/2010 7:15:34	216	-5.486	146.822	13649.1
6.4	27	8/4/2010 12:58:24	216	51.423	-178.649	14406.7
6.1	44	8/4/2010 22:01:44	216	-5.746	150.765	13368
6	27.8	8/4/2010 23:48:02	216	45.980	153.175	16326.9
7.3	25	8/10/2010 5:23:45	222	-17.541	168.069	11152.9
6.4	206.7	8/12/2010 11:54:16	224	-1.266	-77.306	4282.1
6.1	10	8/14/2010 7:30:17	226	12.348	141.487	15580.8
6.3	13	8/14/2010 23:01:04	226	12.273	141.429	15578.7
6.3	174.7	8/15/2010 15:09:29	227	-5.692	148.342	13532.7
6.3	9.8	8/16/2010 3:30:53	228	-17.759	65.647	12295.0
6.2	603.2	8/16/2010 19:35:49	228	-20.799	-178.826	9919.1
6.1	43.1	8/18/2010 16:28:21	230	12.210	141.456	15571.5
6.4	50.9	8/20/2010 17:56:19	232	-6.559	154.088	13070.2
6.3	23.5	9/3/2010 11:16:07	246	51.451	-175.870	14223.8
7.3	12	9/3/2010 16:35:48	246	-43.522	171.830	8801.8
6.1	69	9/4/2010 8:52:04	247	-17.368	-173.999	9792.8
6.3	10	9/8/2010 11:37:32	251	-20.671	169.818	10772.7
6.2	54.1	9/8/2010 11:37:39	251	-20.699	169.810	10771.0
6.2	16	9/9/2010 7:28:02	252	-37.034	-73.412	295.5
6.3	220.1	9/17/2010 19:21:15	260	36.443	70.774	16769.0
6.1	30	9/26/2010 12:12:42	269	-5.314	133.917	14393.7
6.2	10	9/29/2010 17:10:51	272	-4.909	133.712	14444.2
6.7	26	9/29/2010 17:11:26	272	-4.963	133.760	14436.5
6	32	10/4/2010 13:28:39	277	24.270	125.154	17709.9
6.2	19	10/8/2010 3:26:14	281	51.374	-175.361	14187.6
6	27.7	10/8/2010 3:49:11	281	51.287	-175.180	14172.5
6.1	120	10/8/2010 5:43:08	281	2.831	128.217	15482.9
6	57	10/16/2010 20:08:37	289	-20.420	-173.865	9560.0
6.8	13	10/21/2010 17:53:14	294	24.696	-109.156	8118.3

7.3	20.1	10/25/2010 14:42:22	298	-3.487	100.082	15191.1
6	26	10/25/2010 19:37:31	298	-2.958	100.372	15254.3

Table 7.4.2 Magnitude, depth, date, location, and distance to Villarrica of the earthquakes M5.5-5.9 displayed in Figure 4.2.2

Magnitude	Depth (km)	Time	Julian Day	Latitude	Longitude	distance (km)
5.5	8	4/4/2010 23:15:14	94	32.25	-115.3	9147.9
5.8	94.2	4/5/2010 22:36:57	95	-19.86	-68.842	2197.4
5.7	117.7	4/9/2010 22:23:03	99	-28.559	-68.124	1258.7
5.8	7	4/10/2010 6:30:00	100	-41.081	-89.894	1534.6
5.5	49.5	4/10/2010 15:06:34	100	-25.68	-70.667	1534.0
5.5	100.2	4/13/2010 20:27:01	103	-56.331	-27.311	3735.6
5.6	6	4/16/2010 22:41:34	106	-37.46	-73.732	268.9
5.7	24	4/16/2010 23:15:36	106	-37.42	-73.669	269.4
5.5	33	4/17/2010 20:52:42	107	11.678	-86.813	5893.4
5.6	29.9	4/18/2010 1:49:38	108	-37.159	-73.753	297.8
5.7	7	4/25/2010 21:09:44	115	-55.606	-27.73	3695.0
5.7	10	5/5/2010 9:38:23	125	-35.949	-103.058	2755.5
5.5	10	5/6/2010 11:35:30	126	-55.725	-127.942	4433.9
5.8	113	5/16/2010 5:16:10	136	18.4	-67.07	6456.2
5.6	10	5/20/2010 8:06:29	140	-39.063	-92.159	1740.8
5.7	33	5/21/2010 18:52:12	141	-34.512	-71.602	547.1
5.7	18	6/1/2010 3:26:16	152	9.331	-84.206	5573.2
5.8	5.4	6/15/2010 4:26:58	166	32.7	-115.921	9221.5
5.5	104.4	6/26/2010 19:01:18	177	-18.927	-69.164	2296.7
5.8	28.2	6/28/2010 0:59:47	179	-37.91	-75.038	318.1
5.5	17	6/29/2010 1:40:01	180	-37.836	-73.278	211.7
5.7	28.7	7/4/2010 6:57:45	185	-8.469	-80.471	3549.1
5.8	35	7/14/2010 15:05:50	195	-38.224	-73.23	174.5
5.5	55	7/17/2010 6:07:44	198	-24.715	-69.817	1648.9
5.7	10	7/20/2010 17:19:50	201	-29.031	-13.096	5440.5
5.8	18	8/5/2010 6:01:47	217	-37.443	-73.281	249.6
5.5	10	8/13/2010 7:58:49	225	36.877	-32.874	9387.4
5.5	67.7	8/19/2010 22:13:03	231	14.03	-91.121	6274.6
5.6	16.1	8/22/2010 10:23:03	234	37.4998	20.2671	12713.4
5.5	10	8/24/2010 2:11:59	236	18.795	-107.193	7445.7
5.5	53.3	8/28/2010 18:46:30	240	18.72	-107.097	7433.5
5.5	35	8/29/2010 6:37:49	241	-55.8	-26.991	3744.4
5.8	179.8	9/13/2010 7:15:50	256	-14.612	-70.777	2763.9
5.6	16.1	9/14/2010 23:32:02	257	21.487	-105.93	7646.9
5.7	50	9/22/2010 8:00:14	265	-13.39	-76.073	2926.0
5.5	150.3	9/24/2010 19:01:32	267	-7.809	-74.373	3527.3
5.8	37	9/30/2010 0:26:23	273	-36.347	-73.021	355.2

5.8	91	10/9/2010 1:54:05	282	10.211	-84.293	5671.0
5.5	10	10/20/2010 4:09:43	293	24.54	-109.098	8100.3
5.5	10	10/20/2010 6:58:14	293	24.471	-109.026	8090.0
5.7	15	10/23/2010 5:58:28	296	-37.743	-73.362	224.4

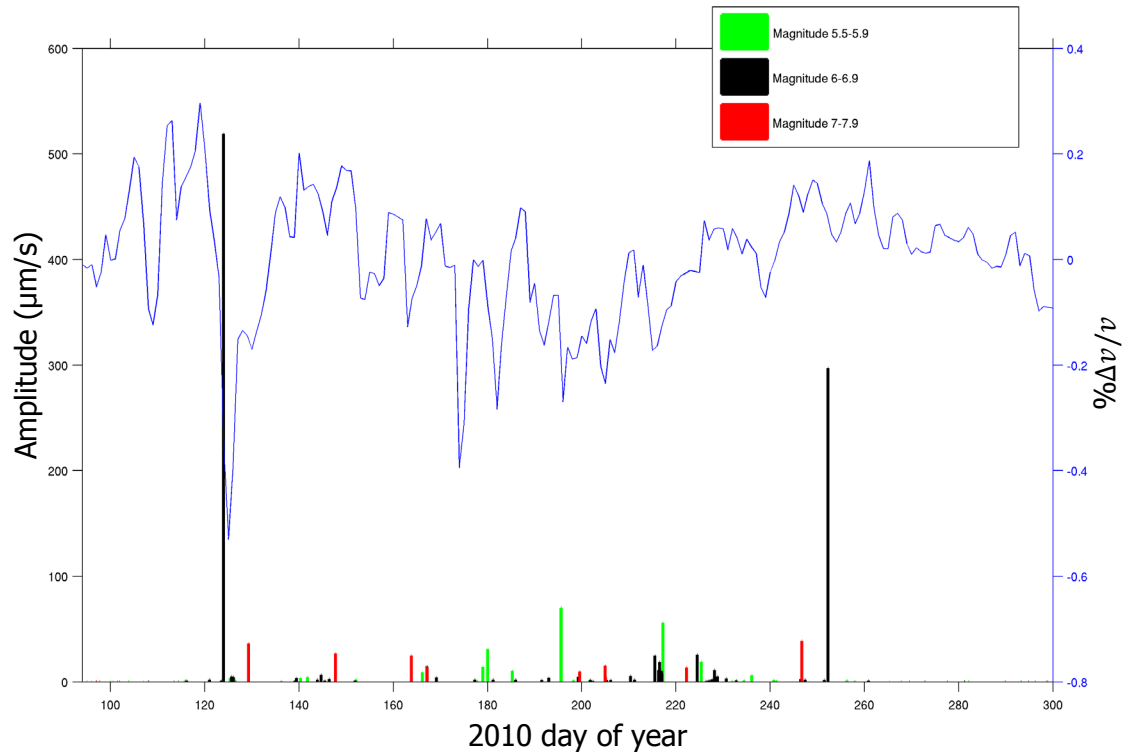


Figure 7.34 V07 radial channel surface wave amplitude versus stacked $\% \Delta v/v$

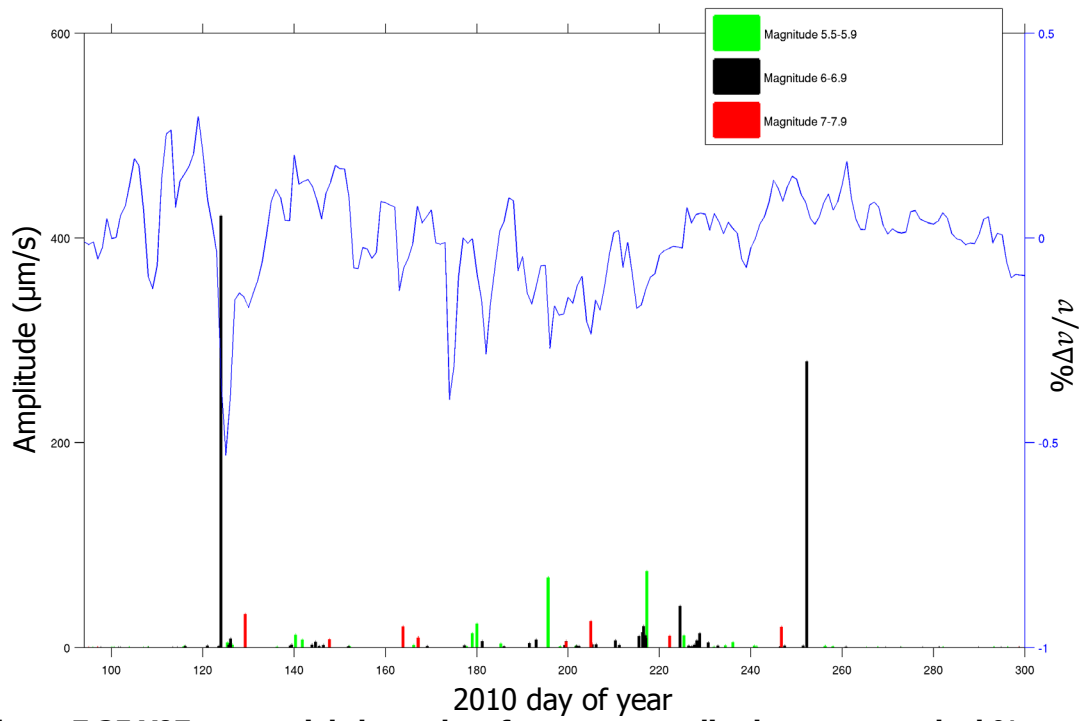


Figure 7.35 V07 tangential channel surface wave amplitude versus stacked $\% \Delta v / v$